Quaternary Geology in Part of the McLeod Lake Map-Area (NTS 093J), Central British Columbia

by

David A. Sacco

B.A. (Hons.), University of the Fraser Valley, 2008

Thesis Submitted In Partial Fulfillment of the
Requirements for the Degree of
Master of Science

in the
Department of Earth Sciences
Faculty of Science

SIMON FRASER UNIVERSITY

Fall 2012

Approval

Name: **David A. Sacco**

Degree: **Master of Science**

Title of Thesis: ***Quaternary geology in part of the McLeod Lake map-area (NTS 093J), central British Columbia***

Examining Committee: **Chair:** Dr. Dan Gibson
Associate Professor

Dr. Brent Ward
Senior Supervisor
Associate Professor

Dr. John Clague
Supervisor
Professor

Dr. Olav Lian
Supervisor
Adjunct Professor

Dr. Alain Plouffe
External Examiner
Research Scientist,
Geological Survey of Canada

Date Defended/Approved: November 2, 2012

Partial Copyright License

Abstract

The Quaternary geology in part of the McLeod Lake map-area was studied through the production and analysis of 1:50 000-scale terrain maps and the examination of stratigraphic exposures and landforms. The surficial geology is dominated by thick, streamlined till that thins where relief is high. Glaciofluvial outwash and ice-contact deposits occur throughout the area and extensive glaciolacustrine deposits blanket low-lying regions. The glacial stratigraphic record spans the Fraser Glaciation and is represented by a sequence of advance glaciolacustrine sediments, till and retreat glaciolacustrine and glaciofluvial sediments. Ice initially flowed into the study area from the northwest and retreated before the arrival of ice from the west and south. Ice-flow during the glacial maximum was northeast and transitioned to the east during deglaciation. Ground penetrating radar suggests that post-glacial aeolian activity was brief. Optical dating on K-feldspar from aeolian material suggests this activity occurred around 9.35 ± 0.64, 9.94 ± 0.77 and 13.3 ± 1 ka and provides minimum ages for ice retreat.

Keywords: McLeod Lake map-area; terrain mapping; Quaternary stratigraphy; ice-flow history; optical dating; ground penetrating radar

Acknowledgements

I would like to first express my deep gratitude to my supervisor Dr. Brent Ward. His valuable and constructive suggestions and sincerity helped form this project and were instrumental in my development as a researcher. A special thank you to my committee members, John Clague and Olav Lian, and external examiner, Alain Plouffe, whose thorough edits and thoughtful discussions greatly improved the quality of this thesis. I would like to acknowledge the guidance provided by Denny Maynard and Marten Geertsema during the mapping and fieldwork. Thanks to all of my friends, family and colleagues who provided support and encouragement throughout this project. I would also like to thank all of those who assisted me in the field, the staff from the Luminescence Laboratory at the University of the Fraser Valley, and the GIS technicians at Chartwell Resources and Geoscience BC. Generous funding for this project was provided by Geoscience BC.

Table of Contents

List of Tables

List of Figures

1. Introduction

Over approximately the last two million years, British Columbia has repetitively been covered by an interconnected mass of glaciers collectively known as the Cordilleran Ice Sheet (CIS; Armstrong et al. 1965; Flint 1971; Clague 1989). The McLeod Lake map-area (NTS 093J) in central British Columbia is situated near the geographic centre of the CIS where glaciers from several source areas coalesced, creating a dynamic glacial environment. Much of the region is characterized by thick drift consisting of sediments of the most recent Fraser Glaciation and in some places, older glacial and nonglacial events. The surface is dominated by glacial landforms including numerous drumlin fields and meltwater features that can be used to establish a relatively comprehensive record of glacial events.

The glacial geology in the McLeod Lake map-area has previously only been studied at a reconnaissance level (Armstrong and Tipper 1948; Tipper 1971a, b). Increased activity in mineral exploration has necessitated a more detailed understanding of glaciation and its impact on the landscape to guide exploration projects. A comprehensive understanding of the ice-flow history is essential in mineral exploration that uses geochemical and mineral tracing in glacial sediments. Different directions and durations of ice flow can impact the dispersal of subglacial sediments by creating palimpsest dispersal patterns (Parent et al. 1996; Plouffe et al. 2011). An ice-flow history can be used to plan exploration surveys, determine the potential vector(s) of glacial transport and locate the source of till geochemical and mineralogical anomalies. The surficial geology maps produced as part of this study can also be used to locate aggregate resources for construction and maintenance of highways and forest service roads and identify areas with possible natural hazard potential. This project also adds to our knowledge of the last glaciation in central British Columbia.

In 2007, central British Columbia was targeted by Geoscience BC for its Quesnellia Exploration Strategy (QUEST) Project. The QUEST Project is designed to attract

mineral exploration companies by providing regional-scale geologic, geochemical and geophysical data. The focus of these surveys is the Quesnel Terrane, which has high potential to host undiscovered economic mineralization (Fig 1.1a). This Masters project provides a model for glaciation based on the description and interpretation of the surficial geology, stratigraphy, geomorphology and chronology from a part of the QUEST Project area (NTS 093J05/06/11/12/13/14; Fig 1.1b) that can be used to interpret regional-scale till geochemical and mineralogical data (e.g. Ward et al. 2009, 2011, 2012; Sacco et al. 2010).

1.1. Location and access

The study area is part of the McLeod Lake map-area (NTS 093J). It comprises six, 1:50 000-scale map sheets (NTS 093J05/06/11/12/13/14) and covers an area of approximately 5350 km^2 (Fig. 1.1b). Highway 97, which links Prince George to Fort St. John, runs along the east side of the study area and Highway 16, which links Prince George to Fort St. James, runs to the south. A network of forest service roads provides access to most parts of the study area for fieldwork based out of Prince George, Fort St. James and Mackenzie. The majority of fieldwork was done by truck and all-terrain vehicle traverses. Some areas were not accessible due to road conditions or lack of roads.

1.2. Physiography

The study area lies within the Interior System of the Canadian Cordillera and includes parts of the Fraser Basin, Nechako Plain and Nechako Plateau physiographic regions (Holland 1976; Fig. 1.2). However, the majority of the study area is within the Fraser Basin and Nechako Plain that are characterized by moderate to low relief between 675 and 1000 m a.s.l. with thick surficial deposits and rare bedrock exposures. Till commonly exhibits a streamlined expression and thick, flat glaciolacustrine units occur in the southern regions. Large meltwater corridors occur in the northeast and east, and esker systems, ice stagnation landforms and smaller meltwater channels occur throughout the region.

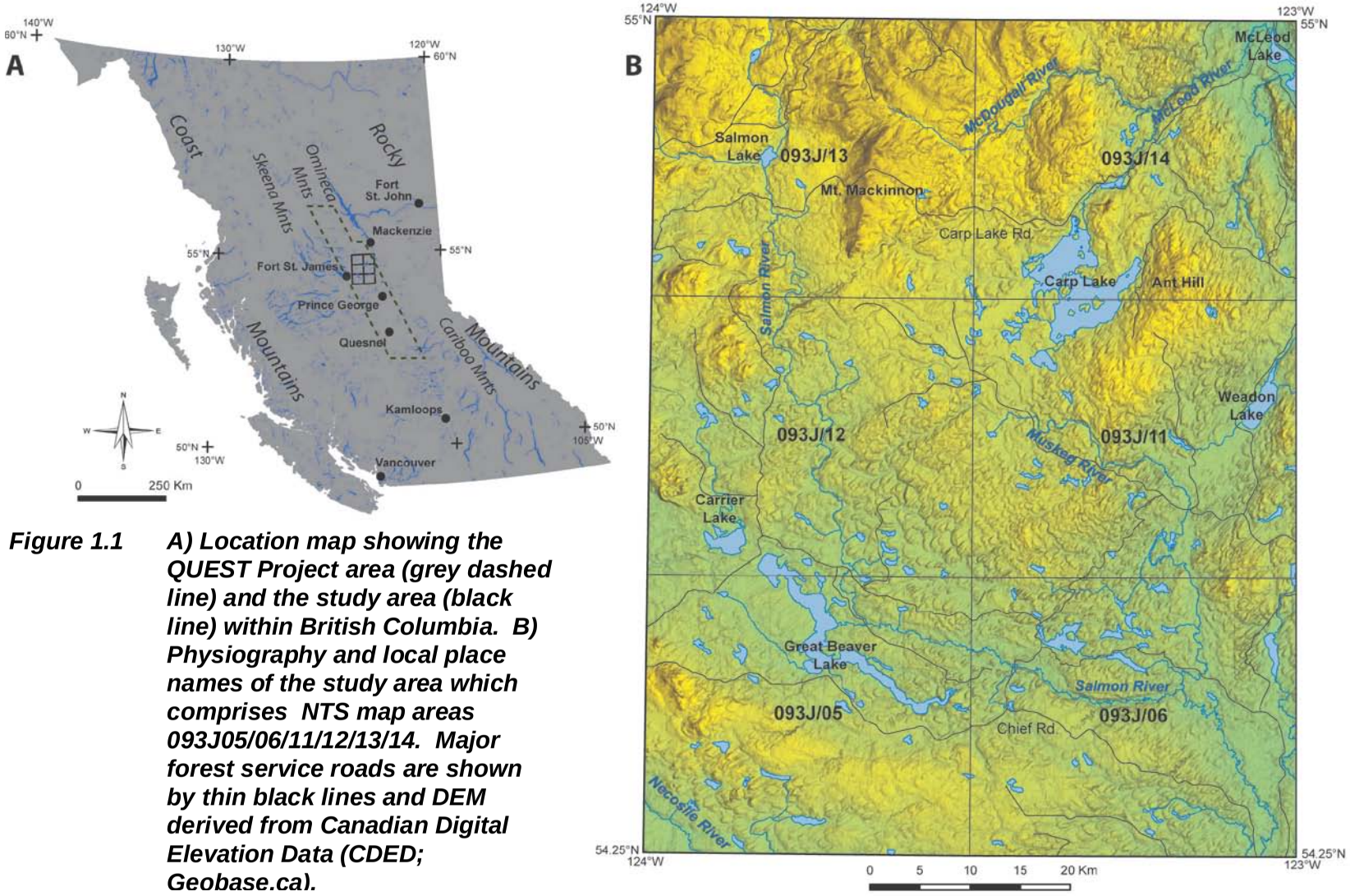

Figure 1.1 ***A) Location map showing the QUEST Project area (grey dashed line) and the study area (black line) within British Columbia. B) Physiography and local place names of the study area which comprises NTS map areas 093J05/06/11/12/13/14. Major forest service roads are shown by thin black lines and DEM derived from Canadian Digital Elevation Data (CDED; Geobase.ca).***

The northwestern part of the study area is within the Nechako Plateau. Here, the southern portion of the Wolverine Mountain Range is notably steep and rocky with some peaks over 1500 m a.s.l. Similar to lower relief areas, till is the dominant surficial material but bedrock exposures are more numerous. Glaciofluvial, fluvial and glaciolacustrine materials are typically confined to valley bottoms with colluvium on the valley sides.

A major drainage divide that separates the Arctic and Pacific watersheds runs northwest-southeast through the study area (Fig. 1.2). In the northeast part of the study area, the Peace and Nation river basins carry water north to the Slave River and eventually drain into the Arctic Ocean via the Mackenzie River. The western edge of the study area is drained by the Stuart River, which flows into the Fraser River. The central area drains via the Fraser River, which flows south through the Lower Fraser Valley and into the Strait of Georgia.

1.3. Climate and vegetation

The study area occurs within the Sub-boreal Interior Ecoprovince of the British Columbia ecoregion classification system (Demarchi 2011). It is characterized by a sub-continental climate with cold winters and warm summers. Prevailing westerly winds moderate the climate, but during the winter and spring Arctic air invades the region from the north and east, bringing extended periods of cold. Precipitation is evenly distributed throughout the year with a minor decrease between February and April. East-flowing moist Pacific air and summer surface heating of lakes and streams bring summer rains, and in the winter, southward-flowing cold Arctic air meets moist Pacific air, causing snowfall.

The study area is dominated by white spruce and subalpine fir but contains a variety of other tree and shrub species. Lodgepole pine is common on well drained soils and in areas of forest regeneration, although the pine beetle infestation has left many of these stands dead. Trembling aspen and paper birch may develop extensive stands where fine soils impede drainage. Common plants of the understory include prickly rose, soopolallie, willows, black twinberry, thimbleberry, devil's club, bunchberry, arnicas,

twinflower, fireweed, trailing raspberry, oak fern, creamy peavine, and aster. Sedge fens are common in wetlands with scrub birch and willows. Wetlands may also contain sphagnum and black spruce. Primary colonizers in disturbed areas are sitka alder, fireweed, prickly rose and trailing raspberry.

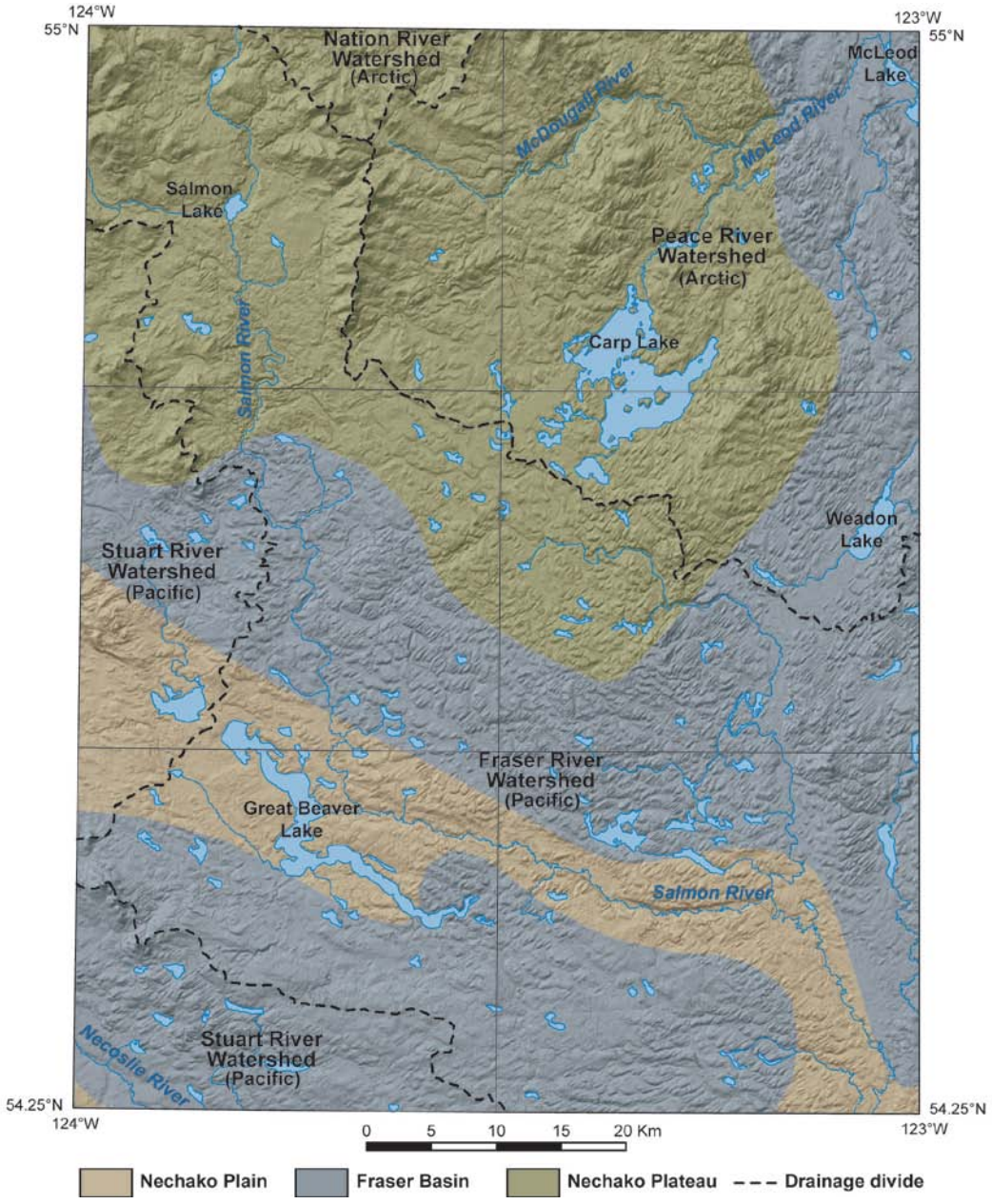

Figure 1.2 Physiographic regions of the study area (after Holland 1976) and major watersheds (DEM derived from CDED; Geobase.ca).

1.4. Bedrock geology

The study area comprises the Kootenay, Cache Creek, Slide Mountain and Quesnel terranes. The northeast corner extends into the Rocky Mountain Assemblage and several overlap assemblages occur throughout the study area (Fig. 1.3).

The Kootenay Terrane, in the north-central part of the study area, is composed of Late Proterozoic – Late Paleozoic rocks of the Wolverine Metamorphic complex consisting mainly of muscovite and biotite schist; amphibolite and calcsilicate paragneiss; and quartzite with pegmatite, granodiorite and quartz porphyry (Logan et al. 2010). The Slide Mountain Terrane comprises the Early Mississippian – Late Permian Antler Formation of basalt, basalt breccia, gabbro, diorite and chert (Struik 1994; Logan et al. 2010). The Cache Creek Terrane occurs in the southwest portion of the study area and is composed of Pennsylvanian and Permian massive grey and light grey limestone, limey mudstone and chert of the Pope succession. The majority of the study area is located on the Quesnel Terrane, which is dominated by the Nicola Group (Logan et al. 2010), formerly referred to as the Takla Group (Struik 1994). Within the Nicola Group is the Hogem Batholith, an undated intrusion of gabbro, diorite, granodiorite, monzonite and syenite (Logan et al. 2010); the Middle – Upper Triassic Slate Creek Succession of black phylite, slate, siltstone and quartzite; the Upper Triassic Cottonwood River Succession consisting of volcanic sandstone, siltstone and breccias; and the Upper Triassic Witch Lake Succession comprising basalt and breccias. In the northeast corner of the study area, the Rocky Mountain Assemblage comprises Upper Cambrian – Lower Ordovician sandy limestone, slate and phylite and Upper Silurian – Lower Devonian sandy limestone and quartzite (Struik 1994).

Overlap assemblages include the Sifton Formation, the Wolverine Range Plutonics, the Ootsa Lake Group and the Chilcotin Group. The Sifton Formation occurs in the southwest corner of the study area, adjacent to the Pinchi Fault. It is Cretaceous – Tertiary in age and comprises conglomerate, breccias, sandstone, shale and minor coal (Struik 1994). The Wolverine Range Plutonics are also Cretaceous – Tertiary in age and consist of muscovite-biotite granite and pegmatitic intrusions (Logan et al. 2010). The Ootsa Lake Group is Eocene in age and consists of felsic and intermediate volcanic flows, tuffs and breccias of subordinate mafic rocks and minor conglomerate and wacke

(Logan et al. 2010). The youngest rocks in the study area are the Oligocene – Pliocene Chilcotin olivine basalts and coarse sedimentary rocks (Struik 1994; Logan et al. 2010).

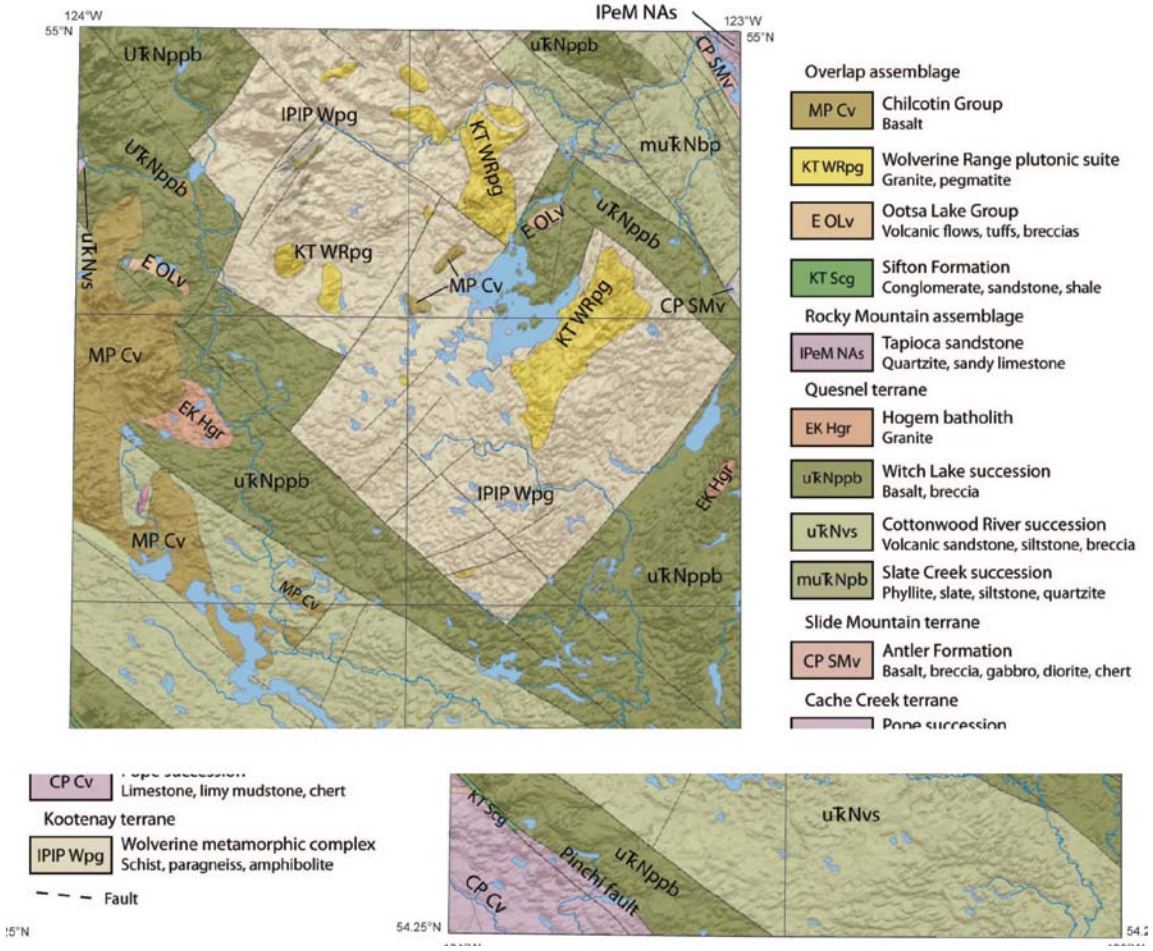

Figure 1.3 Bedrock geology of the study area (after Struik 1994 and Logan et al. 2010). DEM derived from CDED (Geobase.ca)

1.5. Thesis objectives

This thesis describes the glacial geology of a part of the McLeod Lake map-area (NTS 093J05/06/11/12/13/14) in central British Columbia (Fig. 1.1). The objectives are to:

1. Describe the nature and distribution of surficial materials and landforms.
2. Develop a stratigraphic framework.
3. Reconstruct the local ice-flow history.

4. Determine the local pattern and chronology of deglaciation.

These objectives were achieved through:

1. The production and analysis of 1:50 000-scale, terrain maps. NTS Map sheets 093J13 and 14 were produced by the author and the remaining four map sheets (NTS 093J05/06/11/12) by project collaborators.
2. The use of ground penetrating radar to characterize aeolian deposits and optical dating to determine their age and evaluate the timing of deglaciation.
3. The description and interpretation of Quaternary stratigraphic exposures.
4. The collection and collation of ice-flow data.
5. The interpretation of surficial material and landform distribution patterns to establish the style of deglaciation.

Chapter 2 reviews the development of the glacial concept in British Columbia and describes the regional stratigraphic framework and chronology, which provide the necessary background for the reconstruction of the regional glacial history. Chapter 3 focuses on the surficial geology of the study area. It explains the terrain mapping methods used to define and delineate map units and describes the surficial materials and landforms. Chapter 4 is an investigation of post-glacial aeolian deposits. Ground penetrating radar was used to characterize the landforms, and optical dating was used to determine the age of the deposits and provide a minimum age for deglaciation. Chapter 5 discusses the local stratigraphy and ice-flow history and the pattern and style of deglaciation. From these data a local glacial history is developed and used to modify the regional ice-flow model and present a refined conceptual model for deglaciation specific to the northern Interior Plateau of British Columbia. Chapter 6 briefly summarizes the main findings of the thesis and provides suggestions for further work. The terrain maps are included in the appendices along with additional GPR profiles and ice-flow data.

2. Regional stratigraphic framework

Several detailed studies have focused on the Quaternary stratigraphy of central British Columbia (e.g. Rutter 1977; Clague 1987, 1988; Bobrowsky and Rutter 1992), and a number of Quaternary geology investigations have been conducted to assist in mineral exploration (e.g. Levson et al. 1997; Plouffe 2000; Levson 2001). This chapter provides a review of relevant previous work focusing on the development of the glacial geology in central British Columbia and a regional glacial history that includes stratigraphy, chronology and ice-flow history.

2.1. Development of the glacial concept in central British Columbia

This section draws heavily from a thorough description of the early ideas of the CIS in Jackson and Clague (1991) and references therein. The initial suggestion that the Canadian Cordillera had once been extensively covered by glaciers was made by J.D. Dana as an explanation for the contrasting linear coastline of Oregon and Washington and the fjord-cut coast of northern North America (Dana 1849 *in* Jackson and Clague 1991). G.M. Dawson (1878, 1881, 1888) published the first data pertaining to Quaternary deposits and the glacial history of central British Columbia, proposing that a widespread glaciation had occurred. His initial theories suggested glaciers first developed in the north and extended south, contemporaneous with land subsidence beneath 1520 m of water (Dawson, 1878, 1881). Over the next decade, he furthered his concept with the idea that the "Cordilleran Glacier" had first accumulated in the northern Coast Mountains and the high ranges of the interior of British Columbia between the 55th and 59th parallel. He postulated that ice flowed outward in all directions, following the valleys, until it formed a great ice sheet that flowed southeast and northwest between the Coast and Rocky Mountains (Dawson 1888, 1889, 1891). Around the same time, R.G. McConnell was defining the northern limits of the CIS (McConnell, 1891) and T.C.

Chamberlin and R.D. Salisbury were defining the southern limits (Chamberlin 1886, 1888 *in* Jackson and Clague 1991). This information culminated into Chamberlin's "Ideal map of North America during the Ice Age" published by Geike in 1894.

Little was added to Dawson's body of research on the Cordilleran Glacier in the early 1900s. However, the effects of glaciation on the landscape were noted by government geologists during bedrock mapping (Jackson and Clague 1991). These data were synthesized by Kerr (1934) who proposed a model of glaciation in the Cordillera that was further refined by Davis and Mathews (1944). This four-phase model consists of: 1) the alpine phase, defined by the growth of alpine glaciers with movement controlled by topography; 2) the intense alpine phase, in which relief only slightly exceeds the thickness of ice; 3) the mountain ice sheet phase, defined by a continuous sheet of ice still controlled by topography; and 4) the continental ice sheet phase in which the ice-flows independently of topography (Fig. 2.1a, b, c, d). At that time, deglaciation was assumed to occur in the reverse order.

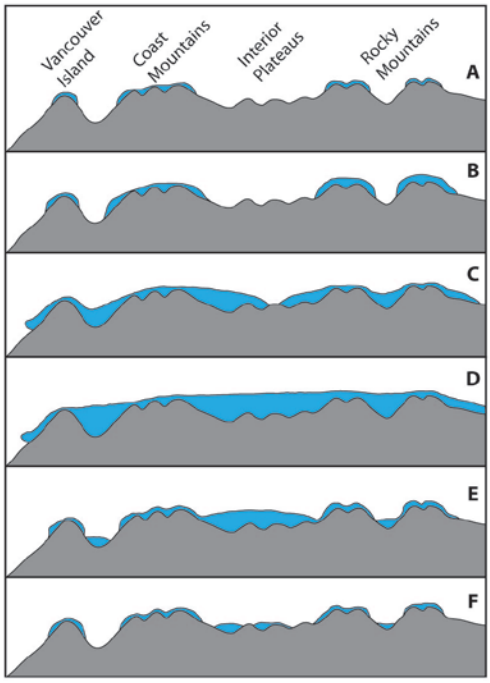

Figure 2.1 ***Conceptual model of the growth and decay of the Cordilleran Ice Sheet (modified from Clague 1989 and Fulton 1991). See text for description.***

Armstrong and Tipper (1948) interpreted glacial landforms from the first available aerial photographs of the region and applied the Davis and Mathews glaciation model to central British Columbia. They proposed that ice accumulated mainly in the Coast Mountains but also in the Cariboo and Omineca Mountains. At an early stage, flow was controlled by topography; in the Coast Mountains flow was easterly and westerly, and in the Cariboo and Omineca mountains flow was mainly northerly and southerly. As glaciation progressed, they envisaged ice coalescing over the Nechako Plateau and Nechako Plain as a large ice sheet that was still confined by topography and flowed dominantly west to east. During the maximum development of the Cordilleran ice sheet, ice moved across the Nechako Plateau in a northeasterly direction, independent of topography. Armstrong and Tipper (1948) were in agreement with previous authors (Dawson 1878, 1881, 1888, 1891; Kerr 1934) that at least two ice advances occurred in central British Columbia, though no evidence was presented to support this hypothesis. They suggested that the first advance only reached the mountain ice sheet phase. Ice flowed east across the Nechako Plateau and Nechako Plain depositing a mantle of till before retreating. During the second advance, the till mantle was rearranged into drumlin fields (previously mistaken as moraines by Dawson (1878)) that illustrate the dominant northeasterly ice flow of the continental ice sheet phase. The second advance was followed by a period of stagnation and decay, inferred from the presence of compound eskers and kettles and the lack of lateral or terminal moraines (Armstrong and Tipper 1948). These authors did not provide any evidence to disprove Dawson's theory of land subsidence beneath water, but did not believe that it was necessary to explain the glacial landforms they studied.

Armstrong and Tipper's (1948) idea of stagnation and decay over the moderate relief of the Nechako Plateau and Nechako Plain was further developed by Fulton (1967) over the Interior Plateau. He proposed a four-phase model of deglaciation for areas of moderate relief: 1) the active-ice phase; regional flow continues but diminishes as the elevation of the fern line rises; 2) the transitional upland phase; uplands begin to appear through the ice with minor regional flow continuing in valley glaciers still connected to the source; 3) the stagnant-ice phase; uplands divide the ice into a series of convex tongues that divert meltwater to the ice margins creating drainage features such as lateral overflow channels and kettled kame terraces; and 4) the dead-ice phase; stagnant ice

melts to a concave profile and englacial drainage creates hummocky gravels and eskers. The models of glaciation (Kerr 1934; Davis and Mathews 1944) and deglaciation (Fulton 1967) were later unified into one conceptual model of the growth and decay of the Cordilleran Ice Sheet (Clague 1989; Fulton 1991; Fig. 2.1).

2.2. Regional stratigraphy

Pleistocene and Pliocene glacial sediments have been reported in British Columbia (Hickson and Souther 1984; Souther et al. 1984; Mathews and Rouse 1986; Fulton et al. 1992; Lian et al. 1999; Hickson et al. 1995; Spooner et al. 1995; Spooner et al. 1996; Edwards et al. 2002; Kelman et al. 2002; Harder and Russell 2007). Many of the ages for these sediments have been obtained from mountainous regions and it is difficult to determine the extents of the glaciers. If these glaciations affected central British Columbia, most of the evidence has been either covered or removed by subsequent glaciations. Thus most sedimentary units have been assigned to the Late Pleistocene, which can be subdivided into the following geological-climatic units, from oldest to youngest: 1) penultimate glaciation ((?) early Wisconsinan); 2) Olympia nonglacial interval (middle Wisconsinan); 3) Fraser Glaciation (late Wisconsinan); and 4) post-glacial (Holocene) (Fig. 2.2.). Due to the limitations of dating techniques, it is difficult of confidently assign sedimentary units to the penultimate glaciation, thus they will be referred to as pre-Fraser Glaciation units.

The following description of the Pleistocene stratigraphy and chronology is subdivided per physiographic regions as defined by Holland (1976) (Fig. 2.3): 1) the central Interior Plateau, which comprises parts of the Fraser Plateau and the southern part of the Fraser Basin, and was affected by ice from the Cariboo and Coast Mountains (Tipper 1971a, b; Clague 1988, 1989, 1990); 2) the northern Interior Plateau, which generally comprises the Nechako Plateau, Nechako Plain and the northern part of the Fraser Basin, and was affected by ice from the Coast and Skeena Mountains (Tipper 1971a, b; Ryder and Maynard 1991; Levson and Giles 1997; Plouffe 1997, 2000; Stumpf et al. 2000); and 3) the northern Rocky Mountain Trench and southern Omineca Mountains, which were dominantly affected by ice from

the Omineca Mountains (Tipper 1971a, b; Rutter 1977; Ryder and Maynard 1991). For the locations of the discussed stratigraphic studies and radiocarbon ages and place names, refer to Fig. 2.4 and Tables 2.1 and 2.2.

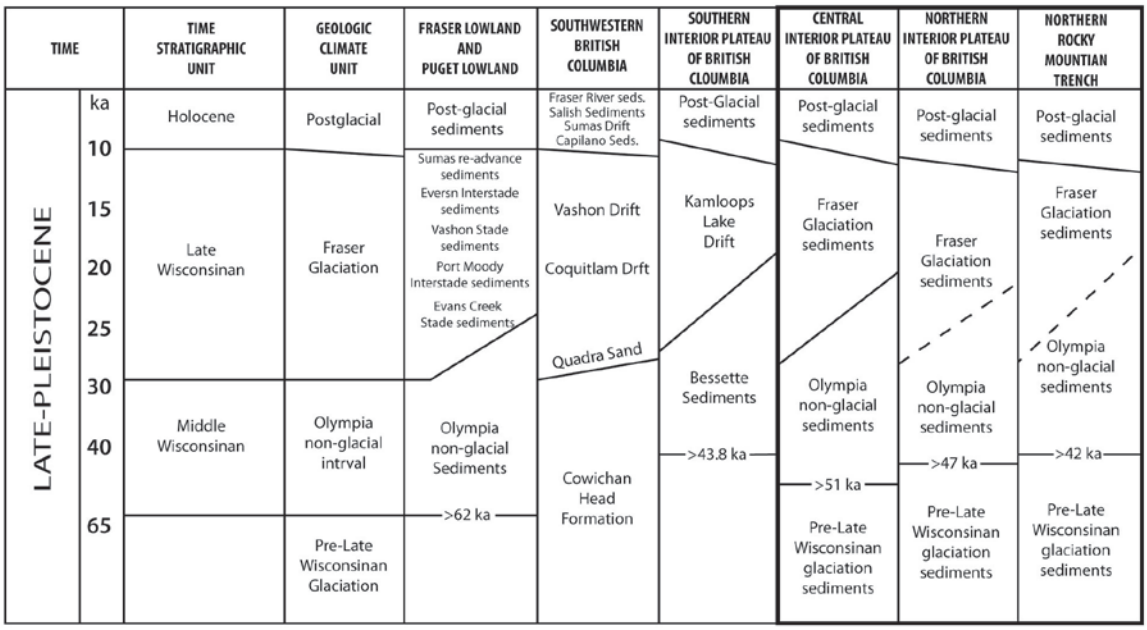

Figure 2.2 ***Late Pleistocene geologic-climate subdivisions and stratigraphic units in south and central British Columbia (compiled from Armstrong et al. 1965; Clague 1981; Stumpf et al. 2000; and modified with references listed in Fig. 2.1). Thick outline denotes regions encompassing the study area.***

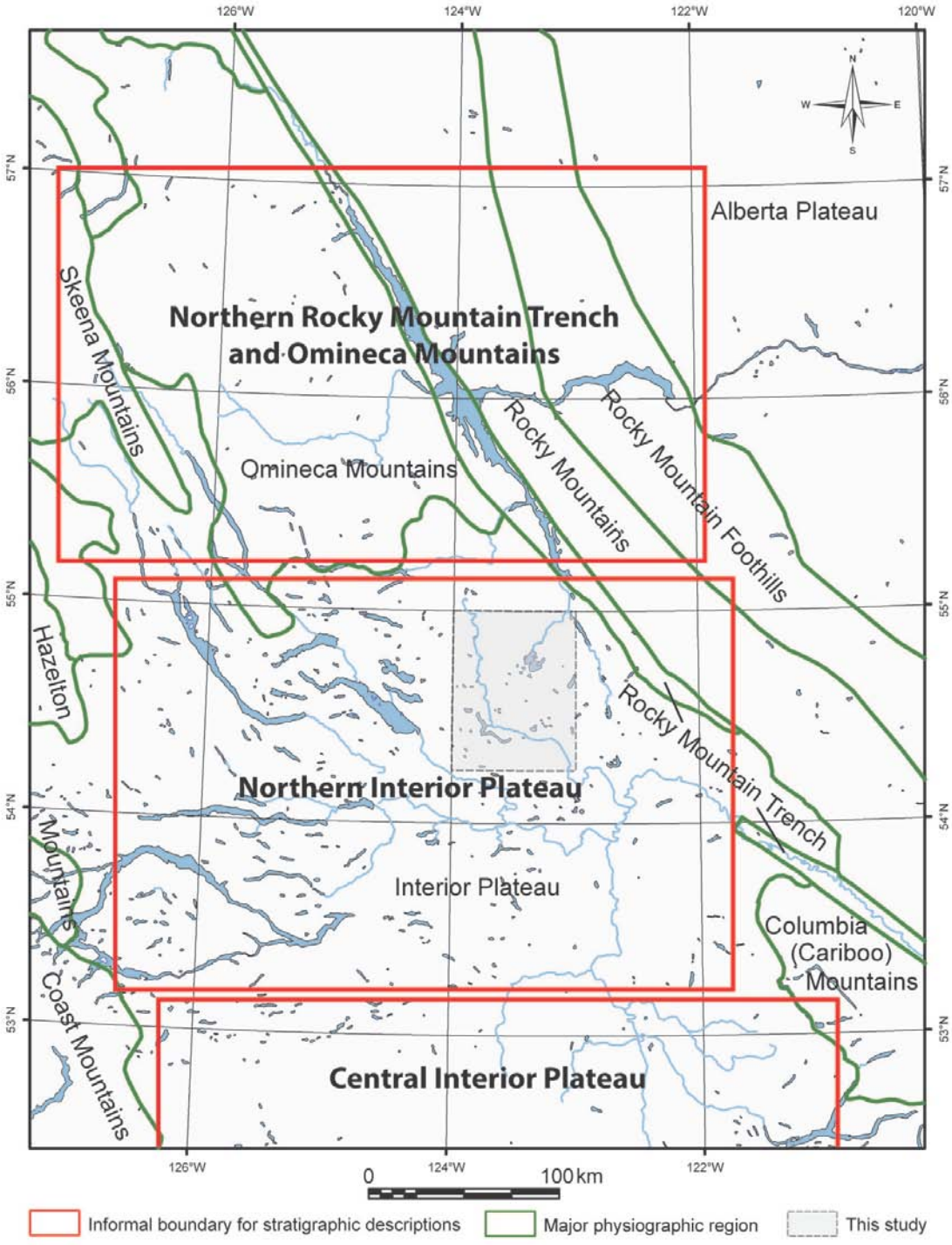

Figure 2.3 Informal division of the region based on physiographic region (Holland 1976) and source areas of ice cover. See text for description.

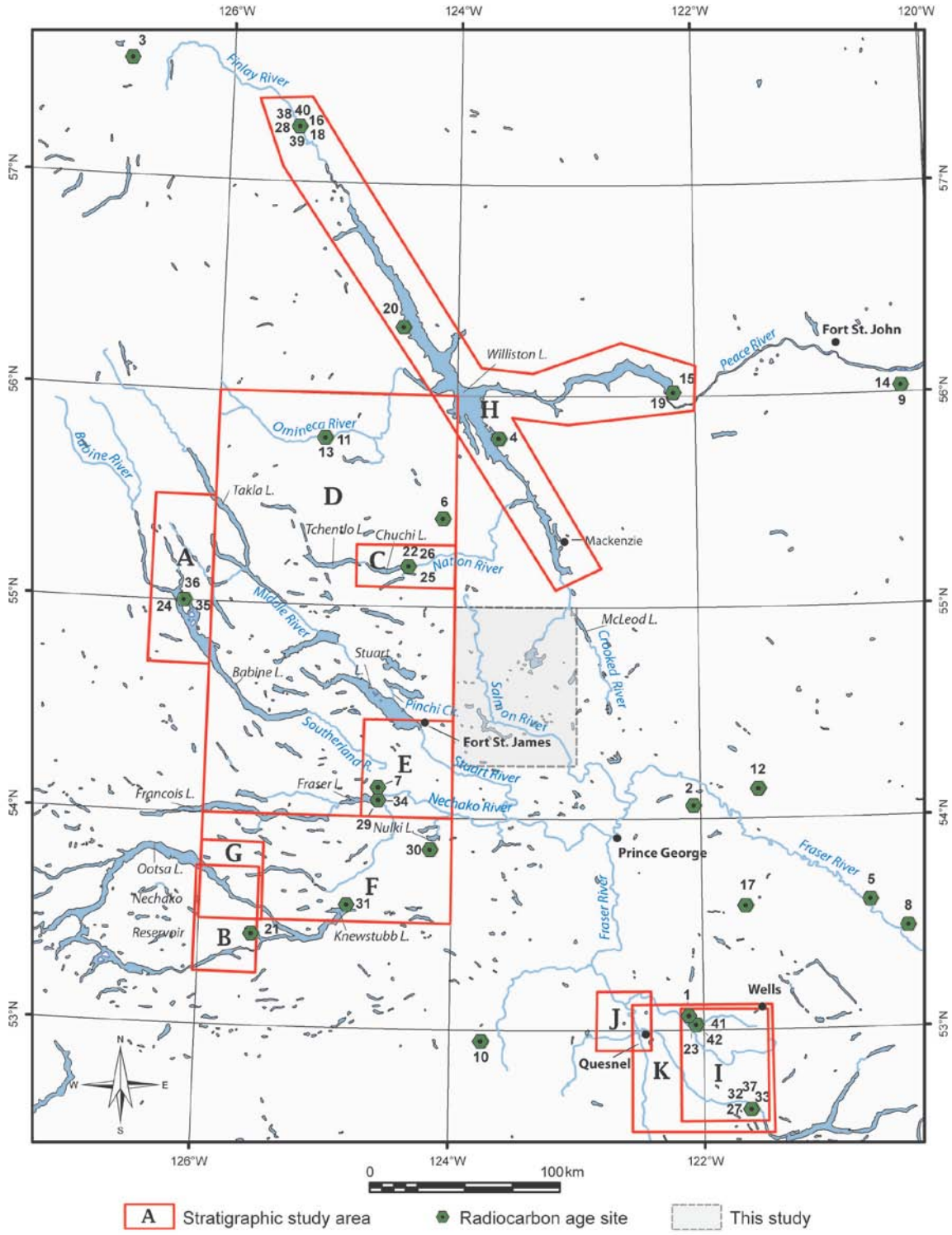

Figure 2.4 ***Locations of radiocarbon ages mentioned in the text (green symbols) and areas where stratigraphic information is reported (red boxes). See Table 2.1 for details on radiocarbon ages and Table 2.2 for references to stratigraphic information.***

Table 2.1 Holocene and Pleistocene radiocarbon ages for central British Columbia (site numbers correspond to locations on Fig. 2.4).

Site	Age (14C yr BP)	Locality	Location (UTM)	Zone	Sample number	Reference
1	8820 ± 80	Mary Creek	560114, 5880055	10	GSC-2974	Lowdon and Blake 1979
2	9117 ± 55	Aleza Lake	562247, 5990854	10	AA78463	Sanborn and Jull 2008
3	9180 ± 80	Cushing Lake	625073, 6385378	10	n/a	Lakeman et al. 2008
4	9280 ± 200	Finlay River	459775, 6184007	10	GSC-1497	Rutter 1977
5	9363 ±77	Morkill Lake	655321, 5942327	10	AA46035	Sanborn et al. 2006
6	9440 ± 110	Skunk Lake	430319, 6141989	10	GSC-5869	Plouffe 2000
7	9830 ± 130	Nautley River	396118, 6000514	10	GSC-5891	Plouffe 2000
8	9863 ± 77	Minnow Creek	675389, 5928525	10	AA46030	Sanborn pers. com. 2011
9	9960 ± 170	Peace River	671210, 6212993	10	GSC-1548	Rutter 1977
10	9990 ± 90	Nazco Cone	450055, 5866782	10	GSC-4116	Souther et al. 1987
11	10000 ± 140	Omineca Valley	368628, 6184920	10	GSC-2036-2	Blake 1986
12	10000 ± 90	Summit Creek	596354, 6000289	10	GSC-2964	Lowdon and Blake 1980
13	10100 ± 90	Omineca Valley	368628, 6184920	10	GSC-2036	Alley and Young 1978
14	10400 ± 170	Kiskatinaw River	671210, 6212993	10	GSC-1654	Rutter 1977
15	11600 ± 1000	Peace River	551695, 6208261	10	I-2244A	Rutter 1977
16	15180 ± 100	Finlay River	355072, 6348998	10	TO-708	Bobrowsky and Rutter 1992
17	19920 ± 130	Bowron Valley	593274, 5927284	10	AA44045	Ward et al. 2008
18	23280 ± 750	Finlay River	355072, 6348998	10	AECV-351C	Bobrowsky and Rutter 1992
19	25800 ± 320	Peace River	551355, 6208360	10	GSC-2859	Rutter 1977
20	25940 ± 380	Williston Lake	409788, 6242873	10	GSC-573	Rutter 1977
21	27790 ± 200	Chelasie Arm	328666, 5924162	10	Beta-101017	Levson et al. 1998
22	30740 ± 220	Nation River	412094, 6116959	10	TO-3653	Harington et al. 1996
23	32020 ± 600	Mexican Hill	563717, 5875474	10	TO-532	Clague et al. 1990
24	34000 ± 690	Babine Lake	677099, 6098496	9	GSC-1754	Harington et al. 1974
25	34800 ± 420	Nation River	412094, 6116959	10	CAMS 17566	Harington et al. 1996
26	35480 ± 1080	Nation River	412094, 6116959	10	Beta-78574	Harington et al. 1996
27	36840 ± 430	Bullion Pit	592850, 5831254	10	TO-392	Clague et al. 1990
28	37190 ± 2870	Finlay River	355072, 6348998	10	AECV-353C	Bobrowsky and Rutter 1992
29	38230 ± 410	Nautley River	396027, 5993941	10	Beta-88557	Plouffe and Jette 1997
30	38600 ± 520	Corkscrew Creek	423367, 5967762	10	Beta-125677	Plouffe and Levson 2001
31	39040 ± 530	Knewstubb Lake	375986, 5936400	10	Beta-101016	Plouffe and Levson 2001
32	41500 ± 1740	Bullion Pit	592850, 5831254	10	GSC-4124	Clague et al. 1990
33	42000 ± 2010	Bullion Pit	592850, 5831254	10	GSC-4334	Clague et al. 1990

Site	Age (14C yr BP)	Locality	Location (UTM)	Zone	Sample number	Reference
34	42460 ± 670	Nautley River	396027, 5993941	10	Beta-88558	Plouffe and Jette 1997
35	42900 ± 1860	Babine Lake	677099, 6098496	9	GSC-1657	Harington et al. 1974
36	43800 ± 1830	Babine Lake	677099, 6098496	9	GSC-1687	Harington et al. 1974
37	46300 ± 940	Bullion Pit	592850, 5831254	10	GSC-4411HP	Clague et al. 1990
38	> 28000	Williston Lake	354640, 6348449	10	GSC-1057	Rutter 1977
39	> 41000	Williston Lake	354640, 6348449	10	GSC-841	Rutter 1977
40	> 44000	Williston Lake	354640, 6348449	10	GSC-837	Rutter 1977
41	>40000	Mexican Hill	563717, 5875474	10	GSC-4383	Clague et al. 1990
42	>51000	Mexican Hill	563717, 5875474	10	GSC-4611HP	Clague et al. 1990

Table 2.2 References to Pleistocene stratigraphic studies in central British Columbia (site letters correspond to locations on Fig. 2.4).

Site	Reference	Locality
A	Levson 2001	93L15, 93M01/08
B	Levson et al. 1998	93F05/12
C	Plouffe 1992	93N01/02
D	Plouffe 2000	93K, 93N
E	Plouffe and Jette 1997	93k01/02/07/08
F	Plouffe and Levson 2001	93F09-16
G	Mate and Levson 2001	93F12/13
H	Rutter 1977; Bobrowsky and Rutter 1992	Williston Reservoir/Finlay and Peace rivers
I	Clague 1990	93A11-14, 93B09/16, 93G01, 93H03/04
J	Clague 1988	93B15, 93G02
K	Levson et al. 1990	93A11-14, 93B09/16, 93G01, 93H03/04

2.2.1. Central Interior Plateau

This section summarizes studies along the Fraser River and its tributaries in the Quesnel area (Clague, 1988; Clague et al. 1990), and in placer deposits in the Ballarat Mine, located about 5 km southwest of Wells in the Cariboo Mining District (Levson et al. 1990; Fig. 2.4). The investigated stratigraphic exposures occur mostly in the southern arm of the Fraser Basin with one in the adjacent Fraser Plateau.

Sediments of a pre-Fraser glaciation

Stratified drift sequences of Early Wisconsinan or older age, which comprise advance glacial sediments, till and retreat glacial sediments have been identified at several locations along the Fraser River and its tributaries (Clague 1988; Clague et al. 1990). At one location along the Fraser River, the lower drift sequence consists of three till units separated by oxidized gravels. The oxidized gravels may represent paleosols, which would indicate that the tills record more than one glacial event, although further investigation is necessary to verify this (Clague 1988). Alternatively, the oxidation may be due to normal groundwater processes during the middle Wisconsinan and the till units may have been deposited during oscillations of the ice margin during a single pre-Fraser glacial event. At both Bullion Pit, located about 60 km southeast of Quesnel, and Mexican Hill, located about 30 km east of Quesnel, pre-Fraser drift sequences are identified based on their stratigraphic location below sediments of the Middle Wisconsinan (Clague et al. 1990).

Sediments of the Olympia nonglacial interval

Several Middle Wisconsinan fluvial, lacustrine and colluvial units have been identified in the southern Fraser Basin and adjacent Fraser Plateau. At the Ballarat Mine, a gold-bearing fluvial unit was deposited in a bedrock channel incised prior to the last glaciation (Levson et al. 1990). At Bullion Pit, interbedded peat and organic rich silt between drift sequences contained twigs and small branches that yielded radiocarbon ages ranging from 46 300 ± 1740 ^{14}C yr BP (GSC-4411HP) to 36 840 ± 430 ^{14}C yr BP (TO-392) (Clague et al. 1990). At Mexican Hill, twigs collected from silt and sand beds above the lower till yielded radiocarbon ages of >51 000 ^{14}C yr BP (GSC-4611HP), >40 000 ^{14}C yr BP (GSC-4383) and 32 020 ± 600 ^{14}C yr BP (TO-532) (Clague et al. 1990). These ages are minimums for the time of deposition for the underlying glacial deposits and loosely constrain the age of the enclosing sediments. The range in ages from non-finite to finite from samples from the same beds either implies reworking of material or contamination; Clague et al. (1990) suggested the youngest results, 36 840 ± 430 and 32 020 ± 600 ^{14}C yr BP, should be considered minimum ages.

Sediments of the Fraser Glaciation

Advance-phase sediments in the Fraser Basin include glaciofluvial gravels and glaciolacustrine clay, silt, sand and diamict. Glaciofluvial gravels are commonly at the base, but the sequences are dominated by glaciolacustrine sediments and overlain by a single unit of till. Stratigraphic exposures along the Fraser River contain thick glaciolacustrine units containing discontinuous subaqueous debris flow deposits (Clague 1988). At the Ballarat Mine, glaciofluvial gravel is overlain by deltaic gravel with interbedded debris flow deposits (Levson et al. 1990). These advance sediments are undated. However, willow twigs collected from a lacustrine unit in the Bowron River Valley to the north yielded a radiocarbon age of 19 920 ± 130 ^{14}C yr BP (AA44045; Ward et al. 2008), which provides a maximum limiting age for overriding by northerly flowing ice out of the nearby Cariboo Mountains. The till can be similar to underlying diamicts deposited in advance glacial lakes, but it typically has a higher clast content and lacks stratification (Clague 1988). The till is generally thin and discontinuous in valleys, contrasting with the more continuous blanket that mantles much of the Interior Plateau outside of these valleys (Tipper 1971a, b; Clague 1988).

A thick unit of retreat glaciolacustrine sediment commonly overlies till at lower elevations in the Fraser Basin (e.g. Clague 1988; Clague et al. 1990). In Fraser River exposures near Quesnel, a complex of silt, sand, gravel and diamict gradationally transitions into rhythmically bedded clay and silt (Clague 1988). Thermoluminescence dating was used to determine the age of clay and silt couplets and yielded apparent ages of 12.8 ± 1.8 ka (QNL84-3, 12) and 13.7 ± 2.3 ka (QNL84-3, 5W) (Berger et al. 1987). At higher elevations in the Fraser Basin, till is exposed at the surface or is overlain by glaciofluvial deposits.

2.2.2. Northern Interior Plateau

Knowledge of the Quaternary stratigraphy of the northern Interior Plateau is based on studies at numerous widely spaced sites in large valleys where thick sediments have been incised by post-glacial processes (e.g. Plouffe and Jette 1997; Levson et al. 1997; 1998; Plouffe 2000; Plouffe and Levson 2001a; Fig.2.4).

Sediments of unknown age

At Swanson Creek, about 20 km north of Knewstubb Lake, two stratigraphic exposures contain units of unknown age (Plouffe and Levson 2001a). At one exposure, a massive, compact and oxidized diamict is overlain by sand, pebble gravel and a second diamict. Both diamicts have a northeast-to-southwest clast fabric orientation and are interpreted to be till. The upper till is Late Wisconsinan in age, but it is unknown if the lower till was deposited during an oscillation of the ice front in the same event or during a separate, earlier glaciation. At the second exposure, a gravel unit is overlain by a crudely stratified, compact diamict with abundant striated clasts, which in turn is overlain by deposits of the Fraser Glaciation. Both the gravel and diamict are heavily oxidized and thought to have been weathered during a nonglacial interval prior to the Late Wisconsinan. It is unknown whether the lower sediments are nonglacial fluvial and debris flow deposits (Middle Wisconsinan), or advance glaciofluvial material and till (pre-Fraser Glaciation).

Sediments of a pre-Fraser glaciation

Till units from the Early Wisconsinan or an earlier glaciation are exposed at two sites. At a site along the Necoslie River, a diamict is interpreted to be till as indicated by its poorly sorted nature, massive character, compaction, and striated clast content. The till is overlain by organic-bearing alluvium that was deposited during the Middle Wisconsinan (Plouffe and Jetté 1997). At Ootsa Lake, a sandy, clayey silt diamict with moderate to high density and jointing is interpreted to be till. The till is overlain by a Middle Wisconsinan organic-bearing lacustrine unit (Mate and Levson 2001).

Sediments of the Olympia nonglacial interval

Sediments of the Olympia nonglacial interval are found beneath Late Wisconsinan sediments locally in the northern Interior Plateau. At Babine Lake, Harington et al. (1974) report about 6 m of finely bedded to massive silt, overlain by sediments of the Fraser Glaciation. Twigs from the silt yielded radiocarbon ages of 42 900 ± 1860 ^{14}C yr BP (GSC-1657) and 43 800 ± 1830 ^{14}C yr BP (GSC-1687), and bone collagen from a mammoth anterior rib yielded a radiocarbon age of 34 000 ± 690 ^{14}C yr BP (GSC-1754). Harington et al. (1974) suggest that the bones were intruded from above, resulting in the younger age than that of the enclosing sediment. Parallel-laminated silt and trough

cross-laminated fine sand are overlain by advance glaciolacustrine sediments in the Babine River valley (Levson 2001). Pollen assemblages similar to those of the aforementioned mammoth site and other units of the Olympia nonglacial period suggest that they could be contemporaneous (Harington et al. 1974; Plouffe and Jetté 1997; Levson 2001).

On the shores of Chelaslie Arm in Nechako Reservoir, a thick sequence of lacustrine deposits is overlain by advance glaciolacustrine, glaciofluvial and till of the Fraser Glaciation (Levson et al. 1998). The lacustrine unit contains fine organic detritus that yielded a radiocarbon age of 27 790 ± 200 ^{14}C yr BP (Beta-101017).

Olympia nonglacial sediments have been described at Knewstubb Lake and south of Nulki Lake on Corkscrew Creek (Plouffe and Levson 2001a). At Knewstubb Lake, fluvial or lacustrine fine sand and silt are overlain by deposits of the Fraser Glaciation. Charcoal from this unit yielded a radiocarbon age of 39 040 ± 530 ^{14}C yr BP (Beta-101016). At Corkscrew Creek, pebbly sand diamict is overlain by clay and parallel and cross-laminated sand. The diamict has been interpreted to be debris flow deposits; the clay was deposited in ponded water, and the sand was deposited in a fluvial environment. The sand contains plant material that yielded a radiocarbon age of 38 600 ± 520 ^{14}C yr BP (Beta-25677).

Olympia nonglacial sediments were also identified at three sites in the Fort Fraser (NTS 093K) and Manson River (NTS 093N) map-areas (Harington et al. 1996; Plouffe and Jetté 1997; Plouffe 2000). At Chuchi Lake, a unit of rhythmically laminated silt and clay containing twigs and bison bones is overlain by sediments of the Fraser Glaciation (Harington et al. 1996; Plouffe 2000). The bison bones yielded radiocarbon ages of 30 740 ± 220 ^{14}C yr BP (TO-3653), 34 800 ± 420 ^{14}C yr BP (Beta-78573; CAMS-17566), and 35 480 ± 1080 ^{14}C yr BP (Beta-78574) (Harington et al. 1996). The twig yielded an age of 55 260 ± 2960 (TO-4785); however the reliability of this age has been questioned (see Plouffe 2000 for discussion). At Nautley River, west of Fraser Lake, a sandy unit containing plant fragments is overlain by sediments of the Fraser Glaciation (Plouffe and Jetté 1997; Plouffe 2000). This unit contains twigs that yielded radiocarbon ages of 38 230 ± 410 ^{14}C yr BP (Beta-88557) and 42 460 ± 670 ^{14}C yr BP (Beta-88558) (Plouffe and Jetté 1997). A unit of sand, silt and minor clay occurs along the Necoslie River (Plouffe

and Jetté 1997). No datable organic material was found in this unit; however, pollen assemblages are similar to other Middle Wisconsinan aged sites (Harington et al. 1974; Plouffe and Jetté 1997). Both the Necoslie and Nautley river middle Wisconsinan sediments are interpreted to be fluvial overbank deposits (Plouffe and Jetté 1997; Plouffe 2000).

Sediments of the Fraser Glaciation

Late Wisconsinan stratigraphic exposures at the lower elevations of the Nechako Plateau typically include a continuous mantle of till, bounded above and below by stratified glaciofluvial and glaciolacustrine deposits (e.g. Levson et al. 1997; Plouffe 1997, 2000; Levson 2001). In the upland areas, localized advance glaciofluvial and glaciolacustrine sediments are typically overlain by till and localized retreat glaciofluvial sediment (e.g. Plouffe 2000; Plouffe and Levson 2001a).

In the Babine River Valley, nearly 20 m of advance glaciolacustrine silt and clay are overlain by glaciofluvial sand and gravel (Levson 2001). In the nearby Dust Creek tributary, about 5 m of glaciolacustrine silt and clay are overlain by a prograding deltaic sequence of sand and gravel nearly 20 m thick (Levson 2001). Similarly, both advance glaciofluvial and glaciolacustrine sediments are reported below Fraser till north and west of Chuchi Lake and in the Sutherland River valley (Plouffe 2000). Stratigraphic exposures containing only glaciofluvial advance sediments occur at Knewstubb Lake and Swanson Creek (Plouffe and Levson 2001a) and north of Tchentlo Lake (Plouffe 2000).

Most stratigraphic exposures in the Nechako Plateau contain only one Fraser Glaciation till, although two sites have been identified that contain multiple diamicts that are tentatively interpreted as tills (Plouffe 2000). At Babine Lake, two diamicts that contain abundant striated and faceted clasts are separated by glaciofluvial sediments. Both diamicts are assigned to the Fraser Glaciation because there is no difference in the degree of weathering of the two units and there are no signs of paleosol development in the intervening gravel. It is possible that one of these units could be a debris flow deposit (Plouffe 2000). At Pinchi Creek, three diamict units have been interpreted as tills. The lowest till is highly compacted and overlain by a looser till that contains sand lenses. A glaciolacustrine unit separates the lower tills from the upper till, which has a

notably lower clast content, and contains a higher clay fraction. The lower unit is suggested to be a lodgement till based on its compaction, and the overlying unit is interpreted as a melt-out till because of the sand beds (Plouffe 2000). The upper till was deposited during an oscillation of the ice front and the low clast content and high clay fraction is attributed to the incorporation of the underlying glaciolacustrine material. The upper till was termed the Pinchi Creek lens by Plouffe (2000) and has only been observed at the southeast end of Stuart Lake to an elevation of approximately 730 m.

Retreat-phase glaciofluvial deposits, including local stagnant ice deposits, single and complex esker systems and outwash plains, occur throughout the region and are shown on surficial maps of the area (e.g. Mate and Levson 2000; Plouffe 2000; Plouffe and Levson 2001b, 2002). In low-lying regions, such as the valleys now occupied by Takla and Babine lakes, the advance glaciofluvial and glaciolacustrine sediments and till is capped by thick glaciolacustrine units of clay, silt and diamicts (Levson et al. 1997; Levson 2001). Similarly, glaciolacustrine deposits occur at the surface in the Omineca, Nation, Middle, Stuart, Necolsie and Nechako river valleys (Plouffe and Jetté 1997; Plouffe 2000).

2.2.3. Northern Rocky Mountain Trench and Omineca Mountains

Construction of the WAC Bennett dam in the 1960s created the Williston Lake Reservoir that now covers a significant portion of the Peace, Parsnip and Finlay rivers. Stratigraphic data are presented here from studies conducted prior to the flooding of the reservoir (Rutter 1977), and in further investigations during the 1980s (Bobrowsky and Rutter 1992). In addition, stratigraphic data are presented from the Omineca River and its tributaries (Plouffe 2000; Fig. 2.4).

Sediments of unknown age

The oldest sediments in the region, located in the Finlay River valley, are oxidized fluvial gravels that locally contain diamict blocks. Wood and peat from the gravels yielded non-finite radiocarbon ages of >28 000 ^{14}C yr BP (GSC-1057), >41 000 ^{14}C yr BP (GSC-841; peat) and > 44 000 ^{14}C yr BP (GSC-837) (Rutter 1977). These sediments were likely deposited during the nonglacial period prior to the penultimate glaciation based on the presence of overlying glacial sediments that are attributed to the Early Wisconsinan

(Rutter 1977). The diamict blocks within the oxidized gravels are interpreted as till rip-ups that may be remnants of a pre-Early Wisconsinan glaciation (Rutter 1977).

Sediments of a pre-Fraser glaciation

Rutter (1977) reports a glacial sequence consisting of advance glaciofluvial gravels overlain by till and retreat glaciofluvial and glaciolacustrine sediments below Fraser Glaciation sediments along the Finlay River. Bobrowsky and Rutter (1992) tentatively assign the lower glacial sediments to the Early Wisconsinan, although it is possible that they were deposited during an earlier glaciation.

Sediments of the Olympia nonglacial interval

The Fraser and pre-Fraser glacial sequences in the Finlay River valley are separated by up to 20 m of fluvial sand and gravel (Rutter 1977; Bobrowsky and Rutter 1992). A series of radiocarbon ages ranging from 37 190 ± 2870 ^{14}C yr BP (AECV-353C) to 15 180 ± 100 ^{14}C yr BP (AEVC-350C) were obtained from this unit (Bobrowsky and Rutter 1992).

Sediments of the Fraser Glaciation

The Fraser glacial sequence in much of the Finlay, Parsnip and Peace river valleys consists of advance glaciofluvial gravels overlain by glaciolacustrine silt, sand and diamict. A till unit of variable thickness and continuity overlies the advance sediments and is locally overlain by glaciolacustrine silt, clay and diamict and glaciofluvial sand and gravel (Rutter 1977). Several diamict units associated with the Fraser Glaciation are laterally continuous and in some areas were initially interpreted as till (e.g. Deserters Canyon and Portage Mountain tills; Rutter 1977). Subsequent facies analysis and improved chronologic resolution indicate that these units are colluvial and only one till from the Fraser Glaciation is present in the Williston Lake Reservoir (Bobrowsky and Rutter 1992).

In the Germansen River valley, south of the Omineca River, four diamicts are separated by glaciofluvial sand and gravel and glaciolacustrine silt and sand (Plouffe 2000). The diamicts are matrix-supported, compact, contain abundant striated and faceted clasts and extend across the width of the exposures. Clast fabrics measured from the diamicts

are unimodal and bimodal suggesting that the diamicts could all be tills (Plouffe 2000). In an adjacent valley, two diamicts are interpreted as till based on their sorting compaction and abundance of striated clasts; however, it is possible that one of the two could be a debris flow deposit (Plouffe 2000).

2.3. Regional glacial history

2.3.1. A pre-Fraser glaciation

Evidence of at least two glaciations is present in the regional stratigraphy. Pre-Fraser glacial sediments are typically only preserved in valleys where they were protected from erosion during subsequent glaciations. In the Fraser River valley, pre-Fraser Glaciation till units are >51 000 ^{14}C yr BP (GSC-4611HP) (Clague et al. 1990). Northwest-trending clast fabrics from these units indicate that the ice flow pattern was similar to that of the Fraser Glaciation (Clague 1988). In the northern Interior Plateau, pre-Fraser glacial sediments are older than 43 800 ± 1830 ^{14}C yr BP (GSC-1687; Babine Lake) (Harington et al. 1974), 39 040 ± 530 ^{14}C yr BP (Beta-101016; Knewstubb Lake) (Plouffe and Levson 2001) and 42 460 ± 670 ^{14}C yr BP (Beta-88558; Nautley River) (Plouffe and Jette 1992). In the northern Rocky Mountain Trench and Peace River Valley, Bobrowsky and Rutter (1992) suggest that the penultimate glaciation was more extensive than the Fraser Glaciation and involved far western-derived ice that crossed the Rocky Mountain Trench and deposited erratics at high elevations in the Rocky Mountains. A radiocarbon age of 37 190 ± 2870 ^{14}C yr BP (AECV-353C) provides an age for a fluvial unit on the Finlay River and loosely constrains the timing of deglaciation of the penultimate event.

2.3.2. Fraser Glaciation

The description of the Fraser Glaciation is presented here in three sections, after Stumpf et al. (2000); 1) the ice-expansion phase; 2) the glacial maximum; and 3) the late-glacial phase.

During the ice-expansion phase, ice sourced in the Pacific Ranges of the Coast Mountains flowed northeast across the Central Interior (Clague 1988, 1989; Stumpf et al.

2000), while ice from the Cariboo Mountains flowed north and west (Clague 1988; Paulen and Bobrowsky 2000). Assuming that ice flowed out of the Bowron Valley contemporaneously with ice moving across the Fraser Plateau, the area was covered sometime after 19 920 ± 130 ^{14}C yr BP (AA44045) (Ward et al. 2008). River valleys in the Quesnel area were dammed by the advancing glaciers, forming a lake of unknown areal extent (Clague 1988). This lake was at least 180 m deep and it persisted long enough for valleys in the area to become completely infilled. The ponding likely destabilized valley walls causing slumps and subaqueous debris flows (Clague 1988). A similar situation is envisaged by Levson et al. (1990) at the Ballarat Mine where advancing ice impounded a lake in which deltaic gravels were deposited and debris flows occurred. This ponding was probably not as extensive as in the Fraser Valley and the debris flows were likely caused by a reduction in vegetative cover associated with glacial conditions.

In the Northern Interior, ice advanced southward from the Skeena Mountains down the Talka and Babine river valleys and from the Omineca Mountains into the northern part of the Nechako Plateau (Tipper 1971a; Plouffe 1997; Stumpf et al. 2000; Levson 2001), while ice from the Kitimat Ranges of the Coast Mountains flowed eastward across the southern part of the Nechako Plateau (Plouffe 1997, 2000; Plouffe and Levson 2001a). Advance glaciolacustrine deposits in the Babine River valley and adjacent Dust Creek valley indicate that southeastward drainage was blocked by advancing ice from the Omineca Mountains prior to being overrun by ice from the Hazelton and Skeena mountains (Levson 2001). This timing of advance is constrained by a radiocarbon age of 34 000 ± 690 ^{14}C yr BP (GSC-1754) obtained from Middle Wisconsinan sediments at Babine Lake (Harington et al. 1974). Multiple tills in the Babine Lake valley may have been deposited during local oscillations of the ice margin at the onset of glaciation (Plouffe 2000). Valley-parallel striations in the Ootsa Lake region and sedimentological evidence in Francois Lake valley and Nechako Reservoir indicate that trunk glaciers from the Kitimat Ranges first occupied these valleys and flowed parallel to them (Levson et al. 1998; Mate and Levson 2001). As the trunk glaciers advanced into these large east-draining valleys, thick glaciofluvial units were deposited and small glacial lakes developed in their tributaries (Mate and Levson 2001; Plouffe and Levson 2001a). At several locations in these large valleys, glaciolacustrine sediment overlies the advance

glaciofluvial material, implying that drainage was blocked by sediment or advancing ice from another source (Mate and Levson 2001; Plouffe and Levson 2001a). The timing of ice advancing over the Nechako Reservoir area is constrained by a radiocarbon age of 27 790 ± 200 ^{14}C yr BP (Beta-101017) from Middle Wisconsinan sediments on Chelasie Arm (Levson et al. 1998).

Ice from the Omineca Mountains flowed eastward and entered the northern Rocky Mountain Trench and flowed southeast down the trench (Ryder and Maynard 1991; Plouffe 2000). Multiple till units in the Germansen River area suggest that several oscillations of the ice front occurred in this region during the advance phase of the Fraser Glaciation (Plouffe 2000). A minimum radiocarbon age of 15 180 ± 100 ^{14}C yr BP (AEVC-350C) from a fluvial unit in the northern Finlay River valley suggests that this area was not covered by ice before this time (Bobrowsky and Rutter 1992). When the ice advanced south past the Peace River, a glacial lake developed against the margin due to the obstruction of northward drainage.

With continued climate deterioration, ice coalesced over the interior of British Columbia. On the Fraser Plateau and the southern Fraser Basin, westerly flowing ice from the Cariboo Mountains was deflected to a more northerly direction by ice from the southern Coast Mountains (Tipper 1971a; Clague 1988; Paulen and Bobrowsky 2000). In the eastern parts of the Nechako Plateau and the northern parts of the Fraser Basin, easterly flowing ice from the Kitimat Ranges and Hazelton Mountains was deflected to the northeast by ice moving across the Fraser Plateau (Plouffe 1997, 2000).

At the glacial maximum, ice flowed independently of topography and was controlled mainly by ice divides over the interior (Tipper 1971a, b; Stumpf et al. 2000). The maximum phase is marked by an eastward shift of a glacial divide from the northern Coast Mountains over the Nechako Plateau (Levson et al. 1998; Stumpf et al. 2000; Fig. 2.5). Reversal of ice-flow indicators in the Skeena, Hazelton and parts of the Coast Mountains indicate the divide shifted east of Babine Lake valley, extending southward into the Ootsa Lakes area (Levson et al. 1998; Stumpf et al. 2000; Fig. 2.5) and possibly northward over the northern Skeena Mountains (Ryder and Maynard, 1991). In general, ice flow at the glacial maximum was easterly across the western Nechako Plateau and southern Omineca Mountains, northeasterly over the northern parts of the Fraser Basin,

the northeastern part of the Nechako Plateau and the Nechako Plain, and northerly over the southern parts of the Fraser Basin (Tipper 1971a, b; Clague 1988; 1989; Ryder and Maynard 1991; Levson and Giles 1997; Plouffe 1997, 2000; Stumpf et al. 2000; Fig. 2.5). Ice covered all of central British Columbia and at this latitude reached an eastern extent at or just beyond the Portage Mountain end moraine in the Peace River valley (Rutter 1977; Bobrowsky and Rutter 1992; Hartman and Clague 2008). The moraine consists of deltaic deposits that developed in a lake occupying the Peace River valley that was probably dammed by Laurentide ice (Rutter 1977; Mathews 1980; Bobrowsky and Rutter 1992, Hartman and Clague 2008). The constraining dates for the Fraser Glaciation in the Williston Lake area suggest that ice cover only lasted for about 5 ka. Bobrowsky and Rutter (1992) proposed that the local glacial maximum was topographically controlled, with ice locally sourced from the nearby Omineca Mountains. However, Bednarski and Smith (2007) provided evidence for ice flow independent of topography at the summits of the Rocky Mountains east of Finlay River; their interpretation suggests more extensive ice cover than Bobrowsky and Rutter. This difference of opinion has yet to be resolved.

During the late-glacial phase, climate amelioration triggered rapid downwasting and thinning of the CIS (Clague 1989; Fulton 1991; Stumpf et al. 2000). In the central Interior Plateau, ice retreated toward the south and separated into valley tongues and masses of dead ice that blocked drainage in major valleys (Tipper 1971a, b; Clague 1988; Plouffe 2000). During this period, glacial Lake Fraser developed in the Fraser Basin (Clague 1987, 1989). Glacial Lake Fraser may have been a single water body or a complex of lakes whose extents and styles of sedimentation where influenced by the location of the ice front. A complex of sand, gravel and diamict was deposited in ice-proximal lakes and transition upward into clay and silt beds deposited when the ice front retreated south of Quesnel (Clague 1988; Eyles and Clague 1991; Plouffe 1997, 2000). Thermoluminescence ages of 12.8 ± 1.8 and 13.7 ± 2.3 ka from these distal glacial lake sediments (Berger et al. 1987) are in general agreement with local minimum deglacial radiocarbon ages of 10 000 ± 90 ^{14}C yr BP (GSC-2964) (Lowdon and Blake 1980) from wood from a stoney clay overlying till; 9990 ± 90 ^{14}C yr BP (GSC-4116) (Souther et al. 1987) from the Nazco Cone, west of Quesnel; and 9863 ± 77 ^{14}C yr BP (AA46030) (P. Sanborn pers. comm. 2011) from basal peat near the upper reaches of the Fraser River.

In the northern Interior Plateau, westerly ice-flow indicators suggest that the glacial divide persisted east of the Skeena and Hazelton Mountains throughout much of the deglacial period (Stumpf et al. 2000). Westerly ice-flow probably continued along valleys

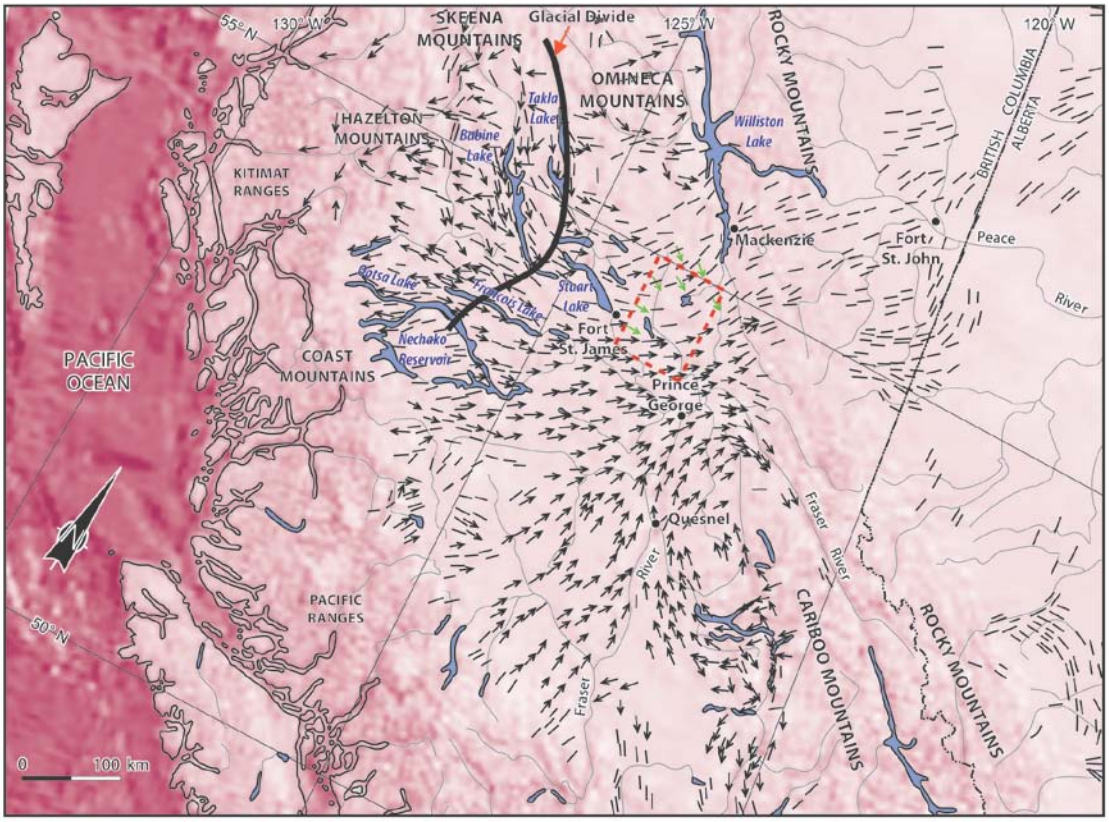

Figure 2.5 Flow directions of glaciers during the Fraser Glaciation. The glacial maximum is marked by the eastward shift of the ice divide (thick black line) from the Coast Mountains to the Nechako Plateau (study area indicated by red dashed box; figure modified from Stumpf et al. 2000 with data from this study (green symbols)).

in the Coast Mountains until the surface of the ice sheet dropped below the elevation of the mountain passes (Stumpf et al. 2000). Deglaciation in the northern Interior Plateau occurred dominantly through frontal retreat in a west to southwest direction, with local ice-flow directions becoming increasingly controlled by topography as the ice thinned (Tipper 1971a, b; Plouffe 2000; Stumpf et al. 2000; Levson 2001). The ice front re-advanced northeast of Stuart Lake and deposited the Pinchi Creek lens. Units that are correlative with the Pinchi Creek lens may occur in the area, but if ice re-advanced over till instead of lake sediments, the lower till would likely be indistinguishable from the

upper till (Plouffe 2000). As the ice front retreated, ice lobes remained in some valleys, disrupting drainage and impounding numerous glacial lakes in the Manson River and Fort Fraser map-areas (Plouffe 1992, 1997, 2000). As the deglacial lakes evolved, subglacial drainage below large ice masses in the valleys deposited eskers in the valley bottoms (Levson et al. 1997; Plouffe 2000). As the ice downwasted, the glacial lakes drained around it, cutting meltwater channels into the valley sides and depositing kettled kame terraces along some valley walls (Plouffe 1997, 2000). In the later stages of deglaciation, a regional lake inundated all valleys of the Fraser River watershed and may have been connected to Glacial Lake Fraser (Clague 1987, 1989; Plouffe 1997, 2000). The timing of westerly ice retreat across the Nechako Plateau is constrained by a maximum radiocarbon age of 9830 ± 130 ^{14}C yr BP (GSC-5891) from peat north of Fraser Lake (Plouffe 2000). There are no ages associated with deglaciation from other parts of the Nechako Plateau.

In the northern Rocky Mountain Trench, a large glacial lake in the Williston Lake Reservoir was dammed by Laurentide ice in the Peace River valley (Rutter 1977). The Portage Mountain end moraine contains deltaic sediments that were deposited into this lake. A mammoth tusk recovered from these sediments yielded a radiocarbon age of 11 600 ± 1000 ^{14}C yr BP (I-2244A) and provides a maximum limiting age on the delta formation. Mollusc shells in the upper strandlines indicate that the lake persisted until at least 9960 ± 170 ^{14}C yr BP (GSC-1548) and 10 400 ± 170 ^{14}C yr BP (GSC-1654). However, the ages of the shells may be too old due to the uptake of older carbon (i.e. the reservoir effect). A lake of unknown extent and duration formed in the Omineca River valley and its tributaries and may have extended to the Williston Lake Reservoir (Plouffe 1997, 2000). Deglaciation of the Omineca River valley is constrained by radiocarbon ages from basal marl (10 100 ± 90 ^{14}C yr BP; GSC-2036; Alley and Young 1978) and peat (10 000 ± 140 ^{14}C yr BP; GSC-2036-2; Blake 1986).

In the upper Finlay River area, large terminal and lateral moraines in tributary valleys have been attributed to a local late advance of alpine glaciers. Radiocarbon ages of 9180 ± 80 ^{14}C yr BP (TO-12475) from a lake core and 9230 ± 50 ^{14}C yr BP (Beta-202609) from organic sediments in a meltwater channel that incised into a moraine provide minimum ages on the time of ice retreat (Lakeman et al. 2008a, b). The advance may have occurred during the Younger Dryas chronozone, suggesting fairly

significant ice persisting until this time. It is unknown if these advances coincide with late-glacial advances farther south in the Omineca Mountains or the Stuart Lake region (Plouffe 2000), as no ages have been obtained on these events.

3. Terrain mapping

Six 1:50 000-scale terrain maps were produced for this study using standardized terrain mapping methods (Resources Inventory Committee 1996; Howes and Kenk 1997). NTS map sheets 093J13 and 14 were mapped by the author (Appendix A1, B1, B2) and 093J05/06/11/12 were mapped by project collaborators (Maynard et al. 2012a, b, c; Ward et al. 2012). Many of the examples used in this chapter draw from areas mapped by the author. However, the information presented characterizes all mapped areas. The map legend uses a closed surficial geology format to assign polygon colours, and individual polygons are labeled using an open terrain classification system that provides detailed terrain information. This section outlines the methods used for terrain mapping and provides information about the map units and landforms.

3.1. Methods

Preliminary terrain interpretations were carried out in the summer of 2009. Surficial material, surface expression and geomorphological processes were used to delineate terrain polygons on high resolution, 1:40 000-scale, 1996 and 1997 black-and-white aerial photographs. Elevation models derived from Canadian digital elevation data (CDED), orthophotographs (www.geobase.ca) and digital NTS data (ftp://ftp2.cits.rncan.gc.ca/pub/bndt/) in a geographic information system (GIS) helped to identify landforms and spatial relationships. Polygon boundaries were delineated using solid lines for defined boundaries, dashed lines for inferred boundaries, and dotted lines for assumed boundaries. Each polygon was assigned a composite terrain symbol that describes its attributes. Specific landforms were identified using on-site symbols.

Field verification was conducted in the summers of 2009, 2010 and 2011 by truck and foot traverses. Navigation and data collection in the field were aided by a handheld GPS connected to GIS software. Data collected at field sites included: sediment type, texture

and density; unit thickness and structures; clast shape, size and lithology; stratigraphy; drainage; and geomorphological features. General observations about the nature and areal limits of surficial materials were input into the GIS during traverses. The initial aerial photograph interpretation was refined using terrain information from 198 field sites and general observations from 1052 locations (Fig. 3.1). Significant areas not accessible by truck or on foot were reached using all-terrain vehicles and data collected from 31 additional field sites were used to finalize the interpretation.

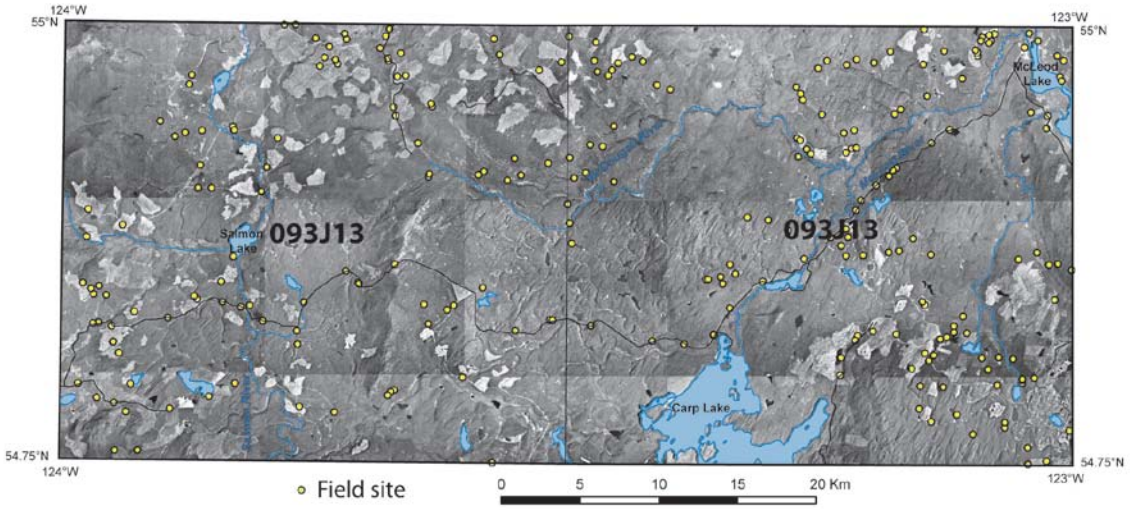

Figure 3.1 Field sites visited in NTS map-areas 093J13/14 for field verification of aerial photograph interpretations.

The aerial photographs were sent to Chartwell Consultants Ltd. for digitizing and georeferencing. Line work and symbols were scanned and transferred into a GIS to produce shapefiles with numbered polygons. Surficial materials, expression and geomorphological processes were manually entered into a database from which a simplified map symbol was derived for each polygon. The final shapefiles and map drafts were produced by Chartwell Consultants Ltd. and the maps were finalized by GIS technicians at Geoscience BC.

3.2. Composite terrain symbols

Unique composite terrain symbols provide detailed terrain information for each polygon (Fig. 3.2). The terrain symbol indicates major and minor surficial materials, surface

expression and geomorphological processes. Texture is only indicated if the polygon was field-checked and the texture is different than described in the legend. Simplified terrain symbols were produced to label map polygons based on assumptions defined in the legend (e.g. glaciofluvial deposits are assumed to overlie till unless otherwise indicated). Terrain symbols were simplified so the information on the maps would be more accessible to users not familiar with the terrain classification system. The simplified symbols consist of a maximum of two surface materials, each with possible subsurface materials with one surface expression, and a maximum of two geomorphological processes. Texture was not included in the simplified terrain symbol. The following sections define the elements of the terrain symbol and draw heavily from the guidelines for terrain classification in British Columbia (Howes and Kenk 1997).

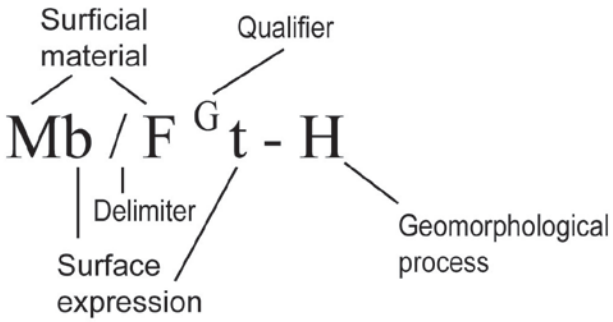

Figure 3.2 Example of a composite terrain symbol used to label map polygons. See text for description of components.

3.2.1. Surficial material

Surficial materials are non-lithified sediments that result from weathering, sediment deposition, biological accumulation and human activity (Howes and Kenk 1997). They are represented by capital letters in the terrain symbol (Fig. 3.2). Up to three components (surficial materials) can be listed in a terrain symbol, in order of decreasing areal extent, and each can have up to two subsurface materials. For the purposes of terrain mapping, bedrock is included in the list of surficial materials (Table 3.1).

Qualifiers can be applied to surficial materials to provide additional information. The glacial qualifier, a superscript "G" (e.g. glaciofluvial: F^G), is used when the material is

influenced by glacial processes. Activity qualifiers are used to indicate whether a surficial material is being formed at the present time. Each surficial material has an assumed activity state (see Table 3.1). The activity qualifier, a superscript "I" (^{I}) for inactive or "A" (^{A}) for active, is applied where the state of activity is contrary to that of the assumed state.

Table 3.1 Surficial materials that occur in the study area (after Howes and Kenk 1997).

Material name[a]	Map symbol	Assumed activity status
Colluvium	C	active
Aeolian	E	inactive
Fluvial	F	inactive
Glaciofluvial	F^{G}	inactive
Lacustrine	L	inactive
Glaciolacustrine	L^{G}	inactive
Morainal (till)	M	inactive
Organic	O	active
Bedrock	R	n/a

[a] Only materials that occur in the map areas are listed.

Delimiters are used to indicate the relative amount of each surficial material represented in the terrain symbols. A point sign (•) is used to indicate that components on either side of the symbol are of approximately equal proportion. A single slash (/) is used to show that the component in front of the symbol is more extensive than the one that follows, and a double slash (//) is used to show that the first component is much more extensive than the one that follows. A reverse single slash (\) is used in front of one material to indicate a discontinuous cover on the previous material. For example, F^{G}p\Ev indicates that an aeolian veneer partially covers a glaciofluvial plain. The reverse slash was defined for this project to simplify the map labels and is not in the Howes and Kenk (1997) guidelines. Surficial materials that constitute less than approximately 10% of the polygon are not included in the terrain symbol. Stratigraphic symbols are used when the nature of the subsurface material is important and not obvious from the context of the units. The units are aligned vertically in the terrain symbol and separated by a horizontal line.

3.2.2. Surface expression

Surface expression refers to the three-dimensional shape and pattern of a surficial material (Howes and Kenk 1997). It is classified according to slope, geometric shape and spatial pattern and is indicated in lowercase letters after a surficial material (Fig. 3.2). Up to three surface expressions can be used to describe each material; they are listed in order of decreasing areal extent. Surface expression can be classified into four broad categories: slope indicators; thin material; thick material; and discrete landforms (Table 3.2).

Table 3.2 Surface expressions used to define map units (after Howes and Kenk 1997).

Category	Surface expression	symbol	description
slope	plain	p	planar landform; 0-3°
slope	gentle	j	planar landform; 4-15°
slope	moderate	a	planar landform; 16-26°
slope	moderately steep	k	planar landform; 27-35°
slope	steep	s	planar landform; >35°
thin material	veneer	v	surface expression derived from underlying material; < 1 m thick
thin material	blanket	b	surface expression derived from underlying material; > 1 m thick
thin material	mantle of variable thickness	w	fills or partly fills irregularities in underlying substrrate;1-3 m thick
thick material	undulating	u	hillocks and hollows with multi-direction slopes ≤ 15°
thick material	hummocky	h	hillocks and hollows with multi-direction slopes > 15°
thick material	rolling	m	linear or elongated hillocks with slopes ≤ 15°
thick material	ridged	r	linear or elongated hillocks with slopes > 15°
discrete landform	fan	f	depositional feature that spreads from an apex with slope ≤ 15°
discrete landform	cone	c	depositional feature that spreads from an apex with slope > 15°
discrete landform	terrace	t	single or assemblage of scarp and associated plain
discrete landform	depression	d	depressions of at least 2 m delimited by an abrupt break in slope

Slope indicators are applied to constructional or erosional landforms with local surface irregularities that are generally less than 1 m: plains; or gentle, moderate, moderately

steep and steep slopes. Thin materials have surface expressions derived from the underlying topography: veneer; blanket and mantles of variable thickness. Thick material cover (undulating, hummocky, rolling and ridged) has sufficient thickness to exhibit a surficial expression independent of the underlying topography. Discrete landforms are fans, cones, terraces and depressions.

3.2.3. Geomorphological process

Geomorphological processes are natural mechanisms of weathering, erosion and deposition that modify surficial materials and landforms (Howes and Kenk 1997). For each polygon, up to three geomorphological processes can be included in order of decreasing areal extent (Fig. 3.2). In the mapped areas, limited erosional (gullying: V), fluvial (irregularly sinuous channel: I), mass movement (slow: F, rapid: R) and deglacial processes (channelled by meltwater: E, kettled: H) were noted (Table 3.3). Comprehensive definitions of the geomorphological processes can be found in Howes and Kenk (1997).

Table 3.3 Geomorphic processes that occur in the study area (after Howes and Kenk 1997).

Group	Process[a]	Symbol	Assumed activity status
erosional process	gully erosion	V	active
fluvial process	irregularly sinuous channel	I	active
mass movement	slow mass movements	F	active
mass movement	rapid mass movements	R	active
deglacial processes	channeled by meltwater	E	inactive
deglacial processes	kettled	H	inactive

[a] Only processes that occur in the mapped areas are listed.

3.3. Map legend

The maps use a hybrid surficial geology and terrain map legend that provides a description of the map units. Map units are defined with a two-letter coding system: a capital letter signifying the surficial material, and a lowercase letter that represents surface expression. Polygons are coloured based on the dominant surficial material and

surface expression. Map units are grouped in the legend under three main headings: Holocene; Pleistocene and Pre-Pleistocene. Additional polygon attributes can be determined using the simplified composite terrain symbols located on the map or the full unit description in the database. This type of system allows the user to quickly identify the dominant features of each polygon, but also provides a more detailed description of the surficial materials, expressions and geomorphological processes when required.

3.3.1. Map unit descriptions and genesis

Map units were categorized based on the genesis and grouping of related landforms. The surficial materials and map units are described in terms of texture, composition, genesis and general distribution and thickness. Assumptions used to simplify the composite terrain symbol for the map label are indicated. Some of these are different than assumptions used in Howes and Kenk (1997).

Holocene

Organic deposits

Organic deposits are composed largely of the saturated accumulated remains of mosses, sedges, or other hydrophytic vegetation and may contain minor lacustrine or fluvial sediments. They commonly develop at the margins of lakes or within slow-moving streams and on floodplains. Organic deposits also occupy depressions on poorly drained sediments or bedrock throughout the study area. Organic deposits are assumed to overlie till unless otherwise indicated.

Organic mantle (Ov;w)

Organic deposits that are less than 1 m thick typically occur at the edges of lakes, slow-moving waterways and on floodplains throughout the study area. Deposits of variable thickness are common in till, glaciolacustrine and bedrock depressions.

Organic plain (Op;b)

Organics plains are generally more than 1 m thick and infill shallow lakes and depressions along floodplains and abandoned meltwater channels. These deposits occur mainly as bogs and fens (Fig. 3.3).

Figure 3.3 Example of thick peat that has infilled a small lake in the northwestern part of map-area NTS 093J12. Photo by B. Ward.

Fluvial deposits

Fluvial sediment (F) is transported and deposited by streams and rivers under nonglacial conditions. Fluvial deposits typically consist of stratified, moderate to well sorted, rounded to well rounded gravels, sand and silt. The sediment size is dependent on the flow regime, distance of transport and sediment source. Steep headwater streams transport larger material. The lower reaches transport mainly sand to pebble-size material. Fluvial deposits are assumed to overlie till unless otherwise indicated.

Floodplain ($F^{A}p;b;v$)

Floodplains are typically indicated as active, occur at or near present-day stream level and are periodically flooded (Fig. 3.4). Units associated with floodplains are commonly composed of gravel, and may be overlain by sand and silt deposited during overbank flow. Areas mapped as floodplains may include minor organic deposits, small tributary fans and narrow terraces. Floodplains typically form along modern streams within large meltwater channels or surrounding streams that meander through large flat areas.

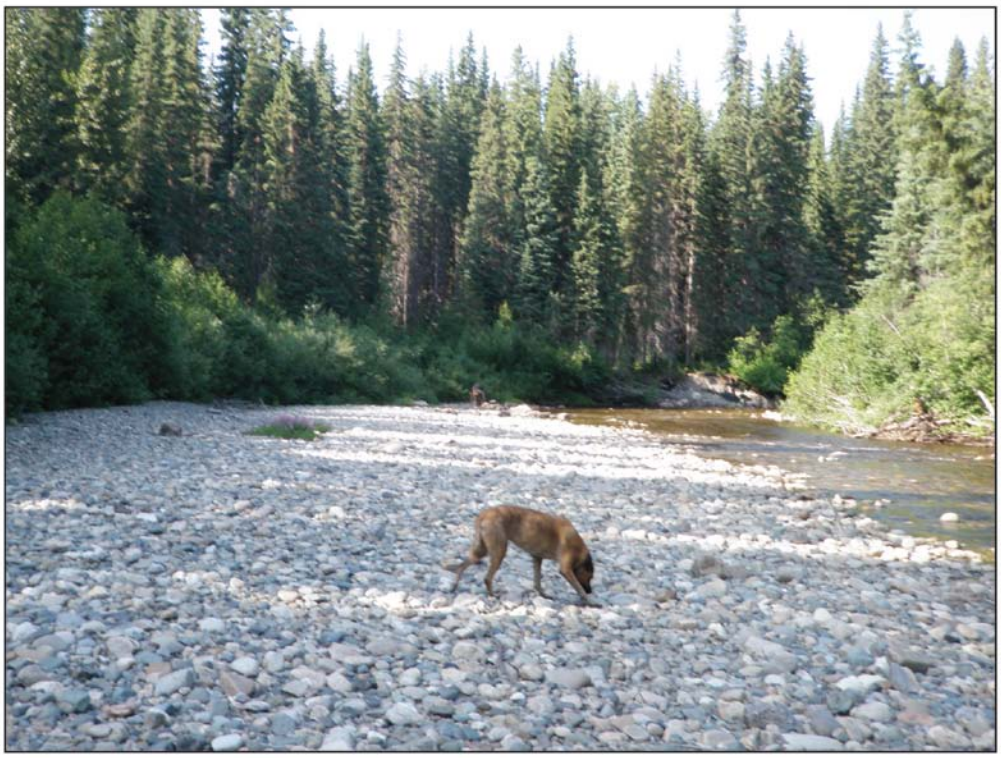

Figure 3.4: Active floodplain adjacent to McDougall River.

Fluvial fan (Ff)

Fluvial fans are constructional features consisting of stratified sand and gravel and may contain diamict lenses. Fans commonly build out onto floodplains at the outlets of steep tributary streams. Those indicated as active have surfaces that are prone to flooding and avulsion, but may contain raised inactive areas.

Inactive fluvial deposits (Fp;t;f;u;v;w)

Inactive fluvial deposits comprise stratified gravel, sand, and minor silt deposited during the Holocene that occur above present-day streams. Most consist of gravel overlain by fine overbank deposits. Deposits with undulating surface expressions typically occur within old floodplains as a result of channelling.

Aeolian deposits

Aeolian sediment (E) is transported and deposited by wind and consists of well sorted silt to fine sand. This sediment was mobilized from unvegetated glaciofluvial and

glaciolacustrine deposits during and immediately after deglaciation. Most aeolian deposits have been stabilized by vegetation, although disturbance by logging has remobilized the sediment in some areas. Units of aeolian material typically occur on or near their source units and can be difficult to discern on aerial photographs because of the vegetative cover. Deposits are assumed to overlie glaciofluvial material unless otherwise indicated.

Aeolian mantle (Eb;v;w)

Aeolian mantles occur as a continuous or discontinuous cover of well sorted sand up to ~1 m in thickness. Aeolian mantles commonly overly glaciofluvial or glaciolacustrine material.

Aeolian dunes (Em;u;r)

Sand dunes have a rolling, ridged or undulating surface expression. “Rolling” and “ridged” represent linear dunes and “undulating” represents complex or barchan style dunes.

Colluvial sediments

Colluvial sediment (C) is transported and deposited by gravitational (mass movement) processes and may include organic detritus. Its texture and composition are dependent on the parent material and the transport mechanism. Most colluvial sediments were deposited during the paraglacial period when ice retreat exposed many unstable slopes. In the mapped areas, colluvial deposits that are derived from bedrock are typically monolithic, poorly sorted, angular and clast-supported (Fig. 3.5a). These types of deposits occur in areas with steeper slopes where bedrock is exposed and the sediment is derived through slow weathering processes. On steep mountain and valley slopes and within incised stream channels, colluvium consists of reworked till, glaciofluvial and glaciolacustrine material. Deposition is generally associated with rapid mass wasting events. These deposits are typically poorly sorted, matrix-supported and may be massive or crudely stratified. Colluvium derived from till can be difficult to distinguish from the parent material (Fig. 3.5b) and is only mapped where it creates a distinct landform (e.g. colluvial fan).

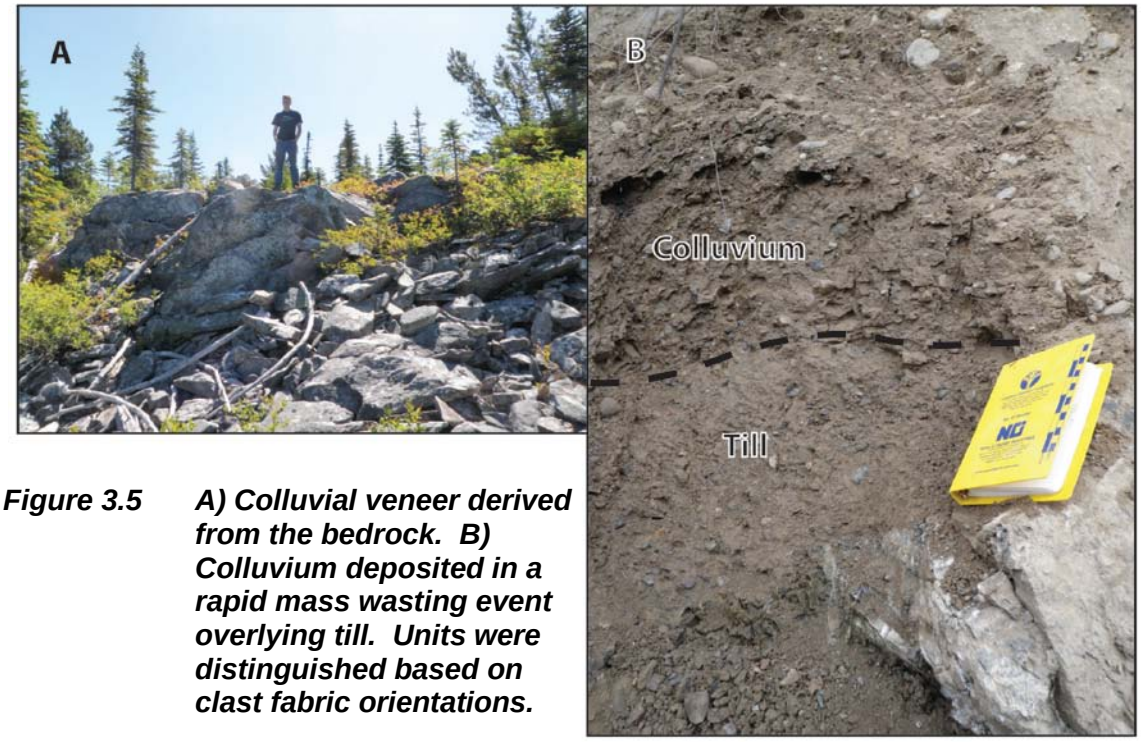

Figure 3.5 ***A) Colluvial veneer derived from the bedrock. B) Colluvium deposited in a rapid mass wasting event overlying till. Units were distinguished based on clast fabric orientations.***

Colluvial mantle (Cb;v;w)

Thin colluvial deposits dominantly occur on moderate to steep slopes where bedrock is exposed. These deposits consist of local angular clasts. Colluvial veneers may also develop on steep unconsolidated slopes from the accumulation of falling, sliding and creeping debris.

Colluvial fans and cones (Cf;c)

Colluvial fans and cones consist of sediments that accumulated during multiple mass wasting events. Fans are a result of rapid mass wasting of saturated debris (usually till). They are typically stratified and may contain fluvial lenses. Many of these features were created by failures from unstable, till-covered slopes during the paraglacial period. Active colluvial fans are typically mapped at the base of gullied terrain that is prone to debris flows. Cones only develop in the study area at the base of some steep slopes from rock and debris fall and are typically too small to be mapped individually.

Pleistocene

Glaciolacustrine sediments

Glaciolacustrine sediment (L^G) is deposited by suspension settling, underflows, littoral action or from floating ice in or at the margins of lakes on, in, under or adjacent to a glacier. Ice-proximal deposits consist of bedded medium to coarse sand and may include lenses of diamict (Fig. 3.6a). Distal deposits comprise: 1) rhythmically bedded silt and sand that may contain dropstones; and 2) slightly coarser lakeshore deposits (Fig 3.6b). Thick deposits are susceptible to post-depositional mass wasting or erosion such as slumping, gully erosion and debris flows. Glaciolacustrine sediments are common in the low-lying southern parts of the study area where southeast drainage into the Fraser River was impeded by ice or sediment during deglaciation. In the northern part of the study area, glaciolacustrine sediments are only observed at surface in south- or southwest-facing valleys where retreating or abandoned ice interrupted drainage (Fig. 3.7). Glaciolacustrine units are assumed to overlie till unless otherwise indicated.

Figure 3.6 ***Glaciolacustrine deposits in the study area. A) Ice proximal deposits are coarse-grained and may include diamict lenses deposited by sediment gravity flows. B) Distal deposits are products of underflows and suspension settling and typically comprise rhythmically bedded sand and silt (B).***

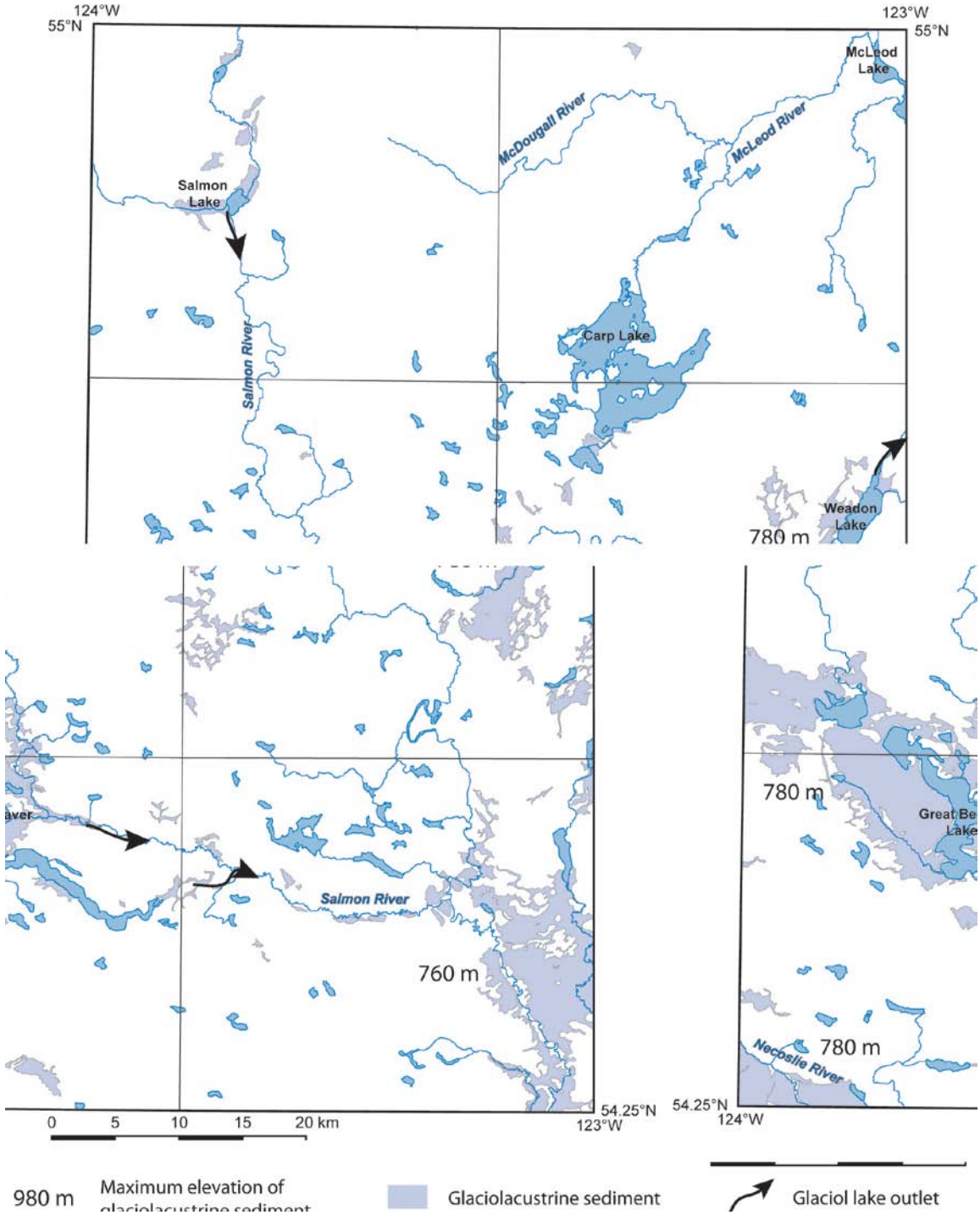

Figure 3.7 Distribution of glaciolacustrine sediments in the study area.

Thick glaciolacustrine (L^Gp;u;t)

Thick glaciolacustrine sediment comprises flat to gently undulating or sloping fine-textured sediment deposited in relatively long-lived proglacial lakes. Aerially extensive glacial lakes developed around the Necoslie River, the southern part of the Salmon River and Great Beaver Lake and deposited silt and sand in them, masking the underlying topography. Deposits may be susceptible to mass wasting and erosion. Minor amounts of fluvial or glaciofluvial sediment may be present within thick glaciolacustrine units.

Glaciolacustrine mantle (L^Gb;v;w)

Thin glaciolacustrine units are typically mantles of fine-textured material deposited in short-lived glacial lakes and at the margins of large glacial lakes.

Glaciolacustrine scarp (L^Gs;k;a)

Erosive glaciolacustrine scarps occur where thick deposits have been incised by meltwater or Holocene streams. They are especially susceptible to gully erosion and mass wasting.

Glaciofluvial sediments

Glaciofluvial sediment (F^G) is transported by glacial meltwater and deposited in supraglacial, englacial or subglacial environments as well as in front of or adjacent to a glaciers. Thick units of glaciofluvial material were deposited in valleys and some meltwater channels due to the increased sediment loads associated with deglaciation. Many of these deposits were incised after deglaciation leaving terraces. Glaciofluvial deposits are differentiated from fluvial deposits by: evidence of ice-contact sedimentation (e.g. hummocky surface expression or internal deformation); location above present base level; texture in relation to post-glacial flow regime; and associated landforms (e.g. meltwater channel). Thin pine stands that grow in the well drained glaciofluvial deposits assist in their identification on aerial photographs.

The texture and composition of glaciofluvial sediments are dependent on their depositional environment. Clasts in ice-contact deposits are subangular to well rounded, and the sediments range from moderately to poorly sorted sandy to bouldery gravels

that may exhibit deformed bedding (Fig. 3.8a). The surface expression is typically complex (e.g. hummocky or a system of ridges), and the thickness can range from a few metres to tens of metres. Ice-contact deposits are not aerially extensive in the study area and dominantly occur in areas of low elevation where ice stagnated or in eskers deposited near the margin of the glacier. Clasts in ice-proximal deposits are subrounded to well rounded, and the sediment is moderately sorted, pebbly to bouldery stratified gravels, but massive units are also present (Fig. 3.8b). These units most commonly occur within meltwater channels, but rarely extend to the surface unless the channels were abandoned prior to deposition of finer, distal glaciofluvial deposits. Distal glaciofluvial material consists of moderate to well sorted, stratified, sandy to pebbly gravels (Fig 3.8c). These deposits are common at the surface in meltwater channels and on terraces. The thicknesses of glaciofluvial units are dependent on the duration of activity, size of the drainage system, sediment load and flow regime. Relatively short-lived, ice-marginal meltwater channels that cross-cut topography may contain less than a few metres of sediment, whereas large meltwater corridors and outwash plains contain much thicker deposits that are commonly mined for aggregate resources. Glaciofluvial units are assumed to overlie till unless otherwise indicated.

Figure 3.8 ***Typical glaciofluvial deposits in the study area. A) Hummocky, crudely stratified and deformed ice-contact glaciofluvial deposit. B) Moderately to poorly sorted and massive ice-proximal glaciofluvial deposit. C) Well sorted distal glaciofluvial deposit. Ice axe is 70 cm long and blue pick is 65 cm long.***

Glaciofluvial outwash (F^{G}p;t;u;f;a;s;k)

Outwash is deposited in front of or adjacent to the glacier. Plains and terraces are typically composed of fining-upward gravel. Fans consist of stratified gravel, sand and minor diamict beds and occur where confined drainage systems open to a larger area. Outwash deposited by braided rivers or that has been affected by post-depositional channelling or kettling may have an undulating surface. Sloping deposits occur where the unit has been incised. Outwash units may be covered with minor amounts of fluvial, organic and aeolian sediment.

Ice-contact glaciofluvial sediment (F^{G}r;m;h;u)

Ice-contact deposits are dominantly stratified gravel and sand with minor diamicton deposited supraglacially, englacially, or subglacially as esker systems, ice stagnation deposits and kames. Rapid facies changes are common within these deposits because of the variable meltwater flow regimes. These deposits are commonly associated with kettles and may display brittle or ductile deformation from the melt of buried or supporting ice. Ice stagnation deposits are generally poorly to moderately sorted.

Glaciofluvial mantle (F^{G}b;v;w)

Glaciofluvial mantles consist of stratified sand and gravel that dominantly occur on elevated surfaces around meltwater channels.

Morainal sediments

Morainal sediments (M) include diamicts that have been deposited by either primary glacial processes (e.g. lodgement, deformation or melt-out), or secondary glacial processes caused by gravity and water (e.g. flow till), and thus encompass all types of till (Dreimanis 1989). Till is the aerially most extensive surficial material in the study area. The composition and texture are influenced by genesis and the underlying material.

The most common morainal sediment in the study area is basal till, occurring as blankets and veneers in areas of high relief and as thick, streamlined deposits over much of the remainder of the study area. It is over-consolidated, has a sandy silt matrix, and is matrix-supported, with 10-30% clasts. Clasts are commonly striated and faceted and range from granule to boulder in size, with a mode in the pebble fraction. Elongated

clasts are preferentially oriented parallel to ice-flow direction. In the southwest part of the study area, till has a notably lower clast percentage, possibly due to the incorporation of glaciolacustrine sediments. This suggests that there was an advance glacial lake in the area or that a lake existed there during the Middle Wisconsinan.

Ablation till occurs as thin, discontinuous veneers (<50 cm) throughout the study area. It is less compact than basal till and has a sandier matrix due to the removal of silt and clay during deposition. Till is assumed to overlie bedrock unless otherwise indicated.

Streamlined till (Mr;m)

Ridged or rolling till underlies fluted and drumlinized terrain and the down-ice part of crag-and-tail features. Intervening depressions commonly contain minor amounts of glaciofluvial or fluvial material because water is concentrated in these areas. Organic deposits also develop in depressions due to the low permeability of basal till.

Thick till (Mp;j;a;k;s;t;h;u;d)

Thick till masks the underlying topography and has a variety of surface expressions. Hummocks, terraces and scarps are the result of post-depositional erosion and may contain minor amounts of colluvium or glaciofluvial sediment. Hummocky or undulating ablation till is also associated with ice stagnation. Till depressions may contain minor glaciofluvial, glaciolacustrine, lacustrine and organic sediment.

Till mantle (Mb;v;w)

Till mantles dominantly occur in upland regions. Thin till units generally have a higher clast content with larger and more angular locally derived material. Variable thickness is most commonly assigned where the material transitions between blanket and veneer, but is also used to indicate discontinuous till infilling hollows in the underlying substrate.

Pre-Pleistocene

Bedrock

Thick drift mantles most of the study area but bedrock crops out locally. Most outcrops (R) occur in high relief areas where till has moved downslope or was not deposited. Bedrock types vary greatly across the study area and include sedimentary,

metamorphic, volcanic and intrusive rocks of Precambrian to Cenozoic age. Bedrock units are commonly associated with a discontinuous veneer of till or colluvium and may include organic sediments.

Sloping bedrock (Rk;s;h;u;r;m)

Steep bedrock slopes occur in upland areas or as a result of deep meltwater incision and may be susceptible to rock fall. Hummocky, undulating or streamlined bedrock is the result of glacial erosion or preferential water erosion that follows the structure of the rock.

3.3.2. Onsite symbols

Onsite symbols are graphic representations of landforms that are used to depict their location. Refer to map legend for onsite symbols used in this project (Appendix B1, B2).

3.4. Landforms

This section describes glacial and nonglacial landforms that occur within the study area. Some landforms, such as ice-stagnation topography and esker complexes, can be identified in the polygon label. Other landforms that are too small to be incorporated into the label or are otherwise important to the user are illustrated with onsite symbols. The landforms are described in the chronologic order, starting with the oldest.

3.4.1. Striations

Striations, grooves and rat tails are linear, small-scale erosional features developed on bedrock surfaces (Fig. 3.9). They are a result of subglacial abrasion from ice-entrained clasts and are oriented in the direction of ice flow. Striations are long narrow depressions generally a few millimetres in width and a few to tens of centimetres in length; grooves are wider features, generally a few centimetres in width and tens of centimetres in length. Rat tails develop where subglacial erosion is inhibited by a hard element in the bedrock, producing a positive relief feature similar to a crag-and-tail. The

use of these features in determining ice-flow patterns is discussed in more detail in Chapter 5.

Striations, grooves and rat tails are most common on fine-grained, glacially smoothed bedrock where sediment veneers have protected them from postglacial weathering. Few striations, grooves and rat tails were observed in the study area due to sparse bedrock exposures and bedrock lithology or structure that is not conducive to their formation or preservation.

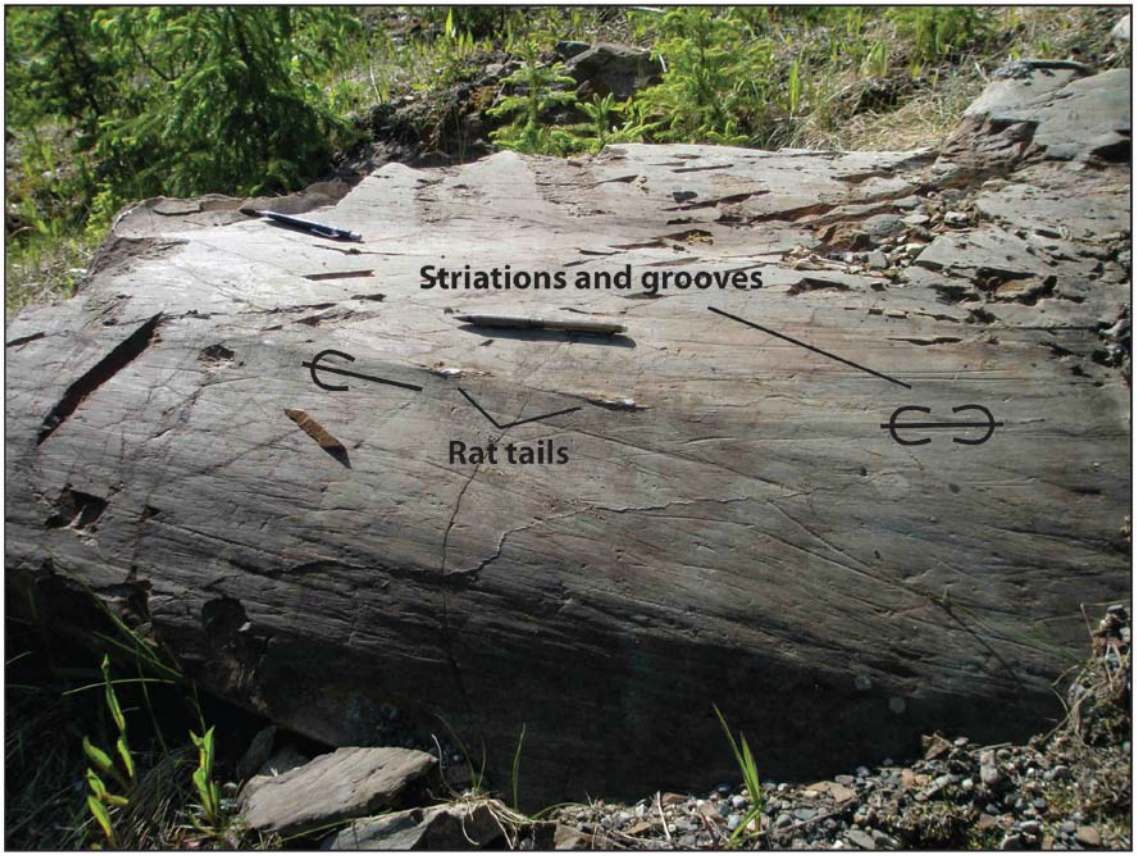

Figure 3.9 Glacially smoothed bedrock with striations, grooves and rat tails. Ice-flow directions indicated by striation symbols. Photograph by B. Ward.

3.4.2. Streamlined macroforms

Streamlined macroforms are elongate, linear features including bedrock, crag-and-tails, drumlins and flutings formed by ice flow. Streamlined bedrock dominantly occurs in

areas of high relief with limited sediment cover. In general, the larger features occur at the summit of Mount Mackinnon and are hundreds of metres wide and up to 2 km in length. At slightly lower elevations, where there are discontinuous blankets and veneers of till, crag-and-tail features are composed of a bedrock knob with a tail of till extending in the down-ice direction (Fig. 3.10).

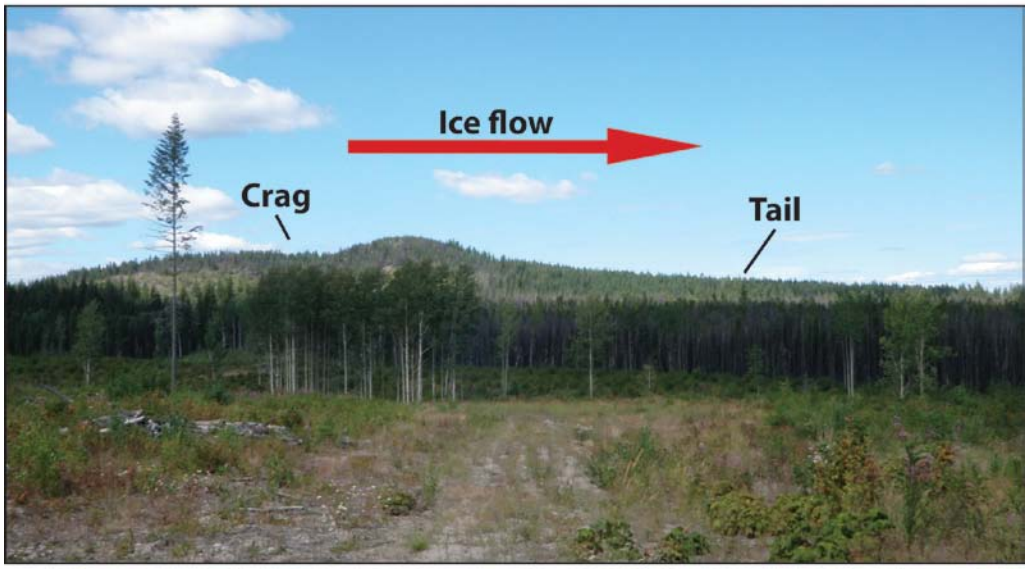

Figure 3.10 Crag-and-tail located in southwestern part of the study area.

Drumlins have a blunt stoss side and a more gentle lee side (Fig. 3.11), while flutings have similar height and slope profiles at both ends. The nature of these landforms is likely influenced by both the thickness and composition of sediment on which they are developed and the effect of local topography. In low-elevation and low-relief terrain in the south and central parts of the study area, drumlins average 30 m in height, 300 m in width and 1 km in length. Some of the larger drumlins have smaller-scale flutings on their tops. In the northern uplands, on Ant Hill and in the southwest corner of the study area, where elevations and relief are greater, drumlins and flutings average 20 m in height, 150 m in width, and about 1 km in length except on slopes leeward of ice-flow, where some of these features are up to 3 km long.

Drumlins and flutings are formed subglacially through a combination of subglacial sediment erosion and redistribution within the subglacial deforming layer (Boulton 1987). They are ubiquitous and exposures in service road cuts indicate that they are composed

of till. The hollows between the ridges commonly contain fluvial or glaciofluvial sediment because drainage is concentrated in the topographic low.

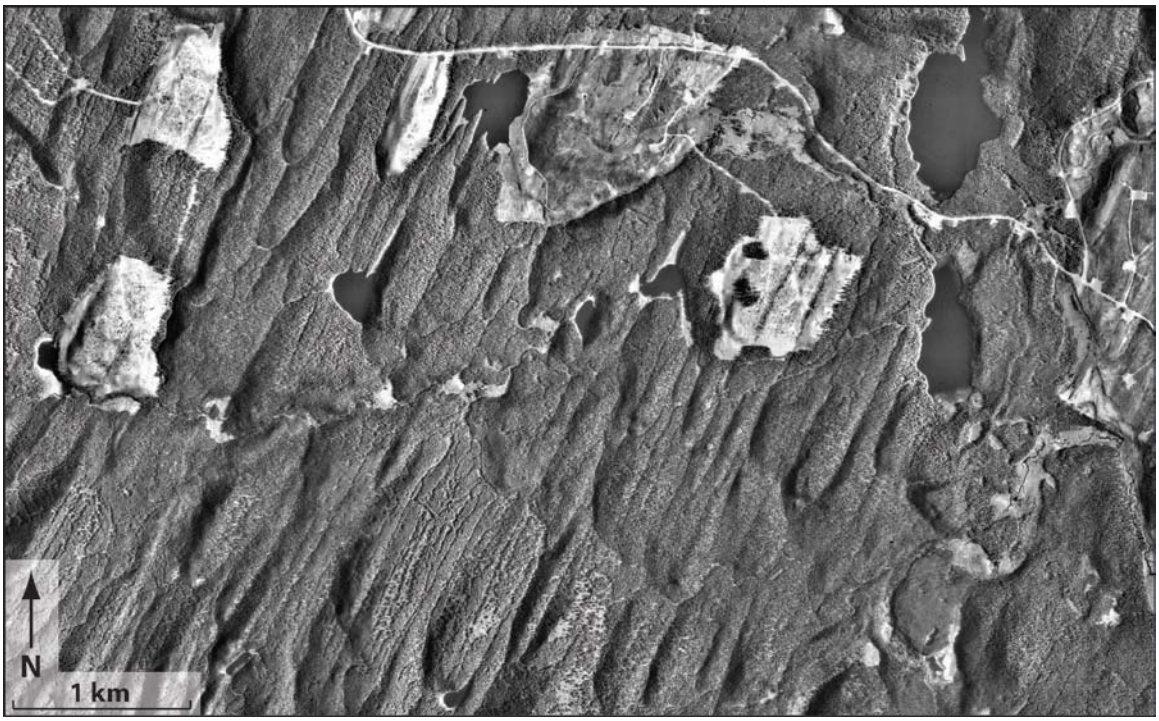

Figure 3.11 Orthophotograph draped over a DEM showing drumlin field east of Carp Lake. Orientation of drumlins indicates north-northeast ice flow.

3.4.3. Eskers

Eskers are sinuous ridges of glaciofluvial sediment deposited in subglacial, englacial or supraglacial drainage networks. They are composed of stratified sand and gravel. Eskers occur as single or multiple ridges (esker complex) or can transition between the two forms (Fig. 3.12). In systems with high hydraulic pressure, eskers are typically aligned subparallel to the direction of ice-flow, reflecting meltwater flow towards the ice margin due to the hydraulic gradient created by the ice surface slope (Brennand 1994; Benn and Evans 1998). Where tunnels are at atmospheric pressure, water flow typically follows the local slope. Eskers usually occur in association with other glaciofluvial materials and landforms such as ice-contact deposits and meltwater channels. Short, straight single-ridge eskers occur on valley sides and commonly follow the local slope. They were likely deposited under stagnated ice within the valleys. They are generally a

few hundred metres in length and are commonly associated with meltwater channels at their upper ends and ice-stagnation topography at their lower ends.

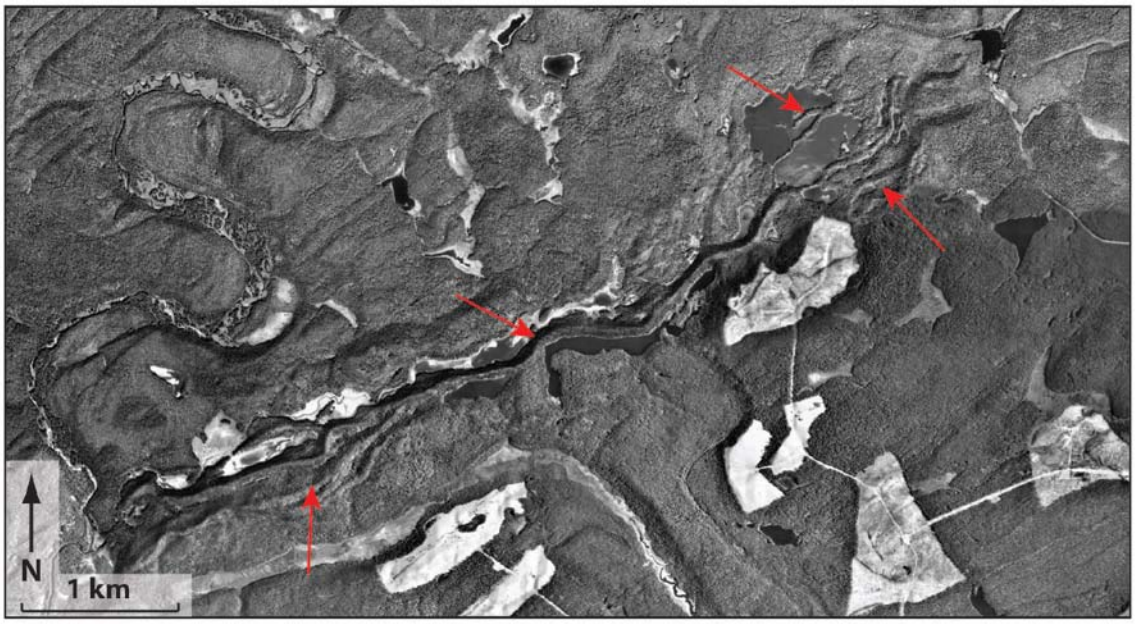

Figure 3.12 Orthophotograph draped over a DEM showing esker complex south of Mount Mackinnon (indicated by red arrows). Northeast orientation of the esker is aligned with ice-flow in the region.

3.4.4. Ice-stagnation landforms

Ice-stagnation landforms, sometimes referred to as kame-and-kettle topography, are composed of mounds (kames) and hollows (kettles) formed of glaciofluvial sediment. The mounds result from deposition within, on top of, or under ice. The hollows represent areas of minimal accumulation or subsidence due to the melting of buried ice blocks. The deposits are stratified sand and gravel that commonly show soft-sediment deformation and faulting due to the melt of supporting ice. Kame-and-kettle topography is commonly associated with small eskers or esker complexes. A good example of kame-and-kettle topography is the corridor between McLeod and Carp Lakes where about 10 km^2 of hummocky glaciofluvial material is pitted with kettle lakes and eskers (Fig. 3.13a). Smaller occurrences of kame-and-kettle topography are present throughout the study area.

Kame-and-kettle features also occur within the study area as individual landforms. Small ice blocks that melted in the glaciofluvial outwash plains north of Mount Mackinnon produced small kettles, between 50 and 150 m across and a few metres deep (Fig 3.13b). Similar-size kettles also occur in glaciolacustrine sediments south of Great Beaver Lake and on the outwash plains west of McLeod Lake. Melt of larger ice blocks likely produced many of the lakes that are scattered throughout the study area, including Salmon Lake and at least some parts of Carp Lake. Kames are steep-sided mounds of sand and gravel formed by supraglacial or ice-contact glaciofluvial deposition. A kame about 200 m across and 30 m high is being mined for aggregate in the central part of NTS 093J06 (Fig. 3.13c, d).

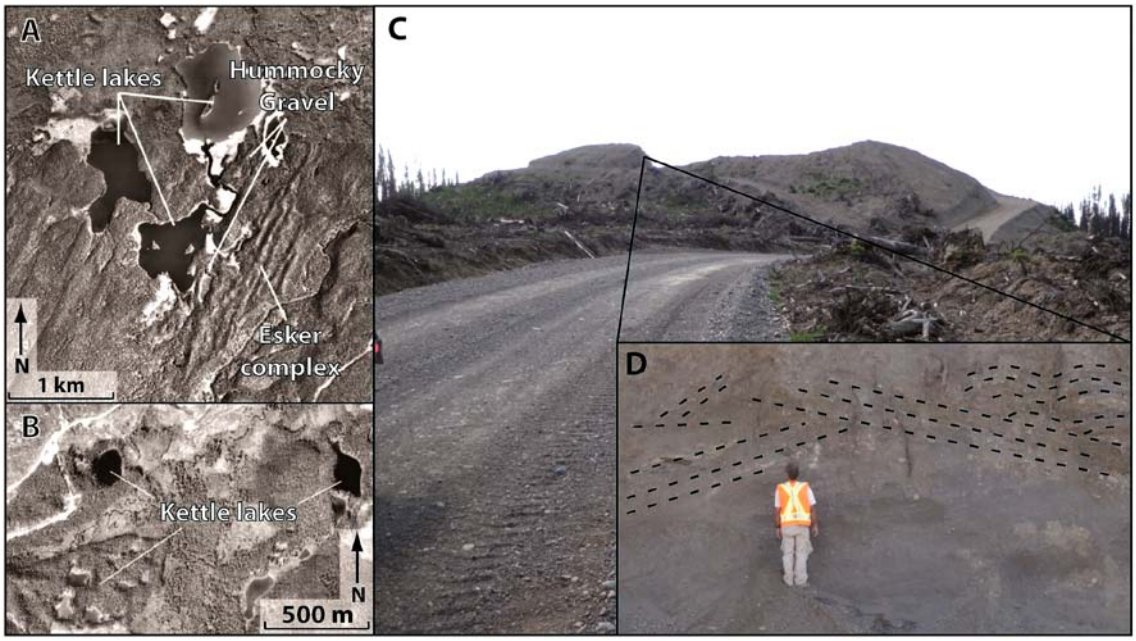

Figure 3.13 Examples of ice-stagnation landforms in the study area. (A) Orthophotographs draped over a DEM showing ice-stagnation landforms between Carp and McLeod lakes and (B) kettle lakes north of Mount Mackinnon. (C) Large kame located in NTS map area 093J06; (D) mining for aggregate has exposed chaotic bedding within the kame.

3.4.5. Meltwater channels

Meltwater channels are eroded into the substrate by glacial meltwater. A complex system of subglacial, proglacial and lateral meltwater channels occurs throughout the

study area. Subglacial channels develop as water flows toward the glacier margin, driven by the hydraulic gradient created by the ice surface; these channels are generally oriented in the direction of ice flow (Fig 3.14b). In some places, meltwater channels transition into eskers as the channels alternate from Nye channels that eroded into the substrate (Nye 1973) to Röthlisberger channels that eroded upwards into the ice (Röthlisberger 1972). As water approached the ice margin, the effect of the hydraulic gradient became less and the flow direction was more influenced by the topography. Where the land sloped away from the glacier, proglacial channels carried water away from the ice margin (Fig. 3.14a). Lateral channels formed along the glacier margin, typically where land sloped toward the glacier (Fig 3.14b).

Meltwater channels are distinguished from post-glacial drainage channels in four ways: 1) they are not connected to a watershed; 2) they are occupied by underfit streams; 3) large glaciofluvial terraces surround the channels; and 4) the channels cross-cut topography rather than flow downslope. Paleoflow directions of channels were determined from their gradients, ice-flow direction and location, and channels junctions. In some channels within complex networks, the paleoflow direction could not be determined.

The size and complexity of meltwater systems differ greatly throughout the study area, affecting the morphology of the channels. Drainage systems that were active for short periods typically have small channels containing limited amounts of glaciofluvial sediment, and are generally only a few hundred metres long. However, variable flow regimes can also cause limited deposition and erosion, thus caution must be taken in this interpretation. Large channels, up to 2 km wide collected meltwater from a number of smaller systems. These channels have extensive thick glaciofluvial deposits within them, and many are now occupied by underfit streams. Examples occur around the present-day Salmon River and the McLeod River between Carp and McLeod lakes.

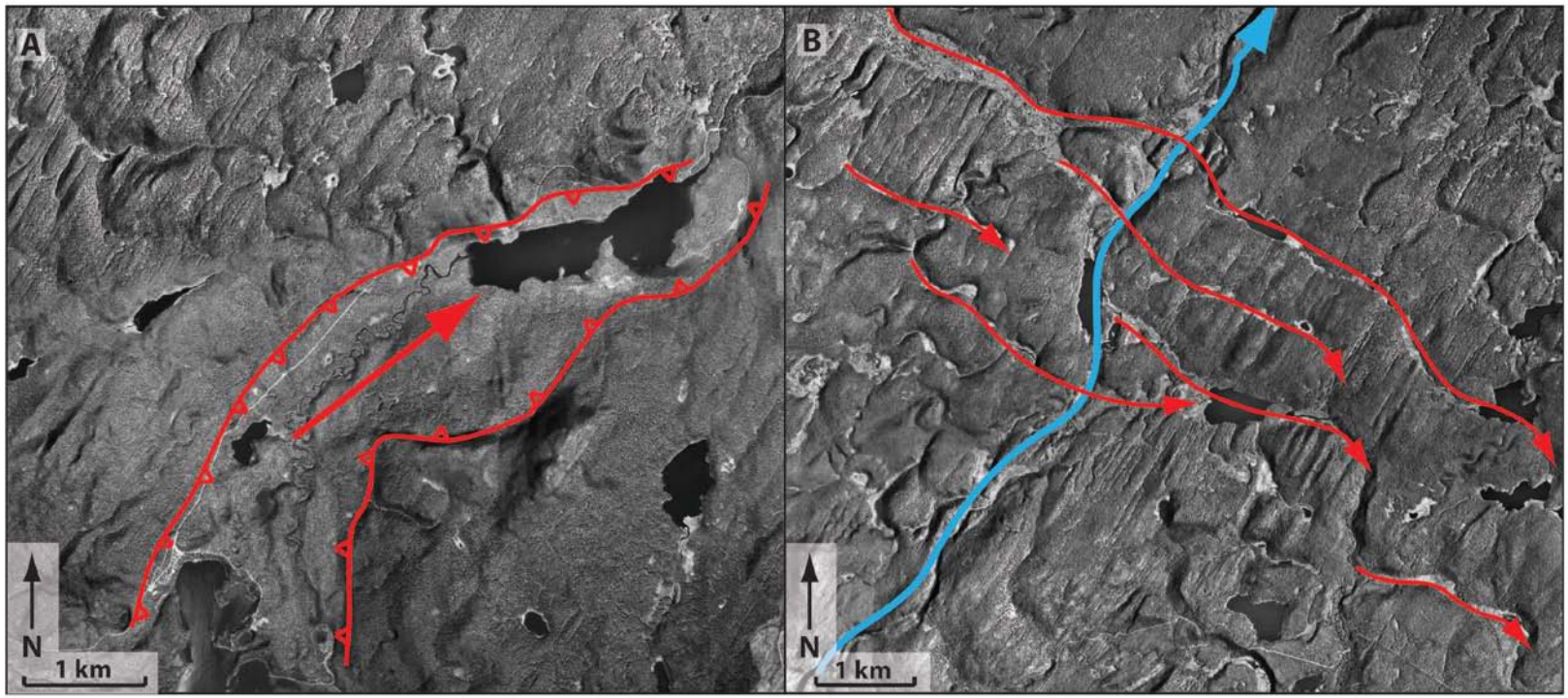

Figure 3.14 Examples of meltwater channels in the study area. A) Proglacial meltwater channel extending off the arm of Carp Lake. B) Subglacial meltwater channel east of Mount Mackinnon (blue arrows) with successive lateral channels delineating the retreating ice margin locations (red arrows).

3.4.6. Aeolian landforms

Aeolian landforms include dunes ranging from one to several metres in height and veneers and blankets that mantle the underlying topography (Fig. 3.15). Care must be taken in interpreting these features as thin aeolian material deposited on irregular surfaces can cause veneers and blankets to look like dunes. In addition, vegetation can mask the subtle surface expression making identification on aerial photographs difficult. Eolian activity began during ice retreat when silt and sand were mobilized from unvegetated glaciofluvial and glaciolacustrine deposits.

Figure 3.15 Aeolian sediments found in the study area. Thick sand occurs in dunes that range from a few (A) to several (B; photo by B. Ward) metres in height. Thin materials occur as veneers (C) and blankets (D) that mantle the underlying topography. Most aeolian sediment overlies the glaciofluvial or glaciolacustrine source units.

Measurements of aeolian bedding plains suggest the material was dominantly transported in a northeasterly direction, potentially by katabatic winds blowing off the retreating ice front (Fig. 3.16). Stabilization of the landforms was likely a result of plant colonization and a decrease in katabatic wind velocity as the ice front moved farther from the area. Few aeolian units have migrated beyond their source areas. The reactivation history is unknown, although no soil development was observed within any investigated aeolian deposits. Removal of vegetation by recent logging and possibly by historic forest fires has caused some local reactivation.

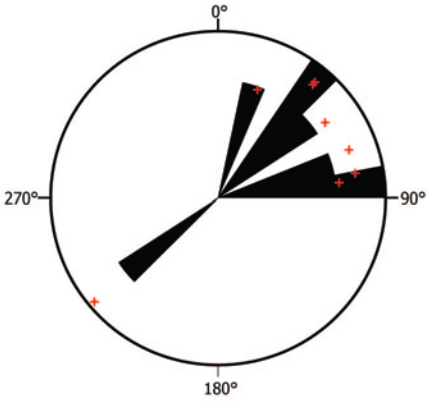

Figure 3.16 ***Rose diagram illustrating wind direction when aeolian landforms were active. Measurements are from bedding plains in aeolian landforms throughout the study area. N = 8; primary eigenvector = 55°; plotted in the lower hemisphere with an equal area projection. Red symbols indicate individual measurements.***

3.5. Summary of surficial geology

The surficial geology of NTS map-areas 093J05/06/11/12 /13/14 was documented by creating of two 1:50 000-scale terrain maps (093J13/14; Appendix B1, B2) and analyzing similar maps produced by project collaborators (093J05/06/11/12; Maynard et al. 2012a, b, c: Ward et al. 2012). The mapping was supplemented with an analysis of digital spatial data in a GIS and detailed field studies.

Most sediments and landforms in the study area are a product of the Fraser Glaciation. During the late-glacial period, sediment fluxes were high due to fluvial, lacustrine, aeolian and mass wasting processes (*cf*. Church and Ryder 1972; Ballantyne 2002).

Since then, sedimentation rates have decreased and rivers have gradually incised drift to reach present base levels.

Till is the dominant surficial material. In low-relief areas, till is thick and streamlined in a northeast direction. In uplands, it mantles the underlying topography as blankets and veneers. Most of the till is basal till. In localized areas in the south, basal till is overlain by a veneer of ablation till. At the highest elevations, till has been removed by mass wasting processes, leaving exposed bedrock and colluvial veneers on the summits and colluvial fans on lower slopes. Bedrock only occurs at the surface as small outcrops in the rest of the study area.

During deglaciation, meltwater modified the landscape by cutting a complex of subglacial, ice-marginal and proglacial meltwater channels and depositing glaciofluvial sand and gravel. Subglacial channels are generally oriented to the northeast, aligned parallel to the deglacial ice-flow direction. Lateral channels are more common and occur as a series of subparallel northwest-and southeast-oriented features over most of the area. Erosional processes were dominant within the subglacial and lateral channels, and only thin units of gravel and sand were deposited. Glaciofluvial sediment was also deposited in eskers, some of which are located within Nye channels, and other ice-contact features. Small eskers and hummocky glaciofluvial deposits commonly occur within valleys or depressions where ice stagnated. Proglacial channels differ in direction and were controlled by the local topography. West of Carp Lake, thick units of sand and gravel were deposited in a series of proglacial and lateral channels that formed large outwash plains. These and other large plains along the McLeod, MacDougall and Salmon rivers were later incised, creating terraces.

Thick silty glaciolacustrine sediments occur in large river valleys and most low-lying areas to the south. Holocene gully erosion has created steep slopes in some of these deposits, making them susceptible to mass wasting. Glaciolacustrine sediments in the northern part of the study area are rare, generally occurring in valleys as thin, coarse-grained sand or gravel typical of more ice-proximal deposits.

Soon after the ice retreated, katabatic winds mobilized silt and sand from unvegetated glaciofluvial and glaciolacustrine deposits, creating aeolian blankets, veneers and dunes.

Although thin, these deposits are extensive throughout the study area. Fluvial deposits are typically restricted to floodplains within meltwater channels. Organics deposits are commonly associated with fluvial deposits, abandoned meltwater channels and small lakes, but occur in depressions on all poorly drained sediments such as till, glaciolacustrine sediments, or on bedrock.

4. Ground penetrating radar survey and optical dating of aeolian landforms

A detailed study of aeolian sediments was carried out because they occur throughout the study area and can provide information on the absolute chronology of deglaciation. Aeolian sediments were imaged using a ground penetrating radar and dated by optical dating.

4.1. Ground penetrating radar

Ground penetrating radar (GPR) supplemented with geomorphic, sedimentological and stratigraphic data was used to determine the architecture of aeolian landforms. The objectives of the investigation were to determine: 1) the three-dimensional form of the aeolian deposits; 2) how the surface form of the aeolian sediment compares to that of its substrate; and 3) the internal structure of the deposits.

GPR has been used to study both aeolian (e.g. Jol et al. 2002; Hugenholtz et al. 2007, 2008) and glaciofluvial deposits (e.g. Jol 2007; Burke et al. 2010). GPR creates a radar image of the subsurface through the generation, transmission, reflection and reception of discrete pulses of high frequency electromagnetic energy (Neal 2004). A transmitter generates an electromagnetic (EM) wave that propagates downwards through earth materials with differing electrical properties, which alter its velocity. When the velocity change reaches a threshold, some of the energy is reflected back to the surface. The reflected energy is detected by the receiving antenna, and the time between the signal being sent and received, the two-way travel time, is recorded. The depth of a reflector is determined by multiplying the two-way travel time by the average signal propagation velocity. A series of traces collected along a survey line creates a two-dimensional profile of reflective subsurface features. A more comprehensive explanation of the

theoretical aspects of GPR and a review of its applications and limitations are provided by Neal (2004).

4.1.1. Study locations

Two of the aeolian deposits sampled for optical dating were chosen for detailed investigation because they have limited vegetative cover due to recent logging, are accessible by forest service roads and are not easily assigned a map unit based on surface expression (Fig. 4.1). The McLeod River site is located within ice-contact deposits in the northeast corner of NTS 093J14. A kettled outwash plain occurs at 740 m a.s.l and delta topsets at about 720 m a.s.l. The delta was later incised forming another plain at an elevation of about 690 m a.s.l. Data were collected on the highest plain, which has an undulating surface. No aeolian material was mapped on the lower plain or delta. GPR data were collected along two survey lines; one crossing a ridge between two adjacent depressions (mcleod1) and the other through the depression (mcleod2; Fig. 4.1).

The second site is located within a large southwest- and northeast-trending ice stagnation complex in the northwest corner of NTS map-area 093J12 (Fig 4.1). The survey was performed on an elevated glaciofluvial deposit, which is overlain in some places by aeolian sediment. Two northeast-trending meltwater channels occur on both sides of the study site, and hummocky to undulating gravel surfaces and eskers occur southwest and northeast of the plain. GPR data were collected along two survey lines that run perpendicular (ocock1) and parallel (ocock2) to a dune crest. A third line (ocock3) covers two terraces and adjacent scarps (Fig. 4.1).

4.1.2. Data collection

The GPR survey, totalling 825 m of line, was performed in October of 2010 using a Sensors and Software PulseEKKO 100 system. The GPR unit was connected to a computer for data acquisition and storage and to provide real-time display. The survey design was based on published parameters (Sensors and Software 1999; Neal 2004) and similar GPR surveys (Bristow et al. 1996; Jol 2002, 2007; Burke et al. 2010), but was modified after field tests. A common midpoint survey was carried out to determine

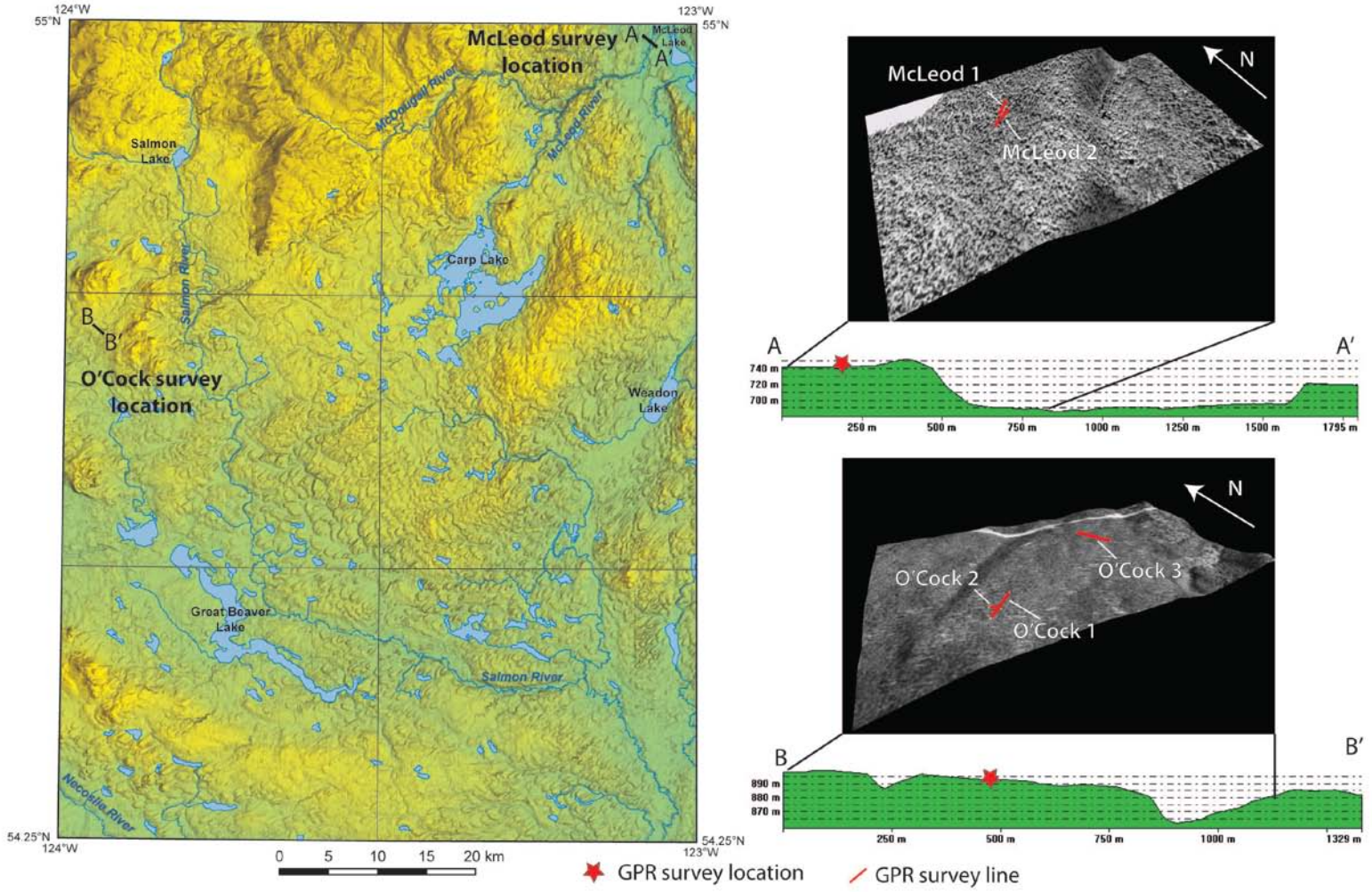

Figure 4.1 Location of GPR surveys with profiles of landforms and 3D images depicting specific line locations.

the average propagation velocity of the EM waves through the sediment. The signal, however, was weak and an accurate velocity could not be determined. Instead, a value of 0.1 m ns^{-1} was used, which is applicable to both unsaturated sand and

unsaturated sand and gravel (Neal 2004). The accuracy of the propagation velocity was later confirmed by excavating pits and augering. Radar profiles were produced with data from common offset surveys with a copolarized, perpendicular broadside antenna setup using 200, 100 and 50 MHz antennas and a trace stacking value of 16 (Fig. 4.2). The 200 and 100 MHz antennas were separated 1 m, and 10-and 25-cm step sizes were used, respectively, for data collection. The 50 MHz antennas were separated by 2 m, and a 50-cm step size was used for data collection. The vertical resolution of the survey is a function of the wavelength of the GPR signal. The wavelength of the signal is calculated using the formula:

$$Wavelength = \frac{v}{f} \quad (1)$$

where v is the average propagation velocity of the substrate and f is the frequency of the antennas. The vertical resolution is one quarter of the wavelength and can be calculated using the formula:

$$Vertical\ resolution = \frac{\left(\frac{v}{f}\right)}{4} \quad (2)$$

Using formula (1), the wavelengths are calculated as: 2 m at 50 Mhz; 1 m at 100 Mhz; and 50 cm at 200 Mhz. Using formula (2), the vertical resolution of this survey is calculated as: 50 cm with the 50 Mhz antennas; 25 cm with the 100 Mhz antennas; and 12.5 cm with the 200 Mhz antennas.

A series of onsite tests were conducted to determine which antenna frequencies would be used for each line. All three antennas were used for mcleod1 and mcleod2. One hundred MHz antennas were used for the three GPR lines at the O'cock site. In addition, the 200 MHz antennas were used at ocock1 and the 50 MHz antennas were used at ocock3. Any surface features, such as large stumps that would have interfered

with the radar were noted during data collection. Topographic variations along the survey lines were recorded with a Leica differential GPS system 500 and were later added to the GPR profiles.

Figure 4.2 Ground penetrating radar unit set up with copolarized, perpendicular broadside 100 Mhz antennas with 1 m separation. Unit was removed from sled for 50 Mhz antennas with 2 m separation.

Independent sedimentological and stratigraphic data were provided from soil pits and auger holes. During initial data collection, one reference soil pit was hand-excavated adjacent to the GPR survey lines at each site. Sediments were described based on unit thickness, texture and structure. After the initial analysis of the GPR data, ocock1, mcleod1 and mcleod2 were chosen for further ground-truthing in 2011 using an Eijkelkamp extendable auger with an Edelman head. However, only the O'Cock site could be revisited due to a road washout. The survey line was augered at 10 m increments. In each hole, the depth of the aeolian and glaciofluvial contact was recorded and samples were taken from above and below the contact and sieved for grain size.

General observations and measurements were made of the landforms around both the McLeod River and O'Cock Road study sites. Hillock crests were traversed and mapped

using a handheld GPS, and the track logs were plotted to illustrate the orientation of the landforms. Multiple locations beyond the lines of the GPR survey were augered with a 1.5 m non-extendable auger to provide additional subsurface data. Dip directions of aeolian bedding were measured throughout the study sites and descriptions of the shape, size and distributions of the landforms were made.

4.1.3. GPR processing

The GPR data were processed using Sensors and Software's EkkoView Delux version 1 release 3. The GPR signal was inexplicably weak, commonly having similar amplitudes to the background noise, and therefore required significant processing to isolate the signal of the subsurface reflectors (Fig. 4.3). The source of the weak signal is unknown and was apparent in all surveys.

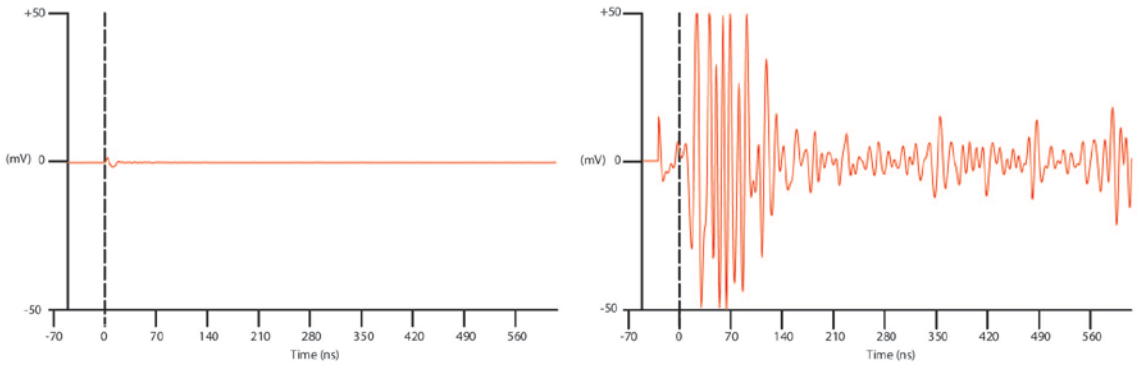

Figure 4.3 Example of an individual trace before (left) and after processing (right). The initial large reflection signal is the arrival of the air and ground waves. The later reflection signals are from subsurface reflectors. Signal loss occurs at ~140 ns. The cause of the weak signal is unknown but was apparent in all surveys.

Automatic time-zero corrections were applied to most lines and datum time-zero corrections were used for lines where time-zero drift occurred. A Dewow function was applied to remove any low-frequency noise due to signal saturation of the receiver. Saturation is an overload resulting from the short time interval between stacked transmissions and the large, nearly instantaneous, input of energy from the air and ground waves (Neal 2004). A vertical averaging filter was applied to each trace prior to application of a gain to remove some of the high-frequency noise before the signal was

amplified. An automatic gain control (AGC) function was used to amplify and equalize the signal down each trace by adding a gain that is inversely proportional to the signal strength. The AGC effectively amplifies the weaker signals at depth; however, it is not frequency-specific so any remaining background noise is also amplified. To overcome this problem, a bandpass filter was applied to isolate the specific antenna frequency. No horizontal (trace-to-trace) averages were applied because they commonly amplify flat-lying reflectors, which are generally background noise in these surveys. Topographic corrections were applied to the processed profiles and time distances were converted to depth using a 0.1 m ns^{-1} average propagation velocity.

4.1.4. Results and interpretations

Radar profiles from mcleod2 and ocock1 yielded the best results and will be discussed here. The remaining profiles are presented in Appendix A2. Radar profiles are divided into packages of similar reflectors, and interpretations are made based on the geometry of the reflective surfaces, augmented with the other field data. Interpretations were drawn from multiple radar profiles, created using several different processing variables that highlight reflections at different orientations. The best overall radar profiles were chosen for the figures. Reflective surfaces interpreted from profiles generated using different processing variables may be difficult to identify in the displayed profiles.

McLeod River site

The 2.1 m soil pit at the McLeod River site exposed two sediment units. Unit 1 consists of 1.55 m of very fine to medium sand. The upper 50 cm is heavily bioturbated with no obvious bedding. The lower ~1 m is only moderately bioturbated, and faint bedding is visible dipping at 4° to the southwest. Unit 1 conformably overlies unit 2, which consists of interbedded sand and gravel. Sand beds are coarse and range in thickness from 5 to 10 cm. The lowest exposed gravel layer is supported by clasts with an average size of 4 cm; the matrix is coarse sand. The gravel layers fine upwards to a coarse sand matrix-supported gravel with an average clast size of 1 cm.

Four traverses, between 26 and 62 m in length, were recorded with a handheld GPS to map the orientations of linear hillocks that resembled sand dunes. The orientations of the crests show little similarity and are not likely the result of aeolian deposition. Three

of the features were rounded and one was linear, trending southwest and northeast. Auger holes on crest of two of the hillocks revealed gravel at 1.4 and 1.6 m depth. A 2-m auger hole within a depression did not reach gravel. However, a single elongated clast with an a-axis of 8 cm was retrieved at ~1.75 m depth and is likely a dropstone and suggests the auger hole reached glaciolacustrine sediment.

Three radar packages (MRP1, MRP2 and MRP3) are identified in the mcleod2 radar profiles (Fig. 4.4). Reflective surfaces are visible from about 1 to 8 m depth; signal loss occurs between 8 and 10 m. The uppermost package (MRP1) is about 1.5 m thick on the sides and thickens to about 2 m in the depression. Reflective surfaces in MRP1 are obscured by the air and ground waves in the 100 Mhz and 50 Mhz radar profiles. In the 200 Mhz profile, discontinuous reflections are identified on the southwest slope and in the centre, dipping roughly at 35° and 30° northeast, slightly steeper than the ground surface. The remaining reflections in the centre and on the northeast slope are roughly parallel to the ground surface. The lower contact of MRP1 is defined by a continuous reflective surface (MRS1) that toplaps the dipping reflections in MRP3 and conformably overlies the flat-lying reflections in MRP2.

Radar package MRP2 is ~2 m thick and fills the depression between 22 and 44 m. The reflections are moderately continuous and slightly convex in the lower part of the package and become flatter higher in the profile. MRP2 and MRP3 are separated by an uneven reflective surface (MRS2). On the sloping sides, MRS2 separates the steeply dipping reflectors in MRP3 from the more flat-lying reflectors in MRP2. The horizontal limits of MRS2 are difficult to discern and may extend farther up the slope of the depression.

MRP3 underlies MRP1 on the slopes and MRP2 in the centre of the profile. It consists of flat-lying reflections on the crests that become steeper toward the centre on the slopes. There are no reflections in MRP3 between about 28 and 42 m. The GPR signal attenuates almost entirely between 723 and 725 m a.s.l. Below this are two faint hyperbolae, indicating the presence of strong point source reflectors.

MRP1 represents a blanket of aeolian material. The surface expression of the aeolian material is nearly identical to that of the underlying material. The discontinuous bedding

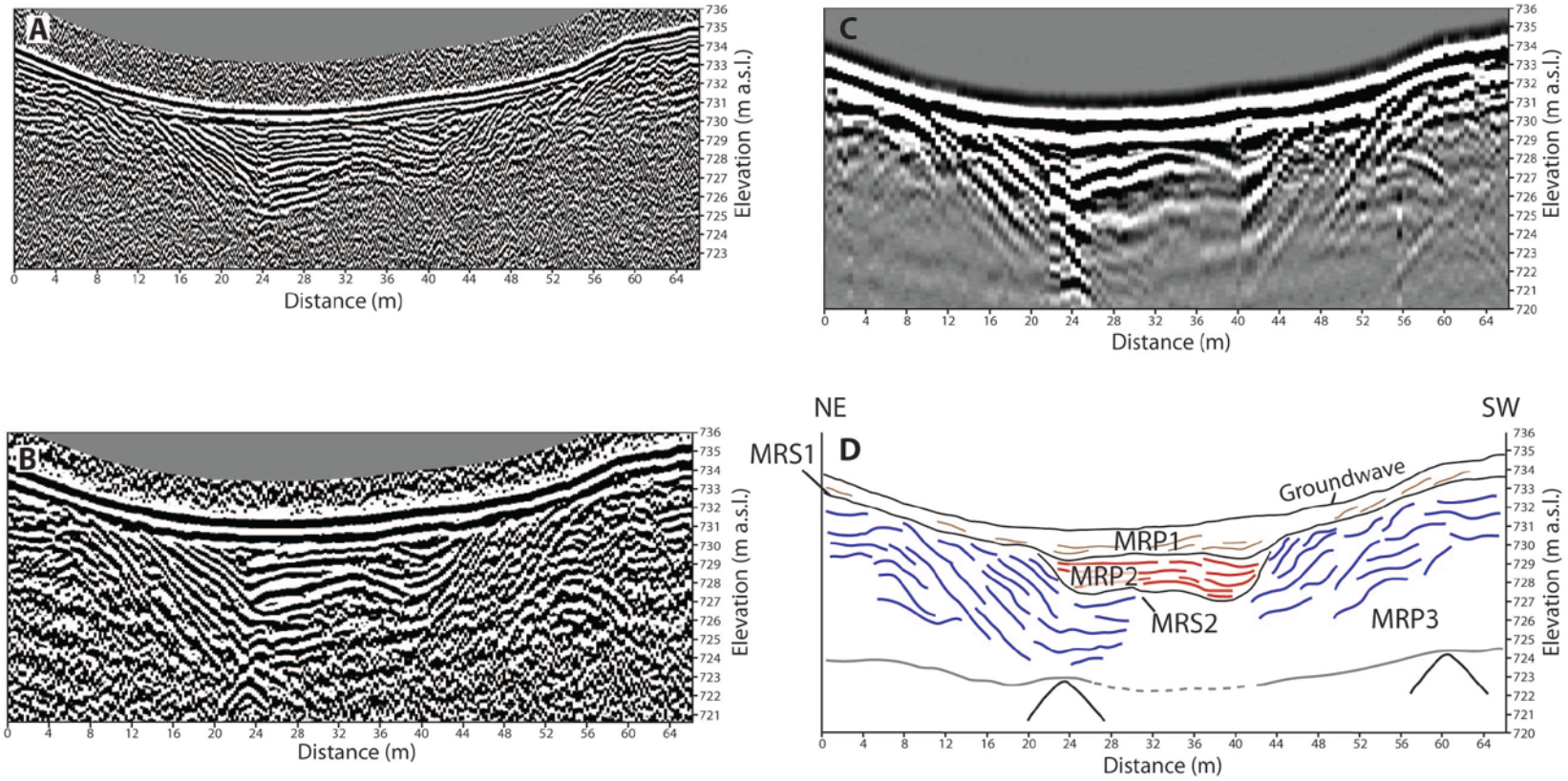

Figure 4.4 ***Radar profiles from GPR line mcleod2 at the McLeod River GPR survey site. Interpretations (D) were made from data collected using 200 Mhz (A), 100 Mhz (B) and 50 Mhz (C) antennas. The lowest package, MRP3, is interpreted as an ice-contact glaciofluvial deposit. MRP2 is interpreted as glaciolacustrine material that has infilled the depression and MRP1 is an aeolian blanket that overlies both.***

reflections are likely caused by the undisturbed finer sand beds noted in the soil pit. The approximate 35° dip angle of the bedding reflections on the southwest side of the radar profile is consistent with stoss-side bedding in sand dunes documented in GPR surveys by Bristow et al. (1996). Similarly, the surface parallel reflections on the northeast side are consistent with leeward bedding, and suggest that the aeolian material was transported in a northeast direction.

The bedding reflections in MRP2 are strong and mostly continuous, which suggests a continuous difference in composition between the beds. This characteristic is more consistent with lacustrine than aeolian sediment, which has less distinctive bedding and in this survey, creates discontinuous reflections. MRP2 was likely deposited during a local ponding event associated with kettle formation. The dropstone found in an adjacent depression indicates that ponding also occurred there.

MRF3 consists of glaciofluvial material, likely interbedded gravel and sand beds, similar to those exposed in the soil pit. The dipping reflectors represent soft-sediment deformation and faulting due to melt of buried ice and possibly sediment gravity flows into water within the depression. The two point source reflectors are likely boulders within till, which is consistent with the loss of the GPR signal.

O'Cock Road site

A single unit of very fine to fine sand is present in the 1.9-m deep soil pit at the O'Cock Road site. The unit is heavily bioturbated in the upper 1.5 m with minimal visible bedding. Below 1.5 m, the bioturbation is less extensive and visible bedding dips 28° northeast. Figure 4.5 depicts the location of the auger holes along the survey line and the depths at which the contact between the aeolian and fluvial sediments occurs. Grain-size analysis indicates that the aeolian material, which is dominated by very fine sand, is only slightly finer than the glaciofluvial fine sand (Fig 4.5). Therefore, the contact is defined by only a slight change in grain-size, except were 1 – 3 cm-thick silt beds were noted within the auger holes at 60, 70 and 80 m along the profile. Four sites beyond the GPR lines were augered to a depth of 2 m. Initial interpretations were that glaciofluvial material was not reached; however, augering was done before the grain-size analysis was performed, and due to the similar texture of the aeolian and glaciofluvial sediment, the contact may have been overlooked.

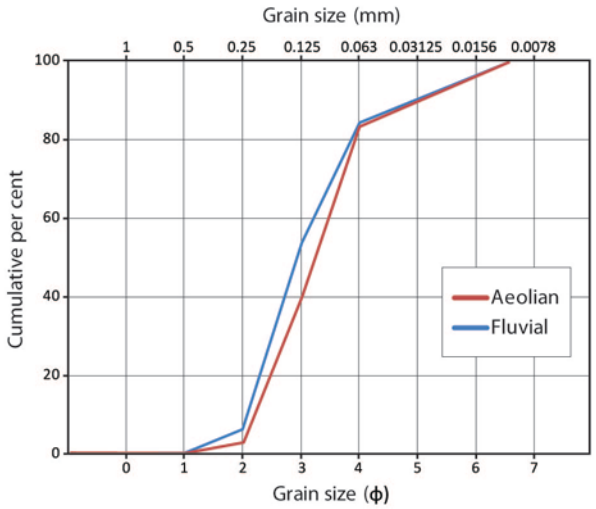

Figure 4.5 ***Cumulative percentage graph for aeolian and glaciofluvial materials at the O'Cock Road survey site. Samples were collected above and below the contact at 10 m intervals along GPR line ocock1. For each material, size fraction weights were combined and divided by the total weight to determine percentages.***

Two radar packages (ORP1 and ORP2) were identified in the ocock1 radar profiles (Fig. 4.6). A reflective surface (ORS1) can be seen between 1 and 6 m depth and signal loss occurs between 7 and 8 m. The radar profiles are dominated by surface-parallel reflection multiples, or ringing, that may have obscured some subsurface reflectors. The cause of the ringing in this survey is unknown, but it could be a result of power overloads on antennas or the bouncing of the GPR signal between the antennas and a high-conductivity reflector (Sensors and Software 1999; Neal 2004).

Radar package ORP1 ranges in thickness from just over 1 m at the beginning of the profile, to about 3.5 m between 28 and 44 m. Several short discontinuous reflections dip ~18° southwest at 12 – 30 m and 74 – 84 m. Similar, short discontinuous reflections at 33 – 58 m dip ~30° northeast. The contact between ORP1 and ORP2 is defined by an uneven reflective surface (ORS1) that is difficult to follow across the profile and was mainly determined using depth measurements of the aeolian and glaciofluvial contact in the auger holes. Radar package ORP2 is dominated by flat-lying, moderately continuous reflections. The flat reflections parallel to the surface are not drawn in the interpretation because it is unknown if they represent structure or are a result of ringing. Several short steeply dipping reflections occur between 21 and 25 m and a series of concaved reflections occur between 52 and 60 m.

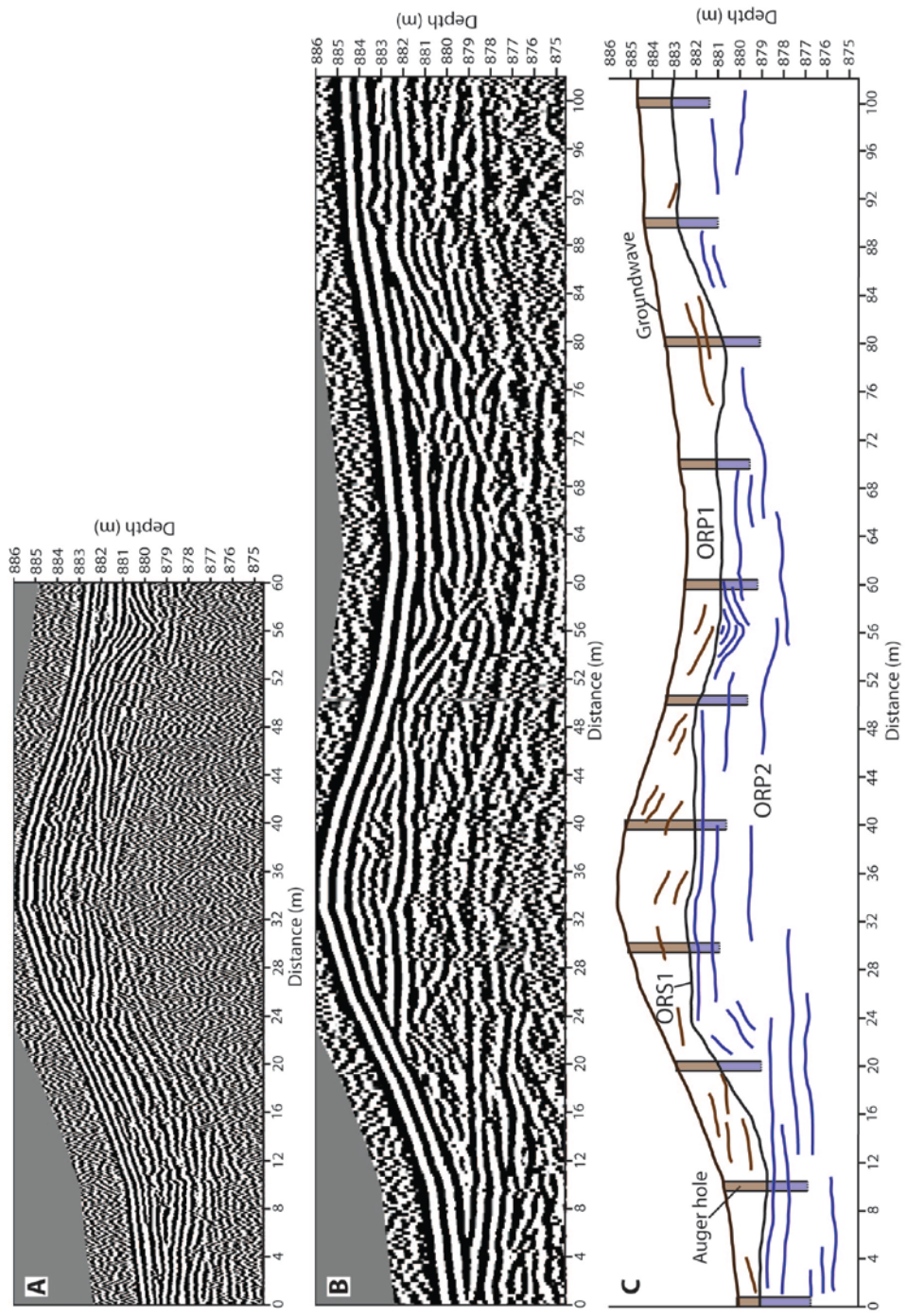

Figure 4.6 ***Radar profiles from GPR line ocock1 at the O'Cock Road GPR survey site. (C) Interpretations were made from data collected using (A) 200 Mhz and (B) 100Mhz antennas. The lower package, ORP2, is interpreted as a channelled glaciofluvial plain. The overlying radar package, ORP1, is interpreted as an undulating aeolian unit.***

The lack of reflective surfaces in radar package ORP1 is attributed to the bioturbation noted in the soil pit. The surface expression is similar to that of the underlying material (defined by ORS1), although the unit ranges in thickness from 1 to 3.5 m. The steeply

dipping beds to the northeast and less steep beds to the southeast suggest a northeast transport direction.

Radar package ORP2 is composed of sandy glaciofluvial material interpreted as a channeled outwash plain in an area of ice stagnation. The flat elevated areas depicted by radar surface ORS1 may represent bar forms. The steeply dipping reflectors could represent bedding in the bar. The lowest section, between 0 and 14 m is interpreted as a more active channel and the slightly higher section in the middle of the profile may represent a short-lived back channel. The concave reflections in the central channel (52 – 60 m) are consistent with scour-and-fill features that can occur in river beds; the thin silt beds noted in the auger holes may have been deposited in standing water left when the channel was abandoned or during overbank flows.

4.1.5. Summary of GPR

The GPR survey indicates that although the two regions have similar surface expressions, the internal geometry of the aeolian deposits is different, necessitating different map unit classifications. At the McLeod River site, the aeolian material has relatively uniform thickness (1.5 – 2 m) and the surface expression directly reflects that of the underlying material. Sediments at the McLeod River site are interpreted as ice-contact glaciofluvial deposits and discontinuous glaciolacustrine deposits overlain by a blanket of aeolian material. At the O'Cock Road site, the thickness of the aeolian deposit ranges from 1 to 3.5 m and the surface morphology is only slightly influenced by the form of the underlying material. The varying thickness and the development of a small dune crest suggest that this unit should be classified as undulating. Bedding structures measured in the radar profiles and the soil pits, at both locations, indicate northeast aeolian transport. I conclude that post-glacial aeolian units cannot be defined by surface expression alone. The orientations of hillocks may assist in determining if they are aeolian in nature, but ground-truthing is recommended when mapping.

At both survey locations, the aeolian deposits are thin and have not migrated beyond their source units. At the McLeod River site, aeolian material only occurred on the upper plains and not on the lower delta, indicating that aeolian activity ceased prior to the

formation of the lower delta. These observations suggest that aeolian activity was limited to a relatively short period and closely constrains the time of deglaciation.

4.2. Optical dating

The chronology of deglaciation in the study area is poorly understood (see Chapter 2). Radiocarbon dating is restricted by the lack of datable material from the earliest part of the post-glacial period. Regional radiocarbon ages suggest that ice retreated from the study area before ~11 000 cal yr BP. For this study, optical dating was performed on post-glacial aeolian material to determine when it was deposited, and thus provides a minimum age for deglaciation.

Optical dating measures the time elapsed since specific mineral grains (quartz and feldspar) were last exposed to adequate sunlight or heat, which for aeolian sediment, corresponds to the time since those grains were buried. The method is based on the fact that ionizing radiation in the environment produces free electrons in natural minerals that can be trapped within impurities and structural defects (Lian 2007). Exposure to light of a specific energy or energy range under controlled laboratory conditions ejects these electrons from their traps, and some recombine at other sites where excess energy is released as luminescence. The amount of luminescence emitted from a mineral is proportional to the radiation dose that it absorbed from the environment during burial in a landform.

Two measurements are needed to determine the optical age of a sample: 1) the laboratory dose of radiation, referred to as the equivalent dose (D_e), which produces the same amount of luminescence as the environmental dose; and 2) the rate at which the sample absorbed radiation in the environment after burial, referred to as the environmental dose rate. The optical age is calculated by dividing the equivalent dose by the environmental dose rate. Comprehensive reviews of optical dating can be found in Lian and Roberts (2006), Lian (2007) and Wintle (2008).

Aeolian sediment is a good candidate for optical dating because it is typically exposed to sufficient sunlight before burial in a landform, which is the most significant factor that can lead to inaccurate results (Lian 2007). Optical ages from these landforms indicate when

they formed and provide minimum ages for ice retreat. The true age for deglaciation is the optical age plus the time of aeolian activity before burial of the sampled sediment. Late Wisconsinan post-glacial aeolian material has been shown to provide good optical dating results when the mineral grains of interest have good luminescence characteristics (e.g. Bateman and Murton 2006; Wolfe et al. 2007). For this study, samples were collected from seven aeolian deposits throughout the study area (Fig. 4.7), four of which were processed and analysed (samples MLD1, CLR5, OCDF4 and OCDF5) and three were archived (samples MLD2, SRDF3 and SRDF6). No material suitable for independent dating control was found at the sample sites.

4.2.1. Sample collection and preparation

Samples were collected by inserting an opaque ABS tube (~15 cm long and ~8 cm in diameter) into a freshly exposed vertical section. Zones with evidence of bioturbation or other post-depositional disturbances were avoided as these processes can introduce grains with different light exposure histories to the sample. The exposed end of the sample tube was capped with an ABS slip cap and the tube was carefully excavated and the inserted end capped. All sample tubes were completely filled with material to keep the contents immobile and the slip caps were reinforced with duct tape to provide an air-tight seal to retain the as-collected water contents.

Under filtered light in the laboratory, all samples were sub-sampled to determine water content. The as-collected, saturated and dry weights were recorded and used to calculate the as-collected and saturated water contents. For each sample, about 20 g of sediment from the end of the tube was removed, dried and milled, and sent to a commercial laboratory where U, Th, and K concentrations were determined (discussed below), which is needed to calculate environmental dose rates. Material from the centre of the tube was extracted for optical dating.

Coarse-grained quartz (180-250 µm) and fine-grained feldspar (4-11 µm) were isolated from all processed samples for dating. Quartz was chosen because it is highly resistant to weathering and requires less exposure to sunlight to empty electron traps and effectively reset the 'luminescence clock'. However, in some cases quartz may not emit measurable luminescence (Lian 2007). Feldspar produces a higher intensity

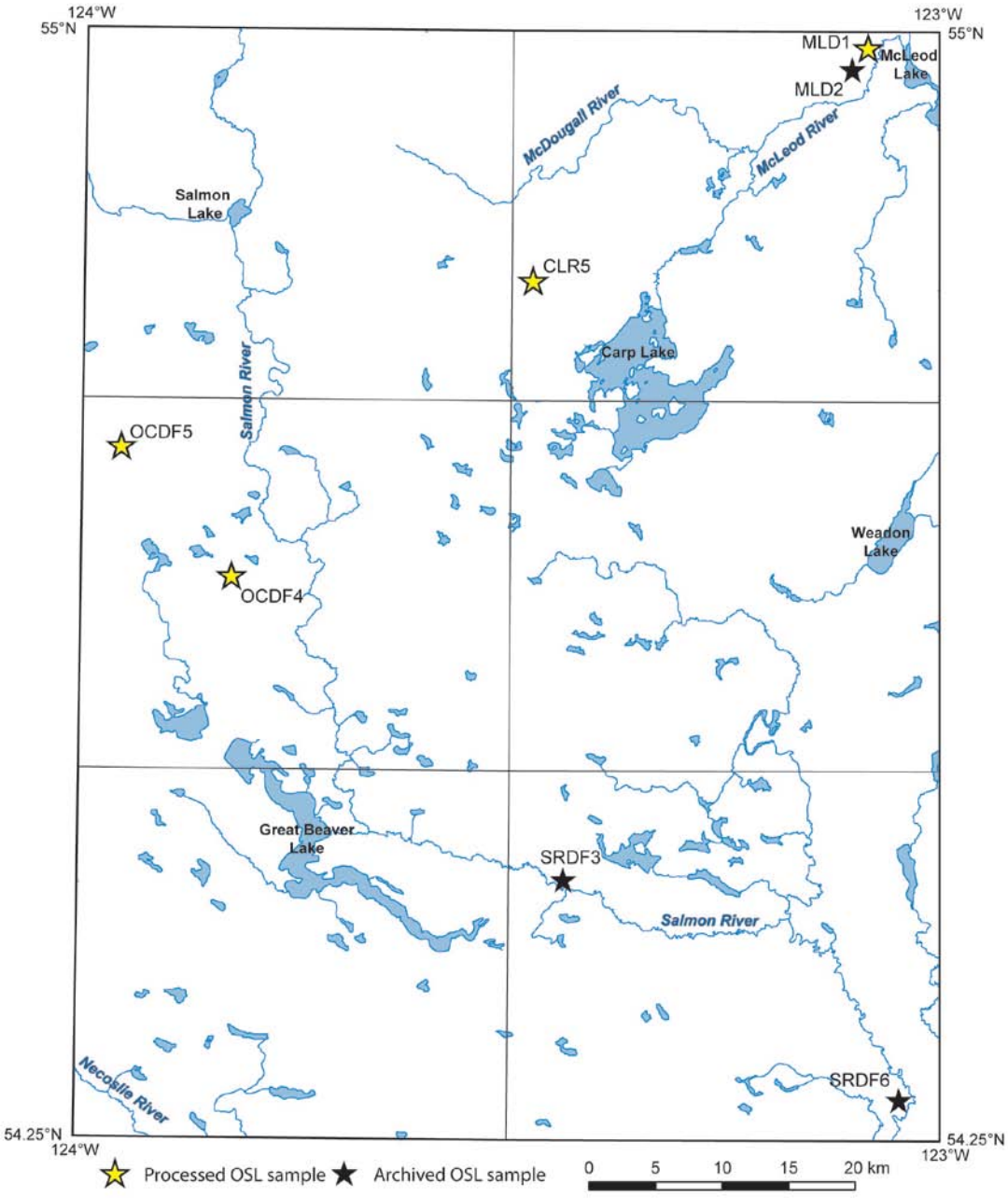

Figure 4.7 Location map of processed and archived optical dating samples.

luminescence signal, but it suffers from anomalous fading (discussed below). To mitigate this effect, the fine-grained size fraction of feldspar was used, as it is thought to be less susceptible to anomalous fading (Lian and Roberts 2006).

Material extracted for dating was first treated with a 10% HCl solution to dissolve any carbonates and then, after rinsing with deionized water, was wet-sieved to isolate the

180-250 µm size fraction; the fine-grained fraction was set aside. Quartz and feldspar were separated from heavier minerals using a sodium polytungstate solution with a density of 2.72 g ml^{-1}. Using a centrifuge, quartz and feldspar were then separated from each other in a sodium polytungstate solution with a density of 2.6 g ml^{-1}. The quartz grains were subsequently exposed to a 48% HF solution for 40 minutes to etch away alpha-affected surfaces and to dissolve any remaining feldspar grains. The feldspar fraction was exposed to a 10% HF solution for 20 minutes to etch away alpha-exposed surfaces.

The fine-grained polymineral fractions were treated with 10% H_2O_2 to remove any fine organic matter that might have been present. The sediment was then deflocculated by adding a 1 g L^{-1} solution of sodium hexametaphosphate and mechanically agitating the slurry on a shaker table. The 4-11 µm size fraction was isolated using the Stokes settling technique that is based on particle settling rates in a column of water. The >11 µm size fraction was removed by allowing the sediment to settle in a 20 cm column of water for 30 minutes and discarding the any settled (>11 µm) material. The <4 µm size fraction was removed by allowing the sediment to settle for 4 hours and discarding the material still in suspension (<4 µm).

Individual aliquots from each coarse-grained subsample were made by sprinkling about 100 grains of quartz on 9.8-mm diameter aluminium discs using silicone oil as an adhesive. Aliquots of fine-grained sediments were made by suspending the 4-11 µm fraction in acetone and pipetting 1 ml of the solution into vials with aluminum discs placed at their bottoms and allowing the acetone to evaporate.

4.2.2. Environmental dose rate determination

Environmental radiation absorbed by the samples after burial comes from alpha, beta and gamma radiation produced by the decay of U, Th, their daughter products, and ^{40}K in the sediment grains and in the surrounding environment. There is also a contribution from cosmic rays which decreases with depth beneath the ground surface. Subsamples extracted for dosimetry were sent to Becquerel Laboratories (Mississauga, Ontario) for neutron-activation analysis to determine the element contents (Table 4.1). Environmental dose rates were calculated using standard formulae (Aitken 1985; Lian et

al. 1995) and the dose rate conversion factors of Adameic and Aitken (1998). Pore water within the sediment attenuates or absorbs radiation differently from mineral matter and therefore must be accounted for in dose rate calculations. For each sample the as-collected water contents were used because it is unlikely that the well-drained sand-rich aeolian sediment was ever water-saturated (Table 4.1). A 10% uncertainty was included with each water content value to account for periodic wet or dry conditions. The contribution from cosmic rays was determined using the current burial depths and the formulae given by Prescott and Hutton (1994) (Table 4.2).

Table 4.1 Sample depths, K, U. Th and water contents.

Sample	*d* (cm)[a]	K (%)[b]	U (ppm)[b]	Th (ppm)[b]	Δ^{w} [c]
OCDF5 (feldspar)	180	1.33 ± 0.07	1.2 ± 0.13	2.6 ± 0.09	0.076 ± 0.008
OCDF5 (quartz)	180	1.33 ± 0.07	1.2 ± 0.13	2.6 ± 0.09	0.076 ± 0.008
OCDF4 (feldspar)	155	1.4 ± 0.1	0.9 ± 0.11	2.7 ± 0.12	0.047 ± 0.005
CLR5 (feldspar)	145	2.07 ± 0.08	1.3 ± 0.14	4.8 ± 0.16	0.046 ± 0.005

[a] *d*: sample depth beneath the ground surface.
[b] K, U and Th contents were determined using neutron-activation analysis.
[c] Δ^{w}: water content = water mass/mineral mass. As collected water contents with a 10% error applied were used for calculations.

Table 4.2 Dose rates, equivalent doses and optical ages.

Sample	$\dot{D}_c$ (Gy/ka)[a]	$\dot{D}_T$ (Gy/ka)[b]	D_e (Gy)[c]	Optical age (ka)[d]
OCDF5 (feldspar)	0.154 ± 0.0077	2.17 ± 0.15	17.6 ± 0.2	9.94 ± 0.77
OCDF5 (quartz)	0.154 ± 0.0077	1.79 ± 0.11	15.7 ± 0.7	8.79 ± 0.51
OCDF4 (feldspar)	0.161 ± 0.008	2.21 ± 0.14	23.8 ± 0.5	13.3 ± 1.0
CLR5 (feldspar)	0.163 ± 0.0082	3.27 ± 0.2	26.4 ± 0.3	9.35 ± 0.64

[a] $\dot{D}c$: dose rate due to cosmic rays, calculated using present day burial depths and the relationship of Prescot and Hutton (1994).
[b] $\dot{D}_T$: total dose rates due to cosmic rays and α, β and γ radiation.
[c] D_e : equivalent dose found using the central age model.
[d] Apparent optical ages (felspar ages corrected for AF) and their analytical uncertainties at ± 1σ.

4.2.3. Equivalent dose determination

Equivalent dose (D_e) determinations were carried out with a *Risø TL/OSL-DA-20* reader equipped with a $^{90}Sr/^{90}Y$ beta source that delivered 5.98 ± 0.12 Gy/min to coarse-grain samples and 5.24 ± 0.12 Gy/min to fine-grain samples. Quartz grains were stimulated using light-emitting diodes that delivered 45 mW cm^{-2} of blue (470 nm) light to the

sample aliquot; the luminescence measured was ultraviolet (~350 nm) detected by an Electron Tubes Ltd. 9235QB photomultiplier tube placed behind a single 7.5 mm-thick Hoya U-340 optical filter. Potassium feldspar on the polymineral fine-grained aliquots was stimulated preferentially using light-emitting diodes that delivered 135 mW cm^{-2} of infrared (870 nm) light; the luminescence characteristic of K-feldspars (~400 nm) was isolated using a Kopp 7-59 optical filter. A Schott BG-39 filter was used to absorb scattered infrared light. The photomultiplier tube was the same as that used for quartz.

A series of pilot D_e determination experiments were first conducted on 5-10 aliquots from each sample to determine the best measurement protocols. The pilot experiments indicated that quartz from samples OCDF4 and CLR5 is not suitable for dating because the measured luminescence was too dim or the samples behaved poorly (e.g. aliquots frequently failed recycling tests and/or their luminescence signal did not appear to consist of the desired fast component; see below). Pilot tests using K-feldspar from sample MLD1 yielded a preliminary age value of ~75 ka, suggesting that mineral grains with different light exposure histories, possibly glaciofluvial, were inadvertently sampled, so no further analysis was done on quartz or feldspar from this sample.

For all of the other samples, D_e values were determined using a standard single-aliquot regenerative-dose (SAR) procedure (Murray and Wintle 2000; see Fig. 4.8 for procedure details). Two additions were made to the procedure for quartz: 1) grains were treated with an infrared wash prior to the measurement of luminescence (Fig. 4.8b, step 3); and 2) after the measurement of luminescence from the test dose, aliquots were treated with an additional blue light stimulation at a higher temperature than the first preheat (Fig. 4.8b, step 9). The infrared wash removes any signal from feldspar contamination (Wintle and Murray 2006), which was only minor when it occurred. The additional blue light stimulation is intended to reduce the effect of thermal transfer of electrons from optically insensitive traps to optically sensitive traps that occurred during the second preheat (Fig. 4.8b, step 6; Murray and Wintel 2003). The SAR protocol used for the fine-grained feldspar samples was based on one found to be successful in dating the same mineral and particle sizes from eolian samples of known age near Clinton in the Southern Interior of British Columbia (W.L. Moon, pers. comm. 2011; see Fig. 4.8a for procedure details). For both minerals, a zero-dose point was included in construction of

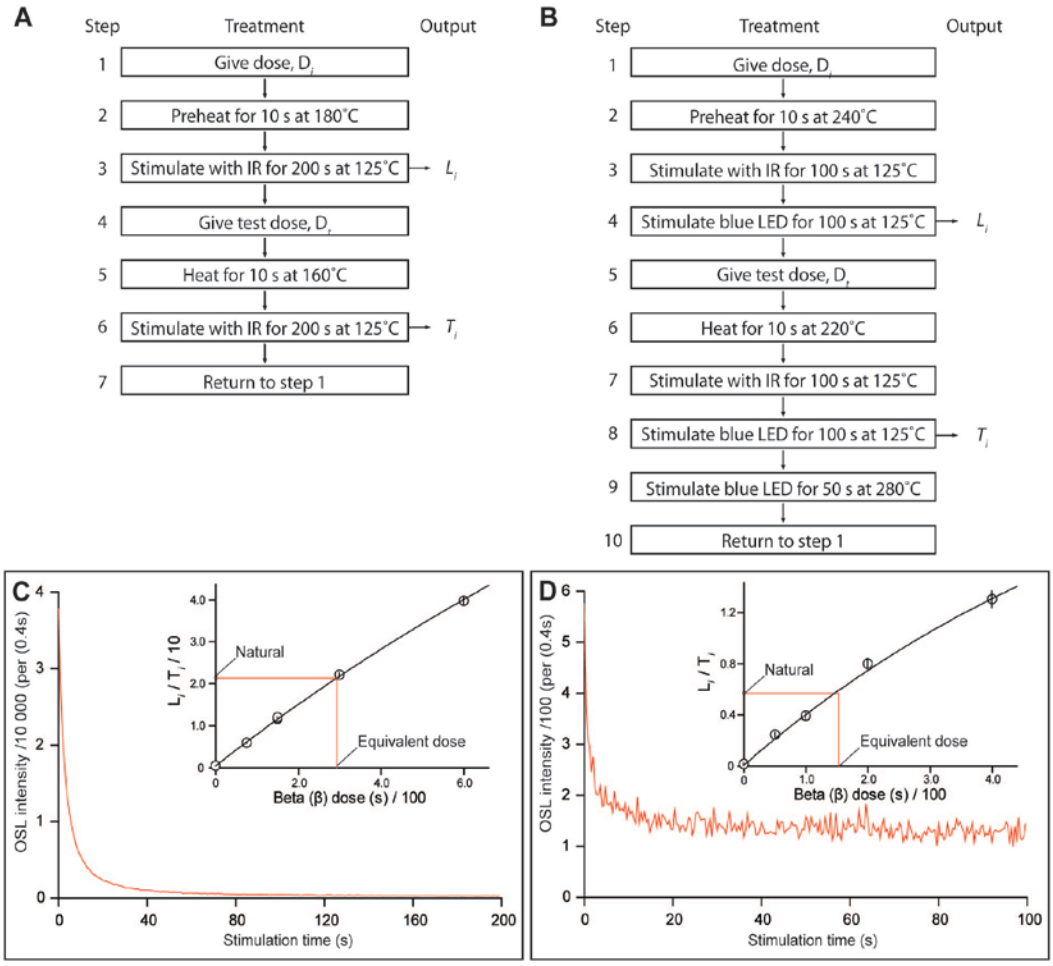

Figure 4.8 ***Modified SAR methods used to date feldspar (A) and quartz (B) fractions of samples. L_i is the luminescence measured after administration of a regenerative dose, D_i. Regenerative doses (i = 1 to 5) for feldspar were 6.55, 13.1, 26.2, 52.4 and 0 Gy and quartz 4.98, 9.97, 19.93, 39.87 and 0 Gy; the 0 Gy data point is used to check for thermal transfer resulting from the preheat, which lasted for 10 s at 180° C for feldspar and 240° C for quartz. T_i is the luminescence measured after a test dose of 0.87 Gy at a cut-heat of 160° C and 14.95 Gy at a cut-heat of 220° C for feldspar and quartz respectively. A higher D_t was used for quartz due to the limited luminescence produced from the grains. The 13.1 Gy (feldspar) and 9.97 Gy (quartz) doses were repeated for each aliquot to determine the effectiveness of the test dose for correcting for sensitivity change. Typical examples of luminescence decay curves for aliquots from OCDF4 (C; feldspar) and OCDF5 (D; quartz). Inset graphs show the dose-response data for these aliquots, determined from the sensitivity corrected luminescence (L_i/T_i) measured over the first 0.4 s of stimulation. The data are fitted with a saturating exponential curve, onto which the natural luminescence is interpolated in order to determine the equivalent dose (De).***

the dose-response curves to assess the severity of preheat-induced thermal transfer and one of the regenerative-dose points was repeated to assess the efficacy of the test dose to correct for sensitivity changes. The luminescence measured over the first 0.4 s of excitation was used to construct dose-response curves from which the D_e was determined by interpolation (Fig. 4.8c, d). Aliquots were rejected for D_e determination if the luminescence measured at the 0 Gy step was above 5 % of the natural signal or if the recycling ratio (repeated dose) was greater than 10 % of unity. D_e values for the accepted aliquots from each sample were plotted on radial plots, and the central age model (Galbraith et al. 1999) was used to determine the weighted mean equivalent doses used to calculate the optical ages (Fig. 4.9; Table 4.2).

Dose recovery experiments were performed on some of the samples to test if the first sensitivity measurement is appropriate to the natural signal in quartz samples (Murray and Wintle 2003; Wintle and Murray 2006). The dose recovery procedure involved exposing a number of aliquots to sunlight to empty relevant electron traps. A known laboratory dose, similar to the sample's D_e, was then given to the aliquots and the same SAR protocol used for the D_e determination was used to attempt to recover this dose. If the SAR protocol is working correctly and if the mineral is suitable for optical dating (i.e., it does not exhibit anomalous luminescence properties; *cf*. Demuro et al. 2008), the procedure should be able to recover the laboratory dose. For quartz, a successful dose recovery test may also indicate that the luminescence measured is dominated by that arising from the thermally-stable fast component of a sample's luminescence signal, and that there is not a significant contribution from the thermally unstable slow and medium components. Less is known about the structure of the luminescence emitted from infrared-stimulated K-feldspar, but it is likely that it arises from a continuum of traps that are thermally stable (Wintle 2008). Measurements on known-aged samples appear to confirm this hypothesis if anomalous fading is taken into account (O. Lian, pers. comm. 2012). Anomalous fading refers to the loss of electrons in thermally stable traps due to quantum mechanical tunnelling of electrons from the traps of interest to traps that are thermally unstable over geological time (Huntley and Lamothe 2001). If not corrected for, anomalous fading can cause erroneously low D_e determinations and result in calculated optical ages that are too young. Thus any discrepancy in the dose recovery test for K-feldspar can be attributed to the choice of an inadequate SAR protocol, or to

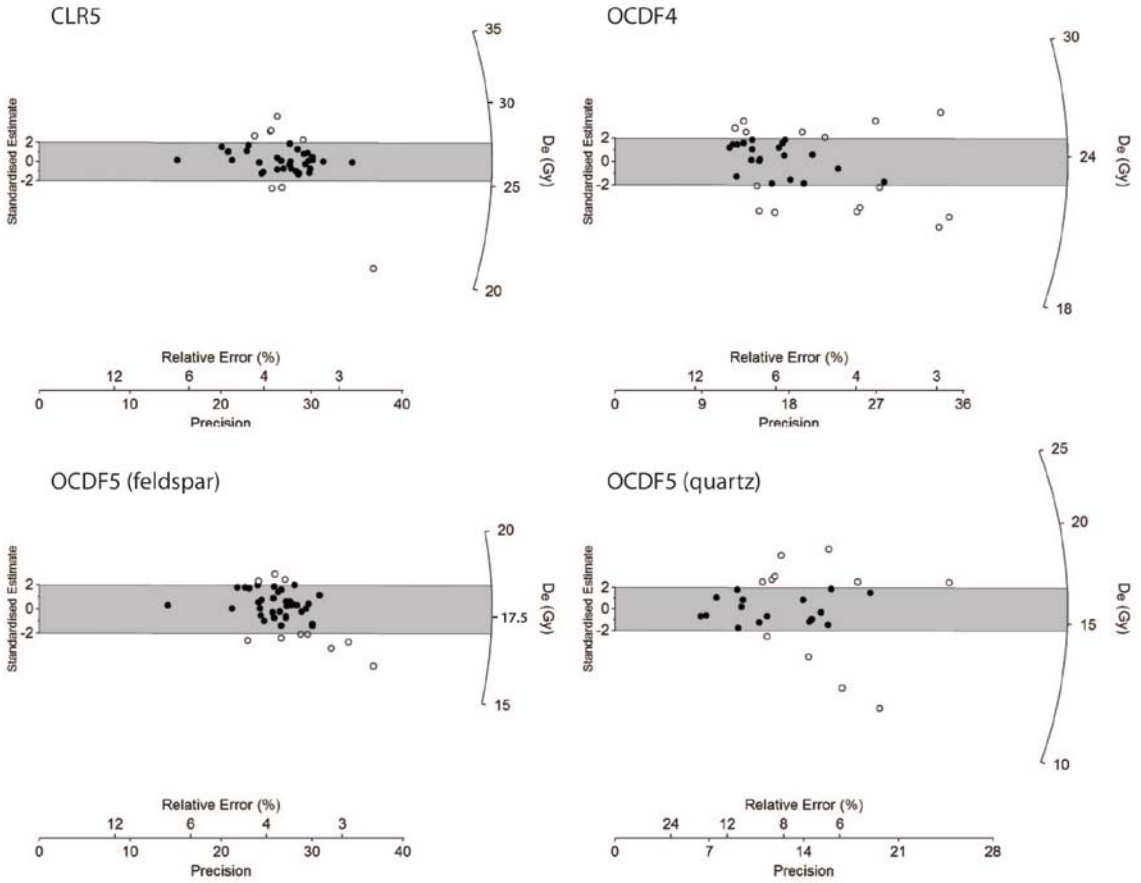

Figure 4.9 ***Radial plots showing the distribution of equivalent doses from each sample. More precise data plot farther from the origin. The gray bands are centred on the weighted mean equivalent dose values provided by the central age model and encompass aliquots with equivalent doses consistent with the mean at a 95% confidence interval.***

AF if there is a delay between irradiation and measurement.. The effect of the latter is best observed if a significant delay is made between laboratory irradiation and measurement.

The dose recovery test for the quartz fraction of sample OCDF5 consisted of 20 aliquots exposed to sunlight for 30 minutes and subsequently given a beta dose of 19.7 ± 0.7 Gy (a value close to its pre-determined D_e). After 3 days, the aliquots were measured using the same SAR protocol originally used to date the sample. A dose of 13.9 ± 0.7 (~70%) was recovered, suggesting that the luminescence signal of the quartz is significantly influenced by the thermally unstable medium and/or slow components.

Dose recovery tests were conducted on feldspar samples CLR5 and OCDF4. For CLR5, 20 aliquots exposed to sunlight for 30 min and subsequently given a beta dose of 26.0 ± 0.5 Gy; after 44 days, a dose of 25.0 ± 0.2 Gy was recovered. For OCDF4, 38 aliquots were given a similar exposure to sunlight and a beta dose of 17.3 ± 0.4 Gy; after a delay of one day, 20 were measured and a dose of 16.1 ± 0.2 Gy was recovered. The remaining 18 aliquots were measured after a period of 425 days, and the difference in the recovered dose was negligible (within the uncertainties of the measurement). Both dose-recovery tests are in agreement, and suggest that a fading rate of no more than 2.0 ± 0.5 % per decade (*cf*. Huntley and Lamothe 2001) must be applied to correct for AF in the fine-grained K-feldspar fraction of these samples. Based on the success of the experiments, using the same SAR protocol, on aeolian material in the lower Fraser River valley, it is unlikely that a significant part of the small difference in given and recovered dose was due to inadequacy of the chosen SAR protocol. However, more fading tests should be done to confirm this assertion as the samples dated in this experiment and those from the lower Fraser River valley are about 300 km apart.

4.2.4. Optical ages and discussion

Sample OCDF5 yielded optical ages of 8.79 ± 0.51 ka for quartz and 9.94 ± 0.77 ka (corrected for AF using the method of Huntley and Lamothe 2001) for fine-grained K-feldspar (Table 4.2). Sample CLR5 yielded a K-feldspar age of 9.35 ± 0.64 ka (corrected for AF), and sample OCD4 yielded a fine-grained K-feldspar age of 13.3 ± 1.0 ka (corrected for AF). A potential source of uncertainty is the assumption that the dated sediments have had similar light exposure histories prior to burial. The underlying glaciofluvial material can have a very similar texture to the aeolian material (see GPR section), thus it is possible that some of this material was incorporated into the samples, resulting in anomalously old ages (e.g. MLD1).

The quartz fraction of OCDF5 yielded an age that is younger than all the feldspar results. Dose recovery experiments indicate that this is likely due to the influence of thermally unstable components in the luminescence signal, which is common in geologically young quartz sediment (O. Lian, pers. comm. 2012). The luminescence decay curve is composed of several components, of which only the fast component is thermally stable. The first 0.4 s of the luminescence signal was selected in an attempt to capture only the

fast component of the curve; however, it appears that despite this strategy a significant amount of luminescence from the thermally unstable medium and/or slow components was selected. This unwanted slow component is apparent in the example luminescence decay curve (Fig 4.8b). A decay curve dominated by the fast component will drop rapidly to the background signal over the first few seconds of stimulation. In the example curve, however, the influence of the medium and slow components is indicated by the more gradual decay to background levels between ~2 and 20 seconds.

Reported radiocarbon ages from west of the study area suggest that ice retreat should have occurred before ~11 300 cal yr BP (GSC-5891) (Plouffe 2000; see Fig. 2.4). The corrected feldspar ages from samples OCDF5 (9.94 ± 0.77 ka) and CLR5 (9.35 ± 0.64 ka) thus are younger than expected. It is possible that aeolian activity continued for over 1000 years. However, this explanation is not in agreement with the morphology of the landforms; if activity persisted for that length of time, the landforms should be better developed and some migration from their source areas would be expected. Alternatively, there may have been a brief period of aeolian reactivation. Between 8000 and 10 000 yr BP, the climate in the Southern Interior was warmer and dryer than it is today (Hebda 1995). If this climate trend extended north to the study area, some of the aeolian deposits could have reactivated, resulting in the younger optical ages. Furthermore, the apparent discrepancy between the expected age of deglaciation and the optical ages might be mitigated by modifying the experimental protocol. After these optical dating experiments were completed, it was found that, for fine-grained K-feldspar samples from the Fraser River valley, a higher preheat temperature (220 ^{0}C rather than 180 ^{0}C) resulted in slightly older ages, closer to the known age of the deposit (O. Lian pers. comm. 2012).

Sample OCDF4 (13.3 ± 1.0 ka) yielded a fine-grained K-feldspar age that is in better agreement with the reported regional radiocarbon ages, but is significantly older than samples OCDF5 and CLR4. If this age is accurate, it suggests there was a period of reactivation in a warmer and dryer climate. If the previously discussed modification to the experimental protocol resulted in older ages for all three samples, it is likely that grains with different light exposure histories were included in sample OCDF4, resulting in an anomalously old age. Alternatively, at two standard deviations the error associated with the ages overlaps at 11.5 ka, suggesting this is the true age of deglaciation.

These experiments demonstrate that K-feldspar is more reliable than quartz as a geochronometer in this region. However, the discrepancy between the optical age from sample OCDF5, does not match the statistically identical results of OCD5 and CLR5, thus the timing of deglaciation cannot be tightly constrained. Although difficult, the best resolution would be to obtain an independent, and reliable, means of dating the aeolian material in the region (e.g., using radiocarbon dating or tephrochronology). This would provide a means of testing variations of the SAR protocol (e.g. different preheat and cutheat temperatures, etc.) to achieve the best result. With this additional confidence in the ages, a more comprehensive explanation for the variation in ages could be determined. Also, experimenting with single grain analysis methods (Galbraith et al. 1999), on K-feldspar in this case, could assist by allowing the removal of grains with different light exposure histories.

4.3. Conclusions

Aeolian activity began immediately after ice retreat and ceased shortly after. The main evidence for this conclusion is that aeolian deposits are veneers and poorly developed dunes and the sediment was transported a short distance from the source material. The landforms did not migrate beyond their source units, which are typically quite large, thus it is unlikely there was a shortage of sediment. Instead, it is likely that the material was stabilized quickly after ice retreat by plant colonization or a reduction in catabatic wind velocity as the ice retreated. This, however, does not discount the possibility of a brief reactivation period. At the McLeod River GPR site, aeolian landforms were present on the upper plain and absent on the delta below. Therefore, aeolian activity in the area ceased prior to the development of the delta topsets, indicating that aeolian activity was limited to the period between the initial exposure of the upper plain and the formation of the delta topsets. As discussed in more detail in the deglaciation section, the elevation of the lake was controlled by the ice margin. The margin would only have to retreat about 40 km before the lake would have drained to the level of the delta. The rate of ice retreat is unknown; however, considering the relatively short distance the ice margin would have to retreat, the aeolian activity was probably limited to hundreds of years. These observations suggest that the chronology of post-glacial aeolian activity can potentially tightly constrain deglaciation.

Optical dating experiments demonstrated that K-feldspar is a better geochronometer than quartz in this region. K-feldspar yielded optical ages of 13.3 ± 1.0, 9.94 ± 0.77 and 9.35 ± 0.64 ka. The discrepancies between the ages make it difficult to assign a date for deglaciation. There are several possible explanations for these discrepancies: 1) all reported optical ages are correct; deglaciation occurred around 13 ka and there was a brief period of reactivation in some areas during climatic fluctuations; 2) none of the optical ages are correct and modification of the SAR protocol will result in older ages for OCDF4 and CLR5 that are consistent with present radiocarbon data and OCDF4 becomes anomalously old; or 3) at two standard deviations the age differences are within the error and deglaciation occurred during the period around 11.5 ka. To verify any of these theories, further experimentation and some independent dating control would be necessary. Although a confident date for deglaciation cannot be determined at this time, the results are favourable and with further experimentation this method could provide a widely applicable alternative to radiocarbon dating to constrain ice retreat.

5. Glacial history

In this chapter, stratigraphy, ice-flow data and the geomorphic relationship of deglacial landforms are used to describe the glacial history of the study area. The local glacial history is applied to the regional setting and modified models for regional ice-flow and deglaciation are presented.

5.1. Methods

Stratigraphic sections were visited and described in the summers of 2009 and 2010. Exposed sections were identified on aerial photographs, Google Earth™ and during field traverses. At each section, units were characterized using colour, texture, sorting, stratification, sedimentary structures and contact relationships. Units were photographed and their thicknesses measured using a hand-held laser range finder or tape measure. Elevations were measured in the field using a hand-held GPS; however, the reported elevations were determined from the DEMs to minimize relative errors between sections. Relative age relationships were determined by stratigraphic position.

The ice-flow history was determined using streamlined macroforms identified on aerial photographs and the DEM and supplemented with striations and till fabric data. Streamlined macroforms are oriented in the direction of the last ice flow sufficiently vigorous to form them (Boulton 1987; Benn and Evans 1996). Thus they typically record ice flow at the glacial maximum or early during deglaciation. Flutes indicate the trend of ice flow but not the direction, except where fluted bedrock has been plucked. Similarly, striations and grooves provide the trend of ice flow but not the direction unless indicated by the shape of the outcrop, or plucking. The lee side of drumlins and the tails of crag-and-tails and rat tails indicate the direction of ice flow.

Clasts fabrics in basal till are preferentially aligned in the direction of ice flow, although subsequent shearing or compressive ice flow may reorient some clasts (Clark and

Hansel 1989; Visser 1989; Hicock et al. 1996; Stokes et al. 2008). Fabric orientations were determined by measuring the a-axis trend and plunge of elongate clasts. Fifty clasts were measured at seven locations and 25 - 35 at six locations, due to low suitable clast contents and time constraints. Data was plotted using a Schmitt equal area projection in the lower hemisphere with Stereo32 Version 1.0.2. Three eigenvalues and eigenvectors were calculated using the same software. Eigenvalues were tested for significance following Woodcock and Naylor (1983). The principle eigenvector represents the average down-plunge orientation of clast a-axes. Because elongated clasts in till commonly plunge up-ice, the apparent ice-flow direction is inferred as 180° from the primary eigenvector. However, when dealing with multi-modal distributions, the eigenvector method may fail to illustrate the ice-flow direction (Hicock et al. 1996). Therefore, flow directions were inferred by considering the principle eigenvectors, a visual inspection of the clast orientation distribution and interpreted information about the local ice-flow.

Relative ice-flow chronologies were determined by several methods: measuring multiple clast fabrics at different depths within the same exposure; truncated rat tails; striations that are formed within grooves; and striations on lee surfaces that would have been protected from later ice-flow. These data were then incorporated into the ice flow history.

Establishing the pattern and style of deglaciation in areas of moderate relief relies heavily on the interpretation of sediments and landforms created by interactions between meltwater and ice (Fulton 1967). Locations of meltwater channels and ice-contact and glaciolacustrine sediments were used to determine the morphology of the glacier and drainage systems (*cf.* Fulton 1967; Plouffe 2000). These features were primarily identified on aerial photographs and supplemented with data collected in the field and from the DEM. The positions of lateral meltwater channels define successive positions of the ice margin. The extents of glacial lakes were determined through aerially extensive glaciolacustrine deposits combined with the elevations of spillways and delta topset beds. Tentative models of glacial lakes that formed and evolved during deglaciation are illustrated by flooding the DEM surface to the determined lake elevations. The accuracy of these models is limited by the error associated with the DEM. The extent of isostatic tilting is unknown in this region and not incorporated into the modeling.

The following sections describe the stratigraphic and ice-flow data used to determine the glacial history. The deglacial landforms are described in the mapping section and the geomorphic data used to resolve the pattern and style of deglaciation will be introduced with the glacial history.

5.2. Quaternary stratigraphy

Six Quaternary stratigraphic sections are described here (Fig. 5.1; Fig 5.2). Several other sections were investigated but are not reported here because they expose only one or two units that do not add to the glacial history. Sections DS-01/02/03/04 and /05 are in the same drainage basin. Section DS-06 is the only exposure located within the southern part of the study area. Three sections occur in natural bluffs on the McDougall River where post-glacial fluvial erosion has incised drift (sections DS-01, DS-02 and DS-03). Section DS-01 is 84 m high and reveals the internal geometry of a large drumlinized feature (Fig. 5.3a). At sections DS-02 and DS-03, the river has incised 21 – 26 m into sediment and up to 14 m into bedrock (Fig. 5.3b, c). These two sections occur under deglacial terraces. Section DS-04 is located south of the Carp Lake service road on the east side of a north-trending valley. The section borders an ice-marginal meltwater channel and was further exposed during road construction. Eleven metres of sediment are exposed above the road (Fig. 5.3d). Section DS-05 is located along Highway 97 on the east shore of McLeod Lake. The 6-m section was created during construction on the highway (Fig. 5.3e). Section DS-06 is a 6-m exposure near several south-trending meltwater channels and was created during the excavation of a gravel pit on the north side of Chief Road (Fig. 5.3f).

Nine units are informally designated to facilitate description and interpretation of the Quaternary succession (Table 5.1).

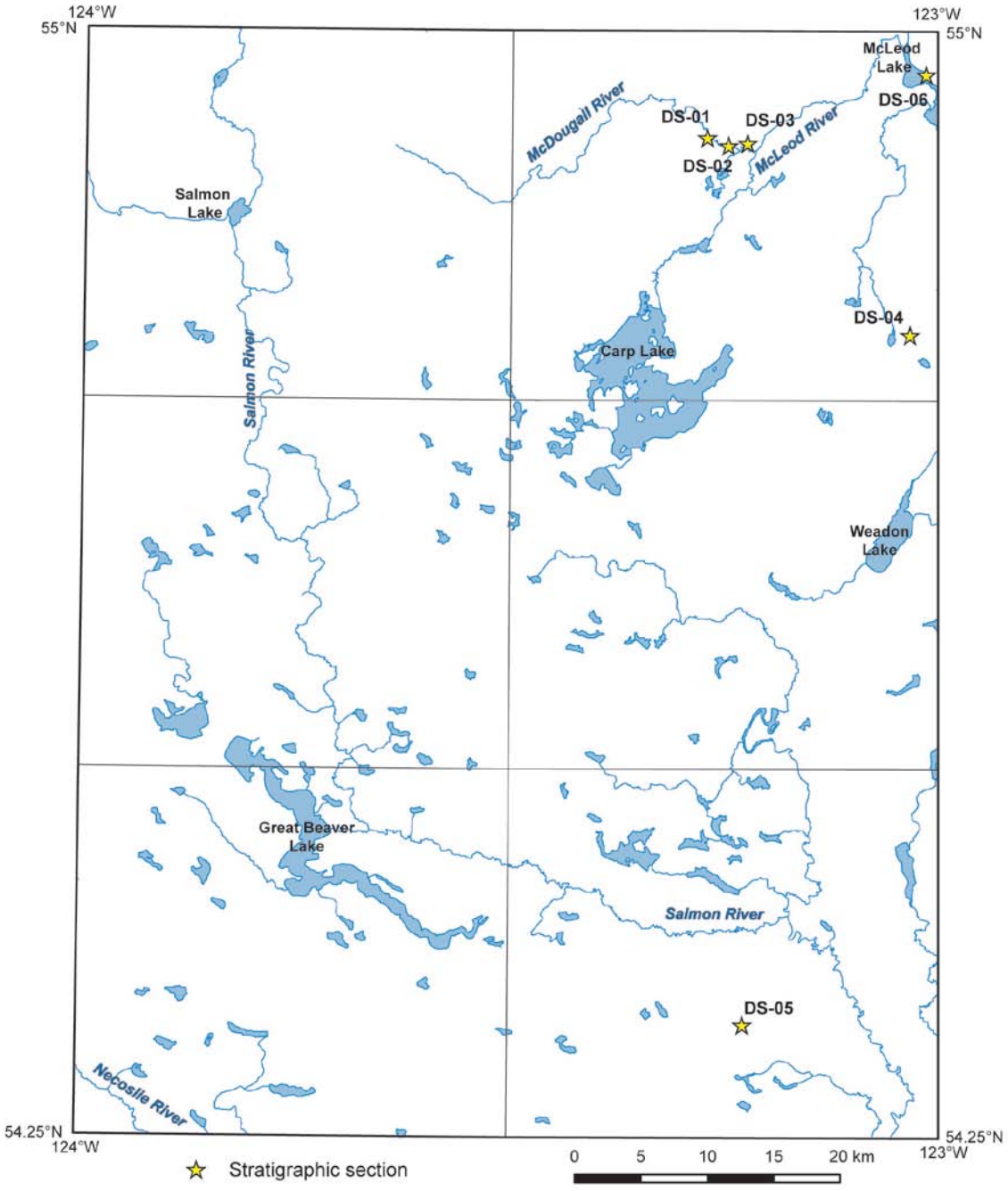

Figure 5.1 Locations of stratigraphic sections discussed in text.

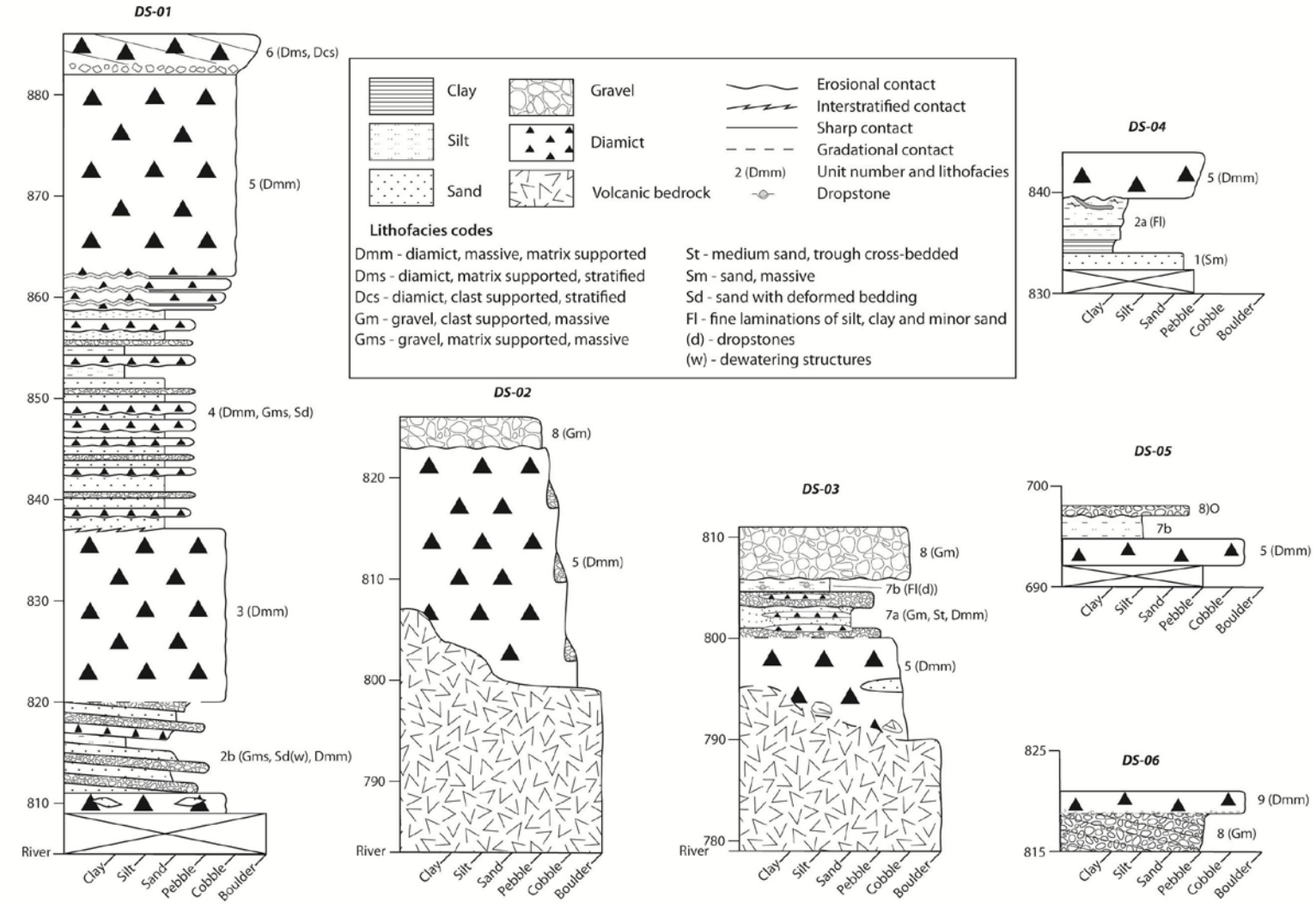

Figure 5.2 Stratigraphic logs from sections visited in the study area.

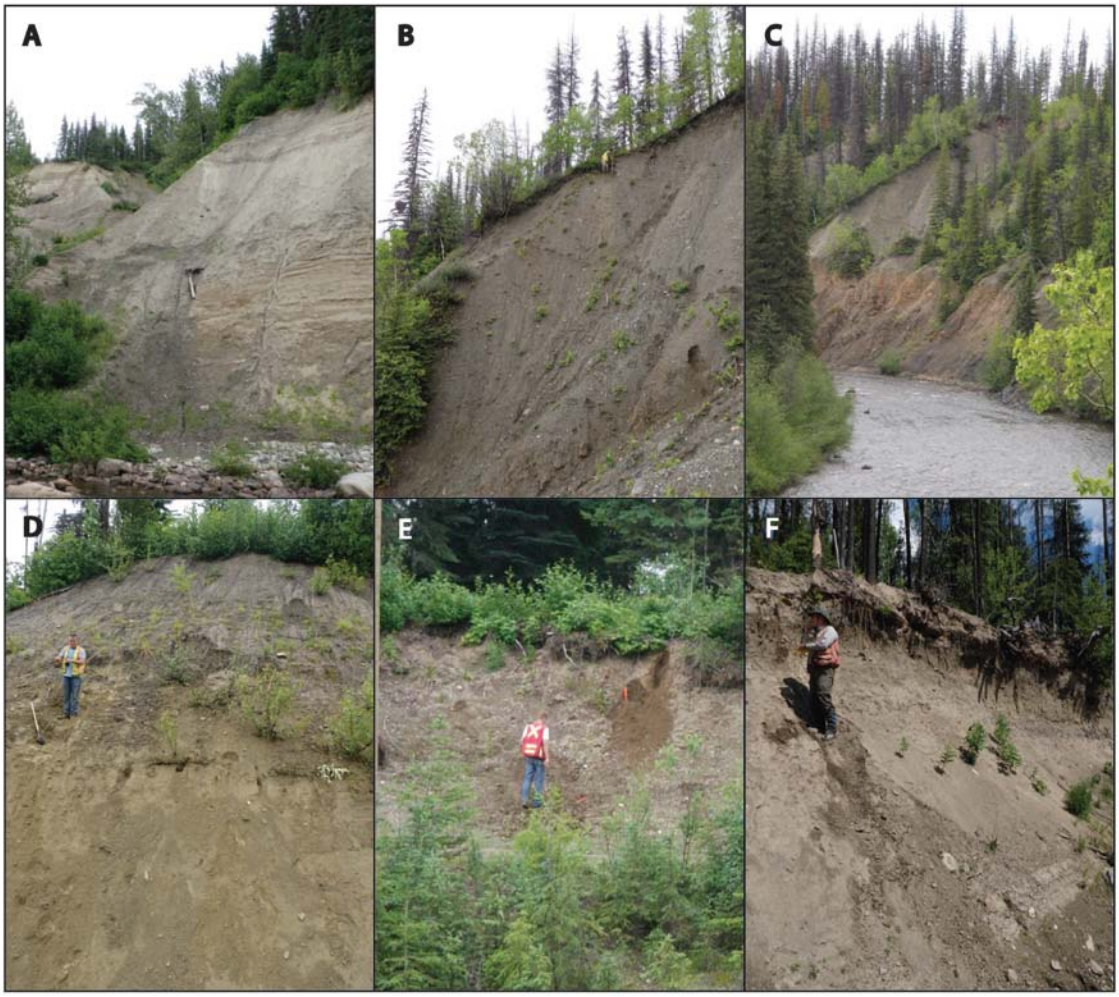

Figure 5.3 Stratigraphic sections described in text. A) DS-01; B) DS-02; C) DS-03; D) DS-04; E) DS-05; F) DS-06

Table 5.1 Summary of stratigraphic units.

Unit	Genesis	Geologic event
9	Glacial (Basal)	Fraser Glaciation (re-advance)
8	Glaciofluvial	Fraser Glaciation (retreat phase)
7	Glaciolacustrine	Fraser Glaciation (retreat phase)
6	Glacial (ablation?)	Fraser Glaciation
5	Glacial (basal)	Fraser Glaciation
4	Glaciolacustrine	Fraser Glaciation (advance phase)
3	Glacial (basal)	Fraser Glaciation (early advance (?))
2	Glaciolacustrine	Fraser Glaciation (advance phase)
1	Glaciolacustrine or glaciofluvial sand	Fraser Glaciation (advance phase)

5.2.1. Unit descriptions and interpretations

Unit 1: advance glaciolacustrine or glaciofluvial sand. Unit 1 was observed at section DS-04 and consists of >1.5 m of massive, moderately well sorted, medium and coarse sand. The sediment size and sorting suggests that this unit was deposited in a shallow lake or as outwash distal to the ice front. The first theory is favoured because there was no apparent bedding consistent with fluvial deposition. The lower contact of this unit is covered.

Unit 2: advance glaciolacustrine sediments. Unit 2 is divided into two sub-units and was observed at section DS-04 (unit 2a) and DS-01 (unit 2b).

Unit 2a is a 5.5-m coarsening-upward sequence of laminated and finely bedded clay, silt and sand with localized faulting and at least one clastic dyke (Fig. 5.4). The lowest portion of unit 2a is composed of laminated clay with minor silt layers that grade into dominantly silt laminations near the middle and finely bedded silt and fine sand at the top. Localized faulting is concentrated in the upper metre and around the clastic dyke (Fig. 5.4). The dyke is 10 – 15 cm thick and composed mainly of laminated clay that generally parallels the dyke walls. It penetrates both sub-horizontally and sub-vertically to a depth of about 1 m over a length of about 3 m. The deposition of clay and silt in unit 2a indicates distal sedimentation in a glacial lake. The upward coarsening indicates increasing energy levels likely due to advancing ice or higher flow regimes. Localized faulting in the upper section is interpreted as glacial tectonization. Brittle deformation around the clastic dyke laminations parallel to the dyke walls suggests it was injected into the substrate as the hydraulic pressure was increased from the overriding ice (*cf*. van der Meer et al. 2009).

Unit 2b occurs at section DS-01 (Fig. 5.5a). It comprises about 11 m of interstratified sand, gravel and diamict beds with an apparent dip of 10°. The bottom 2 m is a dark grey, silty, matrix-supported diamict containing massive to weakly stratified muddy sand lenses. It has 15% subrounded to rounded clasts, and the upper portion passes into 20 cm of normally graded fine sand and silt. The lower diamict is conformably overlain by 5 – 30 cm of undulating and discontinuous beds of fine to coarse sand, well rounded pebble gravel and minor lenses of diamict (Fig 5.5b). Fine sand beds in the upper part of this exposure contain soft-sediment deformation and dewatering structures (Fig 5.5c).

The lower contact is covered. This unit is interpreted as sediment deposited on a subaqueous outwash fan. The gently dipping, discontinuous sand and gravel beds were deposited as the fan aggraded into the water body. The diamict lenses are likely sediment gravity flow deposits resulting from small failures from the ice.

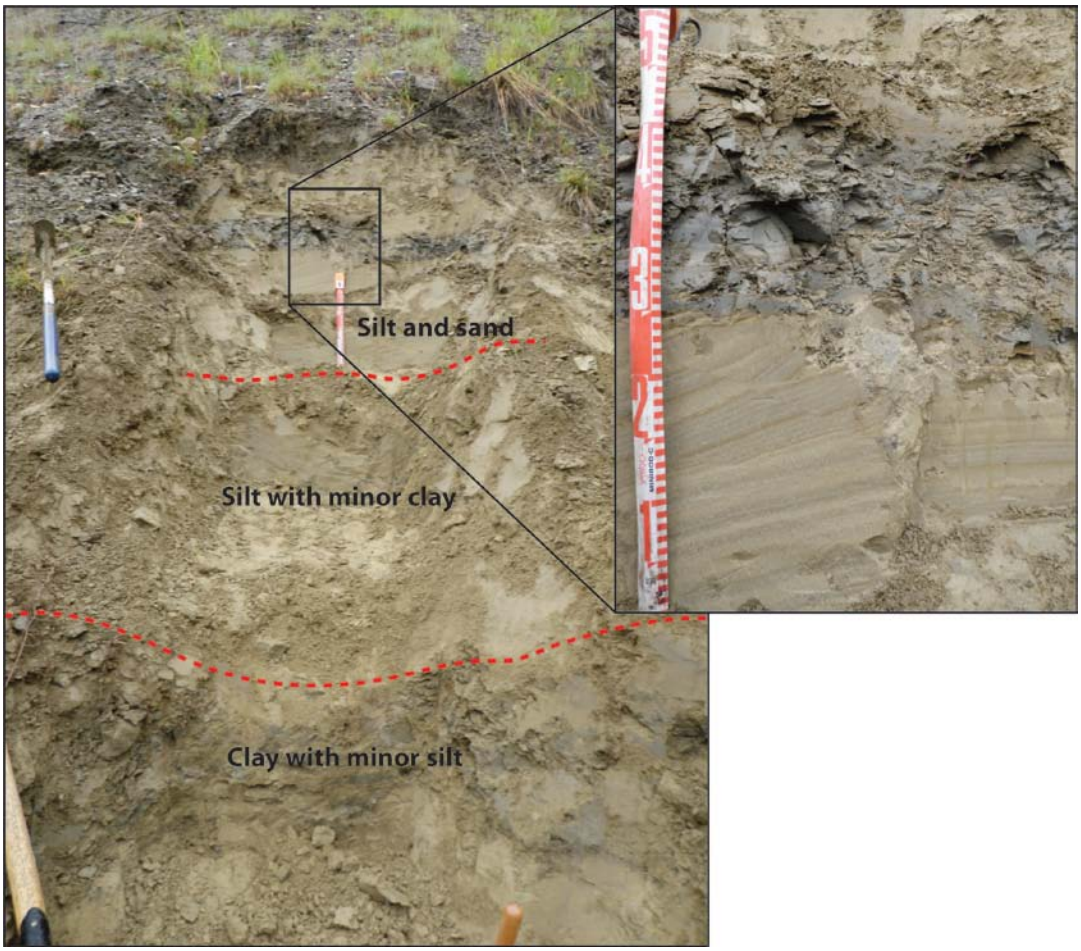

Figure 5.4 ***Coarsening-upward sequence of advance-phase glaciolacustrine material (unit 2a) exposed at section DS-04. Inset shows localized faulting and a clastic dyke injected into the unit when it was overridden by ice.***

Unit 3: lower basal till. Unit 3 is only observed at DS-01 where it comprises 15 – 17 m of dense, grey, sandy silty, matrix-supported diamict with fissility and jointing. It has 10 – 20% of mixed lithology clasts. Clasts are commonly striated and faceted. The lower contact is gradational over about 1 m with unit 2b (Fig 5.6b). This unit is interpreted as basal till based on sorting and the occurrence of fissility and jointing hat indicate overriding by a large ice mass. In the mixing zone, sand and gravel have been

incorporated into the till resulting in a slightly coarser matrix. The upper few metres of this unit contain interbedded sands associated with the overlying unit 4.

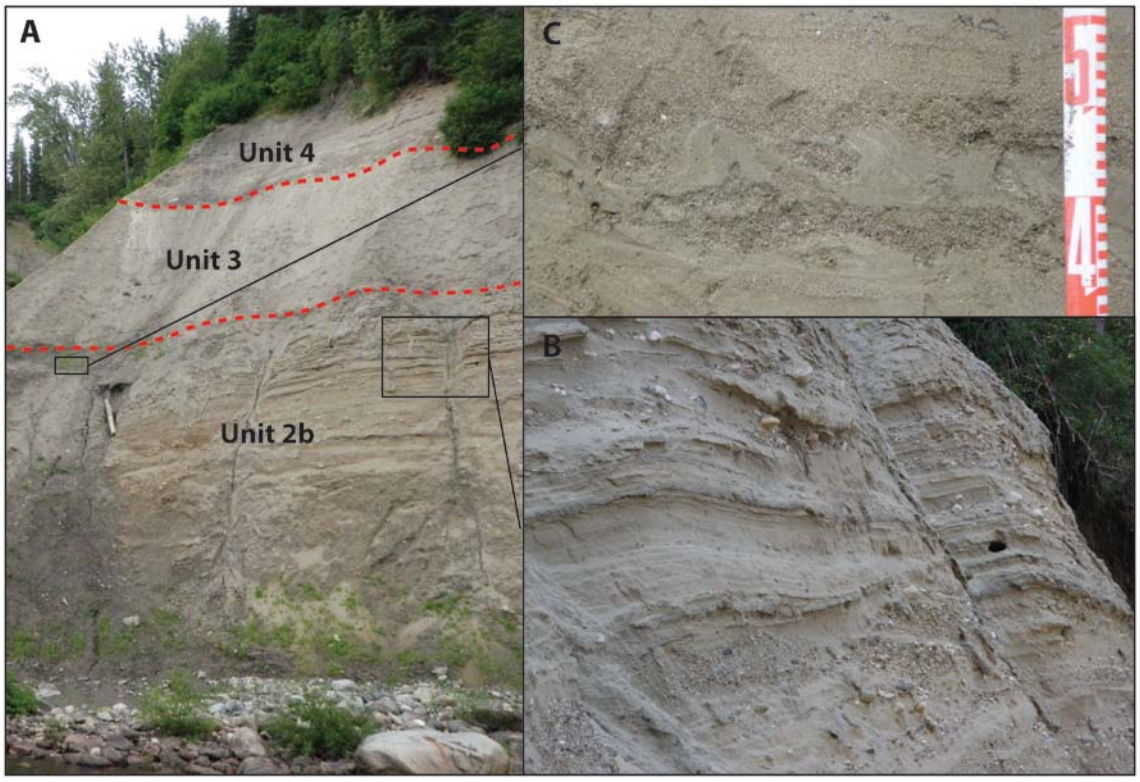

Figure 5.5 ***Lower exposure at section DS-01 exposing a subaqueous outwash fan (unit 2b) below an early advance till (unit 3; A). Insets show undulating, interstratified sand, gravel and diamict beds (B) and dewatering structures in the upper sand beds of unit 2b (C).***

Unit 4: *advance glaciolacustrine sediments.* Unit 4 occurs at section DS-01, overlying the lower basal till (unit 3). It is 20 – 25 m thick and dominated by ~1-m thick diamict layers and interbeds of coarse sand and moderately to well rounded pebble gravel between 0.5 – 1 m thick. Laminated and thin-bedded silt and fine sand beds occurs near the top of the unit. The lower contact is irregular, consisting of chaotically interbedded diamict and sand. Unit 4 was deposited in a glacial lake during an oscillation of the ice margin. It is similar to unit 2b, though the greater frequency of diamict beds suggests it may have been deposited in a more ice-proximal location. The

diamict beds may be flow tills. Thinly-bedded silt and sand deposited by underflows near the top of this unit indicate a temporary lower energy environment.

Unit 5: basal till. Unit 5 occurs in sections DS-01/02/03/04/05 and in most surface and shallow exposures throughout the study area. This unit was deposited during the Fraser Glaciation maximum based on stratigraphic correlation with other units at surface. Most of this unit is dark grey, except where it is exposed at the surface and the upper portion is light brown. Exposed thicknesses range from 5 to 25 m. The till is very dense and supported by a matrix of sandy silt that has good fissility and jointing. In the stratigraphic exposures, subangular to subrounded mixed-lithology clast contents range from 10 – 20%, although in other parts of the study area, clast contents of up to 30% were observed. The clasts in sections DS-02 and DS-03 become slightly more rounded and diverse in lithology higher in the exposures. Sorted lenses of sand were observed in section DS-03. It is possible that the lower parts of unit 5 in sections DS-02 and DS-03 were deposited during the early advance and are part of Unit 3. Thus the change in clast composition and the sorted lenses may represent the contact between the units. Until further investigation is conducted (e.g. till fabrics or tracing the source of clast lithologies), the entire till exposure is tentatively assigned to unit 5. The upper till unit at section DS-01 is assigned to unit 5 because it forms the surface of the drumlinized feature that the section occurs in. The lower contacts of basal till units are commonly erosive (DS-02 and DS-04; Fig. 5.6a), but may be gradational (DS-03) or interbedded (DS-01; Fig. 5.6c).

Unit 6: Ablation till. This unit was only observed from a distance at section DS-01, therefore only a limited description is possible. It is a crudely stratified diamict above the basal till (unit 5) ranging from 3 to 6 m thick. It is dominantly matrix-supported with some clast-supported areas. The clast content ranges from about 20 to 60%. The lower contact is defined by a thin, apparently continuous, poorly sorted, large cobbly gravel lag that is roughly parallel to the surface. This unit is tentatively interpreted as ablation till based on the sorting and crude stratification; however some parts that are more sorted could be glaciofluvial material.

Unit 7: Retreat glaciolacustrine sediments. Unit 7 is divided into two sub-units and was observed at section DS-03 (unit 7a and b) and DS-05 (unit 7b).

Unit 7a is about 6 m thick and fines upwards from well rounded pebble gravel into stratified, cross-bedded medium sand that is sharply overlain by another layer of pebble gravel. The lower contact is gradational over 5 cm with basal till (unit 5). Throughout the unit are discontinuous, 25 – 75-cm-thick, silty sandy matrix-supported diamict beds with sharp upper and lower contacts (Fig. 3.6a). Unit 7a is interpreted as ice-proximal subaqueous outwash. The alternation between sand and gravel suggests different flow

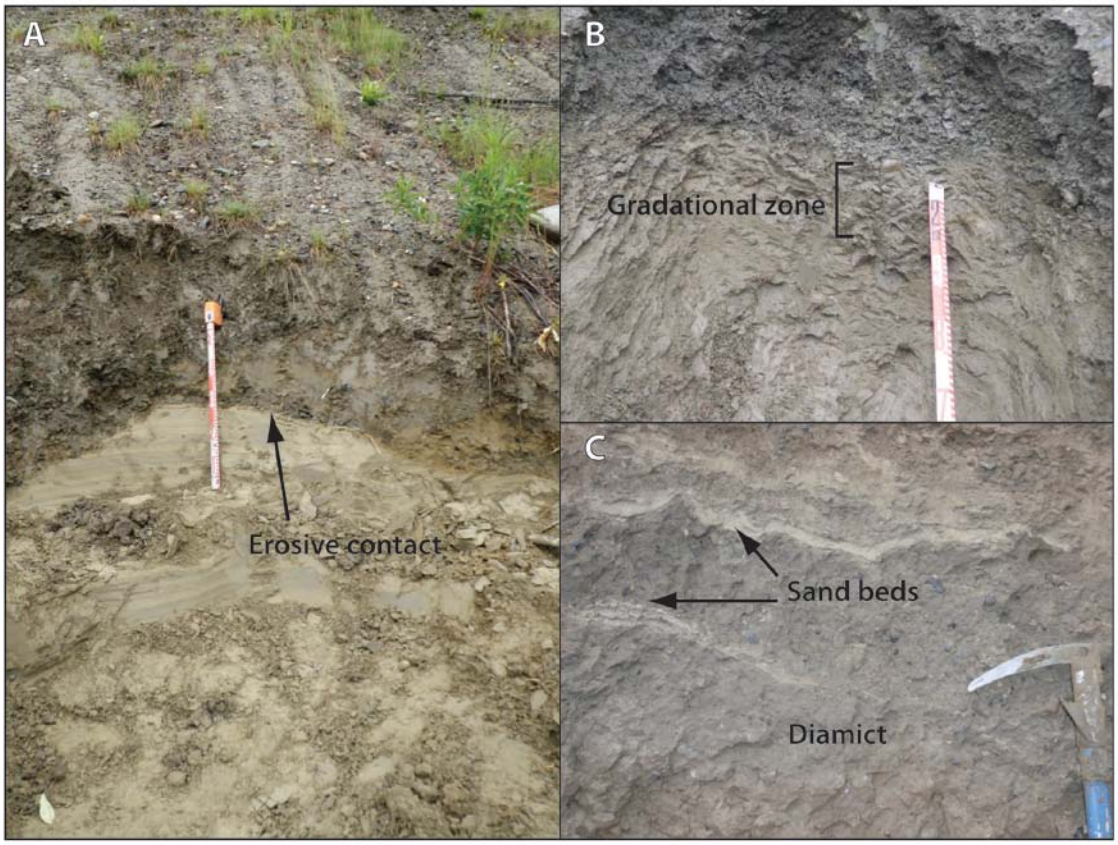

Figure 5.6 ***Lower contacts of basal till units. (A) Erosional contact with glaciolacustrine sediment (unit 2a) at section DS-04. (B) Gradational contact with subaqueous outwash (unit 2b) at section DS-01. (C) Till interbedded with sand (unit 4) at section DS-01.***

regimes, possibly due to different meltwater discharges or distances from the ice front. The discontinuous lenses of diamict were likely deposited by subaqueous debris flows.

Unit 7b consists of laminated and finely bedded silt and sand. At section DS-05, unit 7b consists of 2.1 m of laminated silt and fine sand with 1 – 3 cm clay beds at 10 – 20 cm intervals. At section DS-03, unit 7b consists of 1 m of laminated and finely bedded silt

and fine sand with dropstones. At both exposures, the lower contact is conformable, overlying proximal subaqueous outwash (unit 7a) at section DS-03 and basal till (unit 5) at section DS-05. This unit was deposited by underflows and suspension settling in glacial lakes.

Unit 8: retreat glaciofluvial gravel. Unit 8 occurs at sections DS-02/03/05/06 and in shallow exposures throughout the area. It is composed of moderately sorted to well sorted, rounded to well rounded, pebble to cobble gravel that generally fines upwards. Deposits are typically clast-supported with a coarse sand matrix. All exposed lower contacts are erosive. In stratigraphic exposures, these deposits range from <1 to 5 m thick, but may be thicker in large outwash corridors. At section DS-06, unit 8 is composed of moderately rounded to well rounded, moderately sorted gravel that coarsens and becomes less sorted upwards and shares a gradational upper contact over 10 cm with the overlying till (unit 9). At section DS-03 small pockets of this unit occur perched on narrow terraces in the till at 20, 29 and 35 m above present-day river level, indicating temporary high base levels during the post-glacial incision of the drift. This unit is interpreted as retreat glaciofluvial sediment based on its stratigraphic location over till.

Unit 9: Late re-advance (?) basal till. This unit was only observed at section DS-06 as a dense, dark grey, silty sandy, matrix-supported diamict with moderate fissility and jointing. It has a 20% mixed lithology clast content with stones that are moderately rounded; some are striated and faceted. Unit 9 is slightly less consolidated and considerably thinner that unit 5. This unit was deposited over ice-marginal glaciofluvial sediment (unit 8, section DS-06) during a minor re-advance of the ice front.

5.3. Ice-flow history

5.3.1. Streamlined macroforms: drumlins, flutings and crag-and-tails

In general, streamlined macroforms indicate northeasterly ice flow with some more northerly oriented features in the central part of NTS 093J13 and throughout much of NTS 93J14, and with some more easterly oriented features in the west and south parts

of the study area (Fig. 5.7). The orientations of these landforms record ice-flow during the Fraser Glaciation maximum and early during deglaciation. The northerly deviations are probably the result of local topographic control on a thinning ice sheet; in NTS 093J13, ice would have been deflected by Mount Mackinnon and in NTS 93J14 it would have been funneled into the Rocky Mountain Trench. The easterly deviations represent a more regional easterly shift in ice-flow direction. There was no reorientation of macroforms in the northern part of the study area suggesting that the transition likely occurred after the ice retreated from, or was very thin in, that area. The macroforms in the south are not fully aligned with eastward direction of the striations or till clast fabrics (see below).

5.3.2. Striations, grooves and rat tails

Forty-one sets of features composed of striations, grooves and rat tails were measured in, and slightly north of, the study area and, of those, specific flow directions could be determined from nine locations (Fig 5.8; Appendix A3). From these data, three broad trends and relative ages are identified from oldest to youngest: 1) northwesterly – southeasterly; 2) northeasterly; and 3) easterly.

Striations of the first group were measured at eight locations in the northern part of the study area and range from 320° – 140° to 280° – 100° (Fig. 5.8 green symbols). They are nearly perpendicular to the streamlined features in some areas and are interpreted to record early ice flow from the northwest. The second group of striations has orientations from 190° – 10° to 260° – 80° (Fig 5.8; black symbols). Although the range of orientations in this group is high, they are in agreement with the trend of the local streamlined features; thus they likely developed contemporaneously during the maximum and slightly later stages of glaciation. Striations of the third group were measured at eight locations in the western portion of the study area and range in orientation from 250° – 70° to 95° (Fig. 5.8 red symbols). One of these striations is part of a series of three, from which a relative ice-flow chronology was determined. The oldest flow direction is 60°, the second trends at 80° – 260° and the final is 95°. The oldest striation in the series is aligned with local streamlined macroforms. The younger two striations represent the transition to eastward ice-flow during deglaciation.

5.3.3. Till clast fabrics

Till clast fabrics were measured at 13 locations in the study area (Fig. 5.9; Table 5.2). At four locations, two fabrics were measured at different depths in vertically aligned positions to investigate potential differences in ice-flow and determine their relative chronologies. All fabrics were statistically significant at the 99% confidence level except for fabric 11-06, which was random below the 90% confidence level.

The ice-flow directions determined from till clast fabrics are in general agreement with the local streamlined macroforms with some differences. The dominant trend for fabric 09-01is about 350° – 170°, with a weaker secondary trend at about 225° – 45°. The apparent ice-flow direction from the principal eigenvector suggests north-northwest flowing ice; however, there is no geological evidence to support this interpretation. It is more likely that this fabric represents ice flowing southeasterly from the Omineca Mountains, similar to the first group of striations mentioned above. The secondary trend is oriented in the direction of the streamlined macroforms and is interpreted to represent ice-flow during the glacial maximum.

The ice-flow direction inferred from fabric 09-03 is about 350°. However, the macroforms in the area are oriented in a more northeasterly direction, at about 35°. Similarly, fabric 09-05 has a minor northerly trending component. The primary trend in fabric 09-05 is about 85° - 265° and reflects ice flow during the late-glacial phase. The origin of the northerly components has not been resolved.

The principal eigenvector of fabric 09-06 indicates ice flow to the northeast, which is consistent with the macroforms. Although strong, the clast measurements are spread along the outer edge of the southwest and northeast quadrants. The dispersion of the data suggests that more than one ice-flow direction may have affected the fabric. The distribution of clasts is interpreted to reflect northeast and east components of ice flow, the latter during the late-glacial phase. The chronology cannot definitively be determined, thus it could represent the inverse shift in ice-flow direction that occurred during the ice-expansion phase (see glacial history). The first theory is favoured because, with the thick drift in the region, it is unlikely that the fabric measured at 1.75 m depth would be within till deposited early in glaciation. Conversely, the dispersion may due to till-forming processes (e.g. deformation).

There is no apparent pattern in fabric 11-06 and the diamict from which this fabric was collected has little to no fissility or jointing. This diamict was likely remobilized during a failure and, therefore, does not provide an ice-flow direction.

Relative ice-flow chronologies were determined from two of the vertical series. In the west-central part of the study area, the lower till fabric (10-01) indicates ice flow to the northeast (45°), parallel to the fluting from which it was collected. The upper fabric (10-02) indicates easterly ice flow (85°). In the northeast part of the study area, the lower till fabric (11-02) is in agreement with the macroforms, trending about 15°. The upper fabric (11-01) indicates more northeasterly ice flow at about 50°. These two sets of fabrics indicate an easterly shift in ice flow.

Table 5.2 Till clast fabric details. Refer to figure 5.9 for locations.

Fabric number	Depth (m)	Clasts measured	Vertical location[a]	Eigenvector(°)	Mean plunge	Apparent ice flow direction (°)[b]	Eigenvalue 1
09-01	3	50		172	1	352[c]	0.689
09-02	1.75	50		205	7	25	0.822
09-03	2	50		170	14	350	0.788
09-05	2	50		261	0	81	0.720
09-06	1.75	50		229	1	49	0.683
10-01	2.1	25	1	224	9	44	0.780
10-02	1.2	25	2	268	4	88	0.809
11-01	2	30	2	61	0	241[c]	0.819
11-02	3.5	30	1	202	8	22	0.722
11-03	4	50	1	204	15	24	0.846
11-04	2	50	2	211	11	31	0.880
11-05	2.75	30	1	240	5	60	0.745
11-06	1.5	35	2	61	8	241	0.465

[a] Only refers to fabrics measured in vertical section; assigned from bottom up

[b] Apparent ice flow directions are calculated 180° from the principal eigenvector and may differ from inferred ice flow direction (see text)

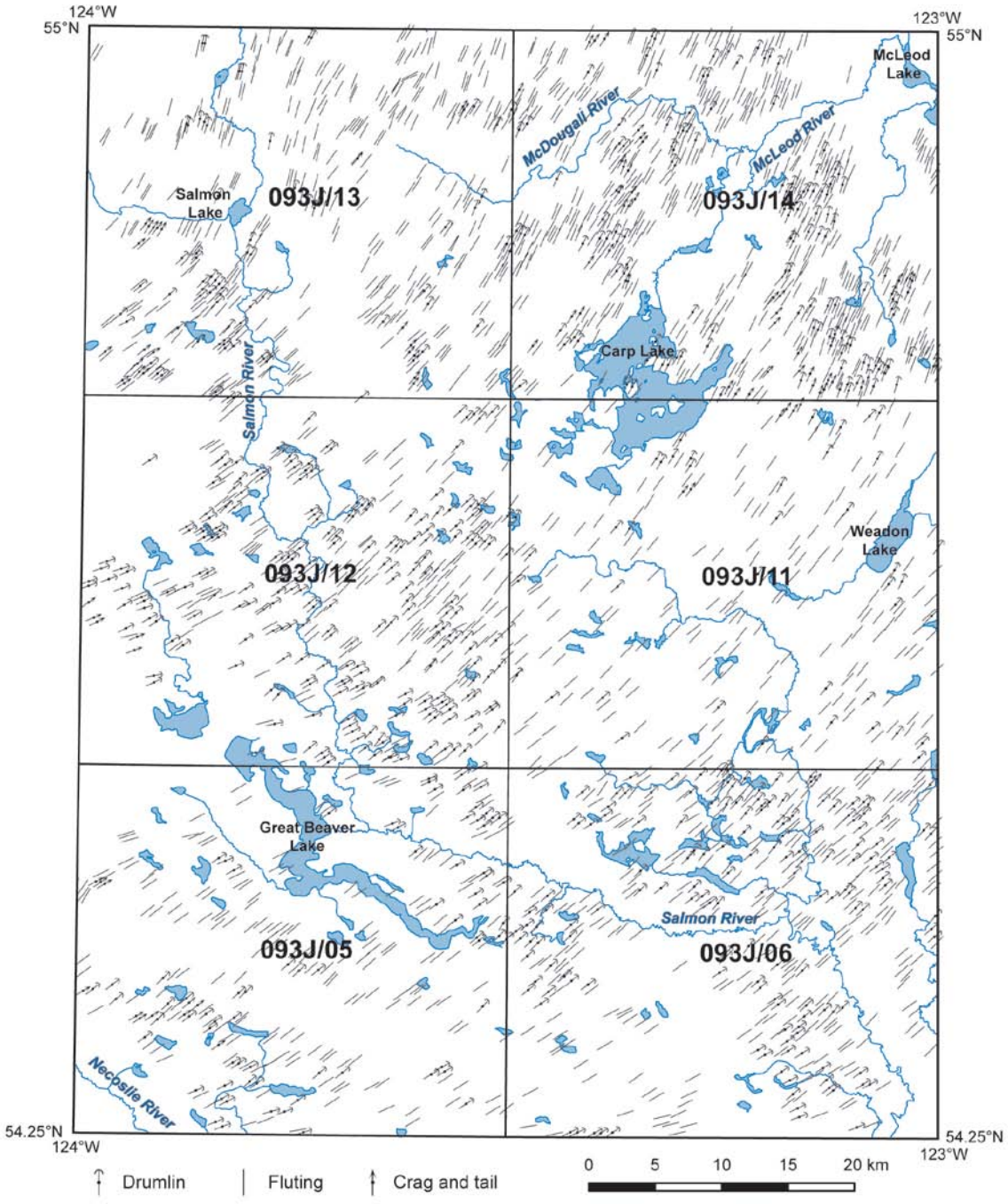

Figure 5.7 Distribution and orientations of streamlined macroforms in the study area. Some features were removed for plotting from areas where density is high.

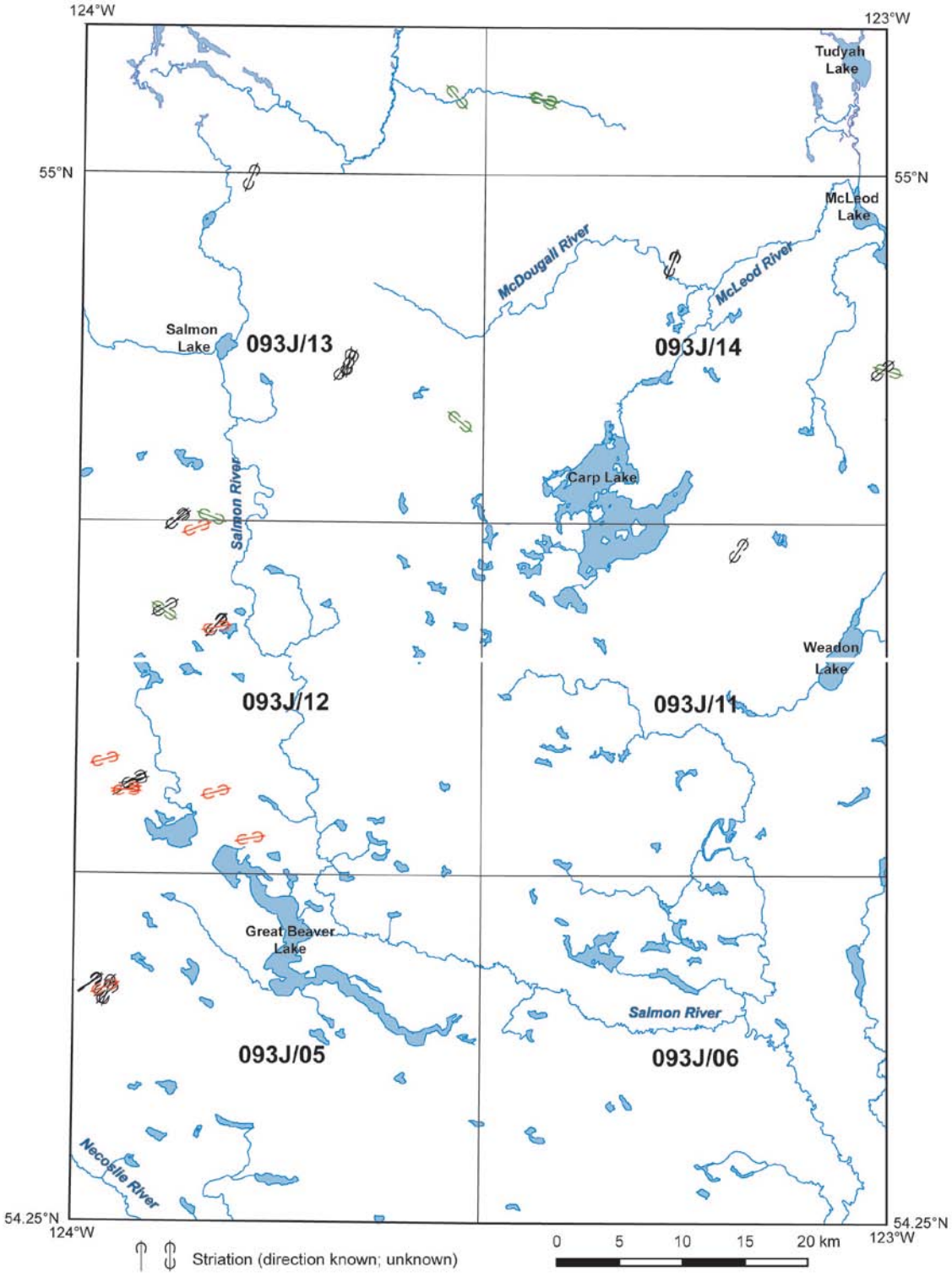

Figure 5.8 ***Location and orientation of striations discussed in text. Striation data indicate early south westerly ice-flow (green symbols), general northeast ice-flow at the glacial maximum (black symbols) and easterly flow (red symbols).***

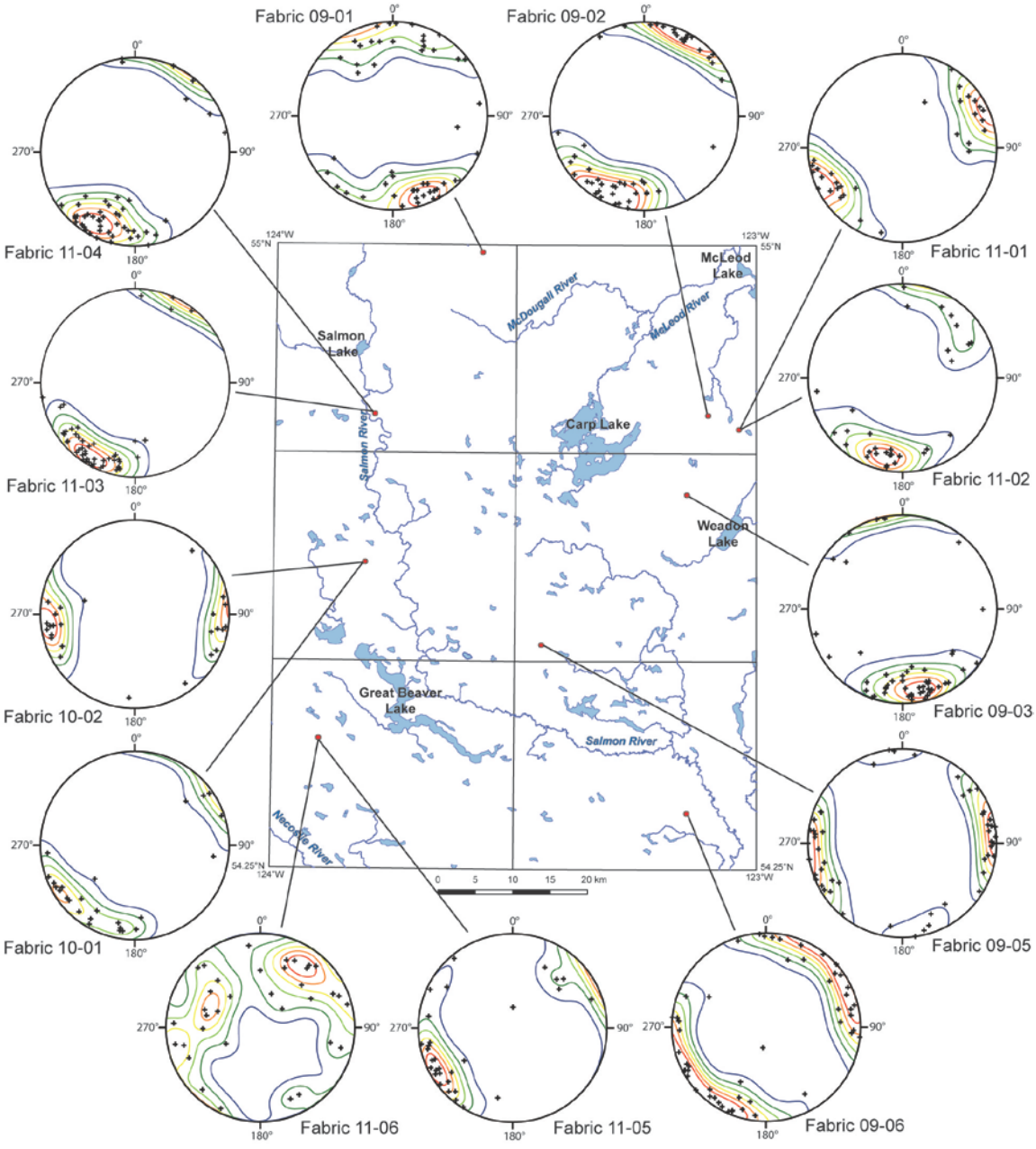

Figure 5.9 ***Locations and measurements of till clast fabrics. Stereonet plots use a Schmidt equal area projection in the lower hemisphere. Refer to Table 5.1 for fabric details.***

5.3.4. Summary of ice flow in the study area

Three stages of ice-flow were determined from the orientations of macroforms, striations, grooves, rat tails and clast fabrics. During the first stage, ice flowed southeast into the northern part of the study area. It is unknown how much of the area was affected by this event. The second stage began with easterly flow but was deflected to the northeast, which was the direction during the glacial maximum. During deglaciation, ice-flow transitioned back to the east, however much of the area was deglaciated by this time and the easterly flow likely only affected the southwest portion of the study area.

5.4. Local glacial history

At the onset of the last glaciation, ice advanced toward the study area from source areas in the Skeena, Omineca, Coast and Cariboo mountains (see Chapter 2). The first ice to reach the area flowed southeast from the Omineca Mountains. The ice impeded northerly drainage through the ancestral Parsnip River north of McLeod Lake, forming a glacial lake of unknown extent north of the drainage divide in the northeast corner of the study area. Unit 1 (moderately well sorted sand, DS-04) was deposited either as outwash prior to lake development or in the early phases of the lake. As the lake level increased, unit 2a (glaciolacustrine clay, silt and sand, DS-04) was deposited. When the ice was near section DS-01, a subaqueous outwash fan (unit 2b) was built. Ice then advanced over section DS-01, depositing the lower till (unit 3). Ice flow during this advance is indicated by the northwest – southeast-oriented striations (Fig. 5.8, green symbols) and the southerly oriented fabric (Fig.5.9, fabric 09-01) in the northern part of the study area. The extent of this early advance is unknown, but no evidence of southerly flow was observed south of about 54.7° N, thus the southern portion of the study area may not have been covered by ice at this time. It is known that the ice retreated back to at least the location of section DS-01 when more subaqueous outwash (unit 4) was deposited over the early advance till.

Easterly flowing ice from the Coast Mountains caused an easterly deflection of the ice from the Omineca Mountains. The transition is recorded in the more easterly oriented striations than during the early advance (Fig. 5.8, green symbols). When glaciers from

the Pacific Ranges and possibly the Cariboo Mountains reached the study area, they produced a northeasterly deflection.

With continued climate deterioration, the advancing glaciers coalesced to form a single ice sheet that covered the study area and extended beyond the Rocky Mountains (Rutter 1977; Bobrowsky and Rutter 1992, Hartman and Clague 2008). The streamlined macroforms, striations (Fig. 5.8, black symbols) and many of the till fabrics (Fig. 5.9) throughout the area indicate northeast ice-flow driven by ice sources to the west and south at the glacial maximum.

As the climate ameliorated near the end of the Late Wisconsinan, the CIS began to retreat. Initially, the ice front thinned along the western flanks of the Rocky Mountains and then retreated to the southwest toward the study area. The macroforms in the northeast part of the study area (Fig. 5.7) indicate that the Rocky Mountain Trench caused local northerly variations in ice flow. The transition from north to northeast orientations in fabrics11-02 and 11-01 indicate that ice-flow shifted back to the northeast, likely when the ice retreated from the topographic influence of Rocky Mountain Trench (Fig. 5.9).

When the ice margin was near the northeast corner of the study area, subglacial meltwater flowed northeasterly through several systems into the Peace River Basin (Fig. 5.10a). The longest meltwater system can be traced from the northern part of NTS 093J12 to the north-central part of NTS 093J14. It transitions between eskers and channels as it crosses the drainage divide between the Pacific and Arctic watersheds and continues over the uplands and beyond the study area. Two meltwater systems developed off the arms of Carp Lake and extended northeast into the northern McLeod Lake valley. The larger system, from the northern arm of the lake, runs through the McLeod River valley. An esker complex, hummocky gravels and kettle lakes occur near the middle of this system. The smaller system begins at the east arm of Carp Lake, passes through a deep channel in a local topographic high and continues northward. Shallow meltwater channels and a series of eskers indicate that, at some point, meltwater from the east arm system was diverted north into McLeod River valley. These landforms are time-trangressive and the systems were not necessarily active in the depicted configuration at one time (Fig. 5.10a).

Ice retreated from the northeast part of the study area along a mostly linear, northwest-southeast-trending margin (Fig. 5.10b). Meltwater continued to be discharged into the McLeod Lake valley, but was blocked just north of the study area, forming a large glacial lake, informally named glacial Lake McLeod. Silt and sand (unit 7b, DS-05) were deposited in this lake about 20 m above the level of present-day McLeod Lake. Meltwater moving through the McDougall River valley was diverted southeast along the retreating ice margin, cutting a series of channels leading to the McLeod River. The youngest channel in the series is the present course of the McDougall River. Meltwater, some of which was likely supplied by subglacial drainage flowing over the north end of Mount Mackinnon, continued to be directed into the uplands and through the McDougall River until the ice retreated to lower elevations (Fig. 5.10b, c). Ice continued to retreat and sediment or ice caused a local ponding event in the McDougall River valley. Due to the ~100 m difference in elevation between glaciolacustrine units in the McDougall River and McLeod Lake valleys, it is unlikely that this lake was connected to glacial Lake McLeod. Underflow currents deposited cross-bedded sands, while failures from the unstable valley walls or ice front deposited discontinuous diamict beds (unit 7a; section DS-03). Eventually the blockage was removed and cobble gravel was deposited on the valley floor (unit 8; DS-02 and DS-03). Water continued flowing from the Carp Lake outlets into the McLeod River. The abundance of isolated ice-contact deposits and kettles in the McLeod River valley suggest that a detached (?) ice mass remained in the area.

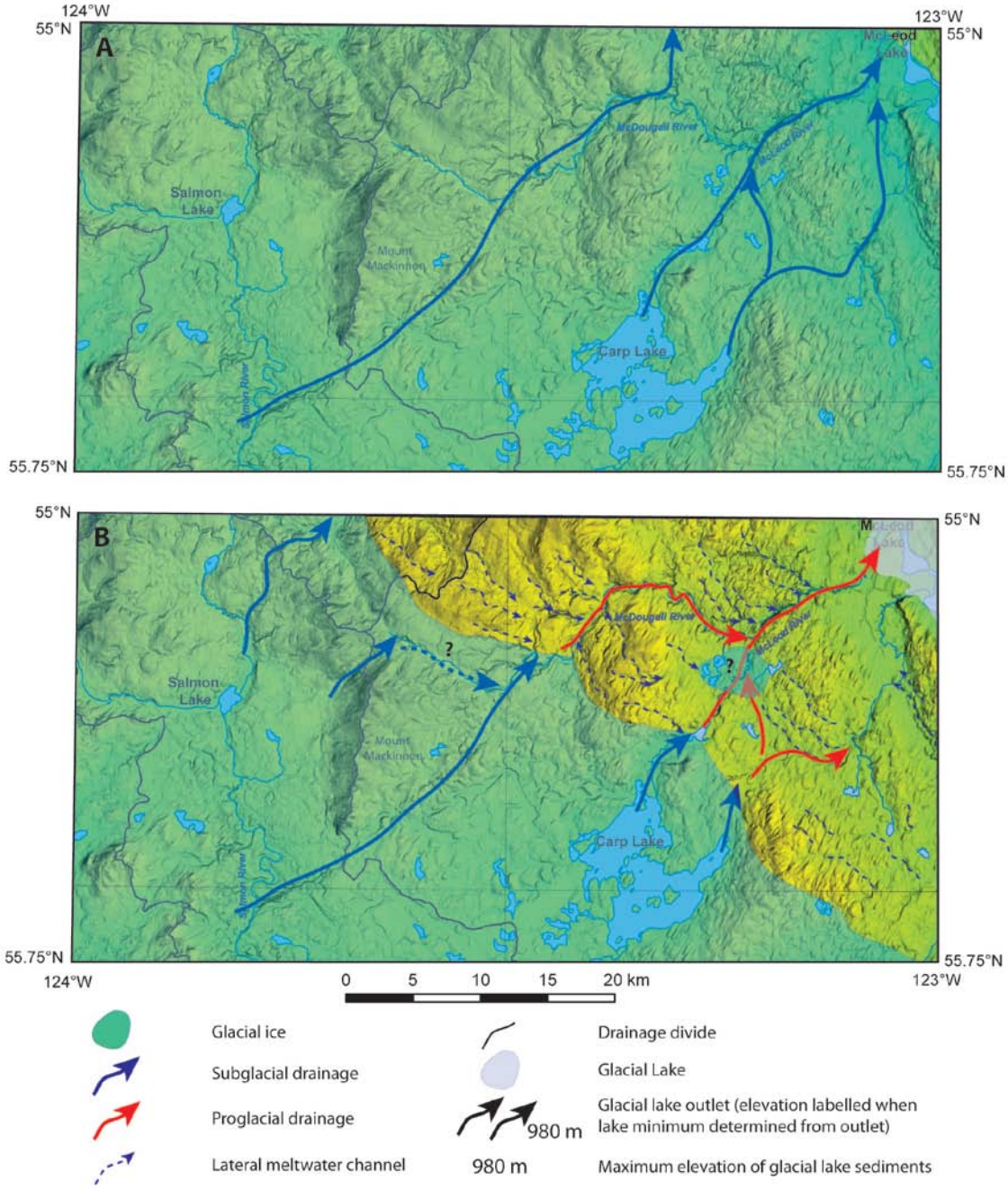

Figure 5.10 A/B

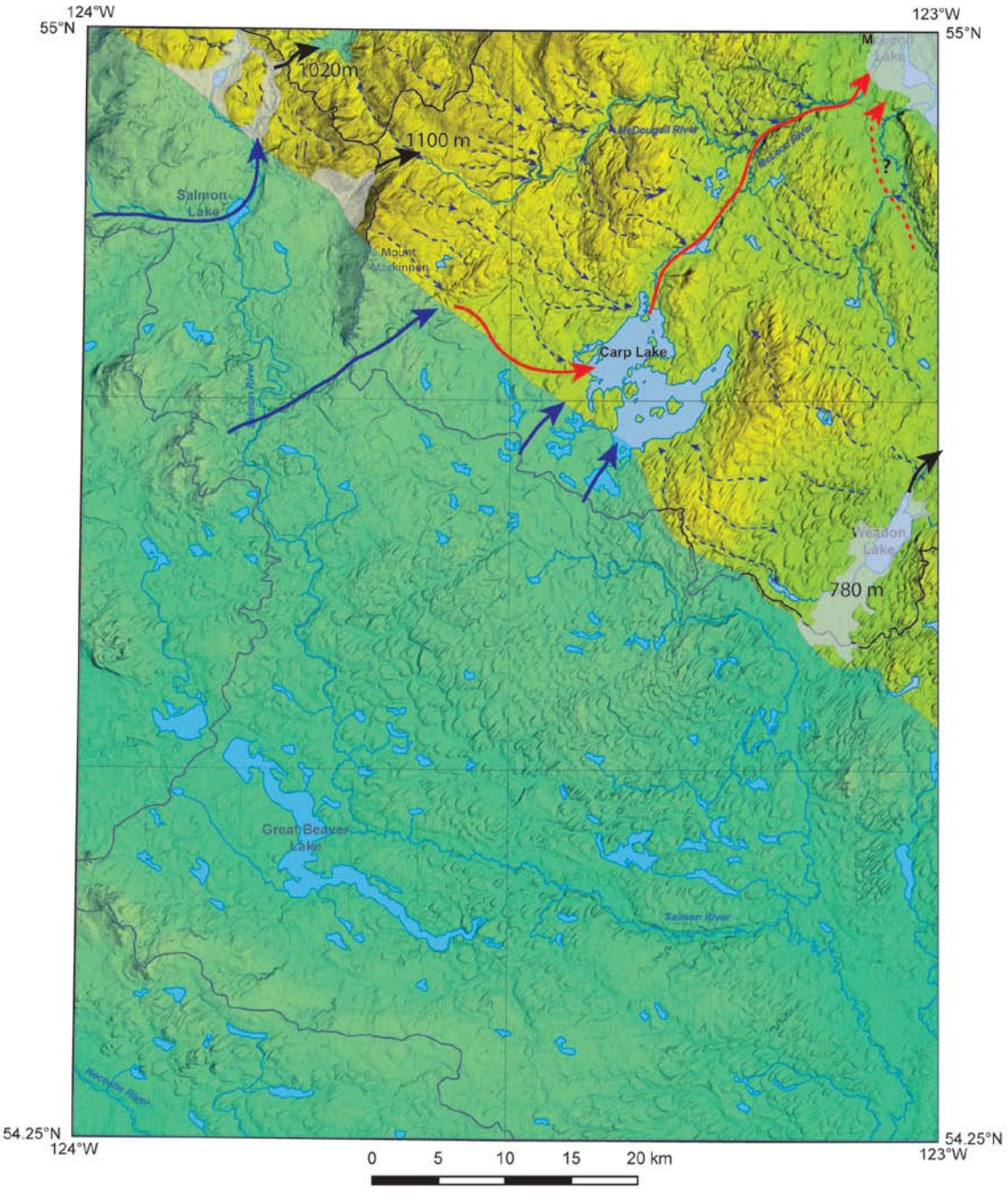
124°W
55°N
123°W
55°N
1020m
1100 m
Salmon Lake
Mount Mackinnon
McDougall River
McLeod River
?
Carp Lake
Weadon Lake
780 m
Great Beaver Lake
Salmon River
54.25°N
124°W
0 5 10 15 20 km
54.25°N
123°W

Figure 5.10 C

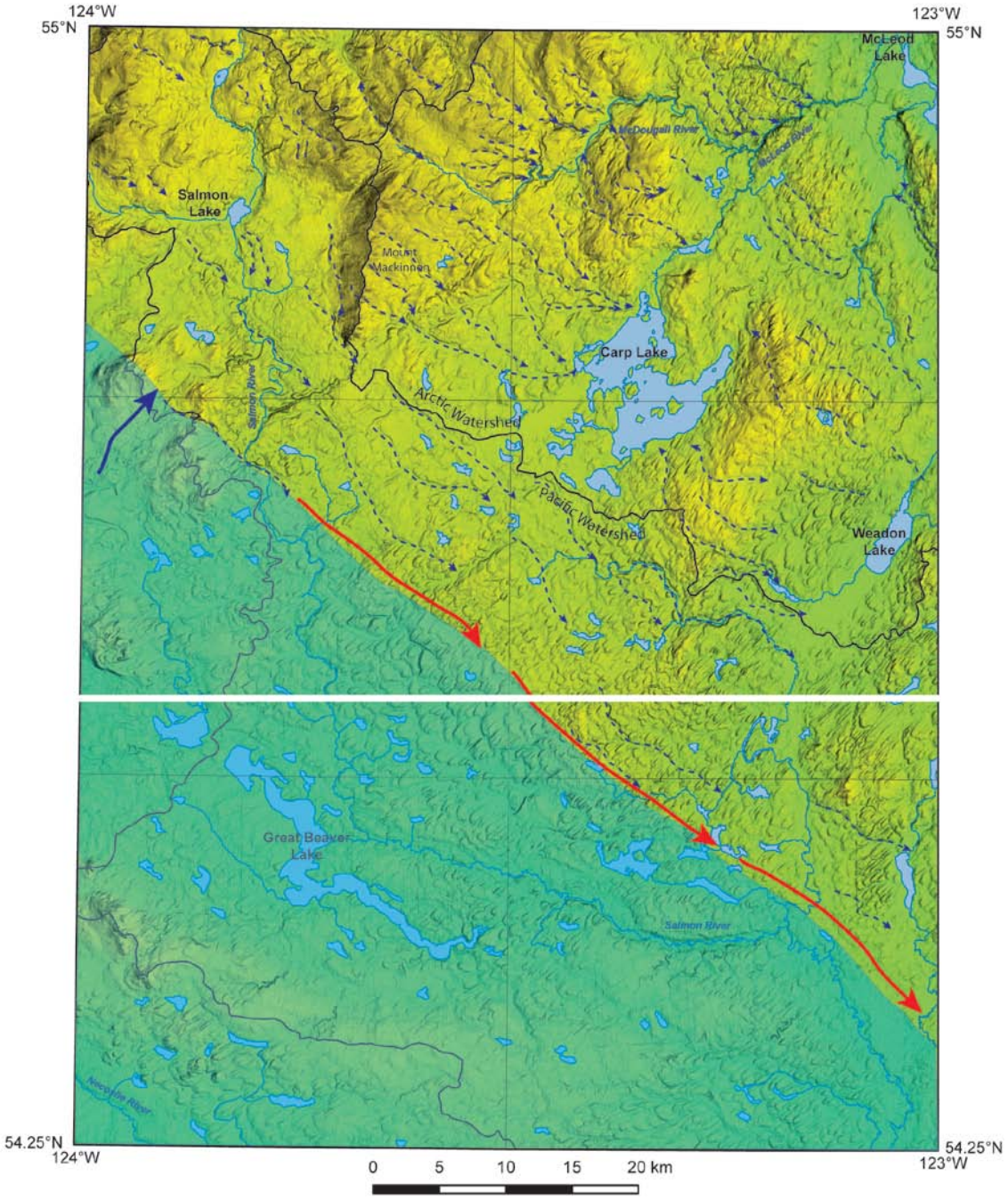
124°W
55°N
123°W
55°N
McLeod Lake
McDougall River
Salmon Lake
Mount Mackinnon
Carp Lake
Arctic Watershed
Pacific Watershed
Weadon Lake
Great Beaver Lake
Salmon River
54.25°N
124°W
0 5 10 15 20 km
54.25°N
123°W

Figure 5.10 D

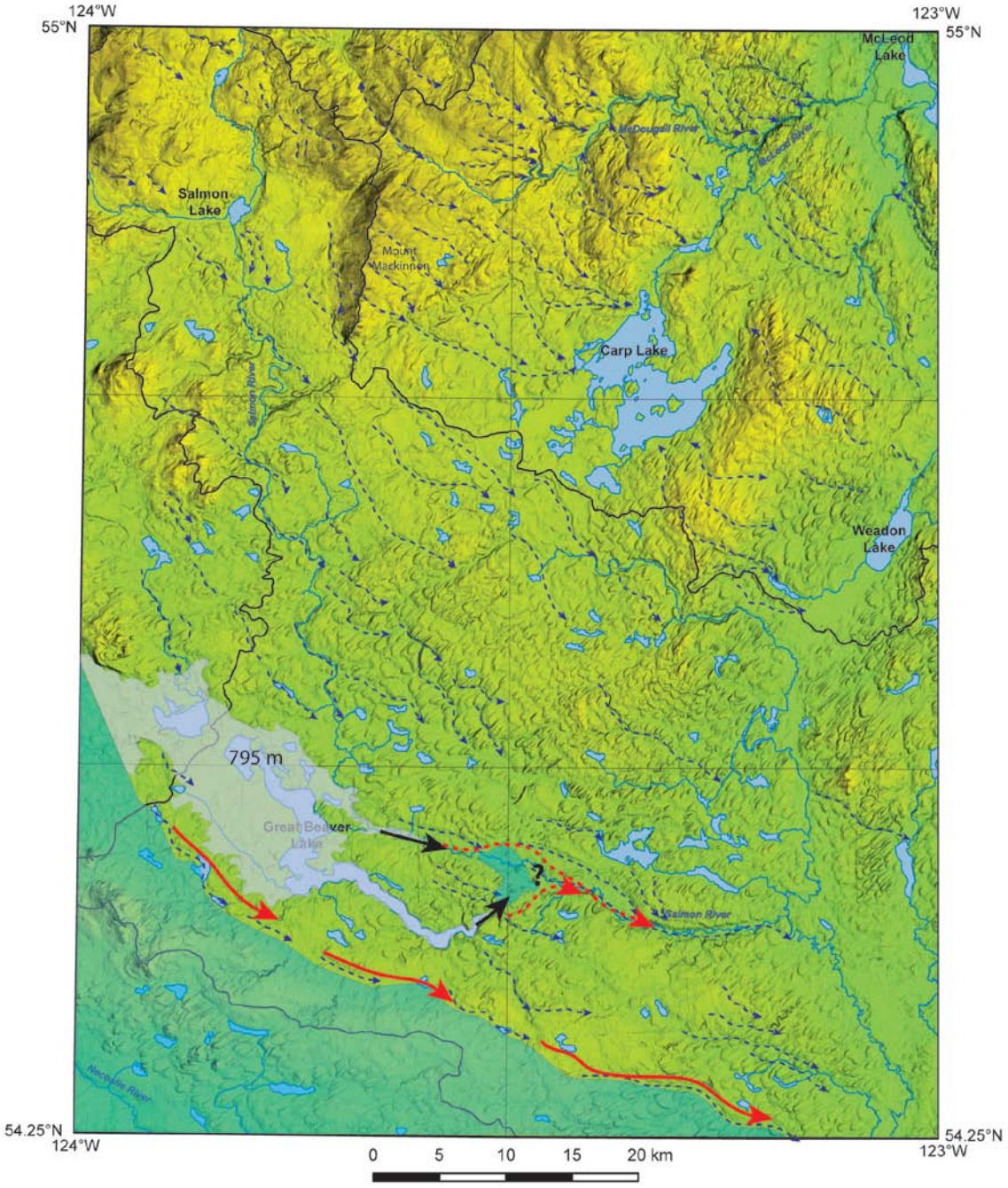
124°W
55°N
123°W
55°N
McLeod Lake
McDougall River
Salmon Lake
Mount Mackinnon
Carp Lake
Salmon River
Weadon Lake
795 m
Great Beaver Lake
Salmon River
Necoslie River
54.25°N
124°W
0 5 10 15 20 km
54.25°N
123°W

Figure 5.10 E

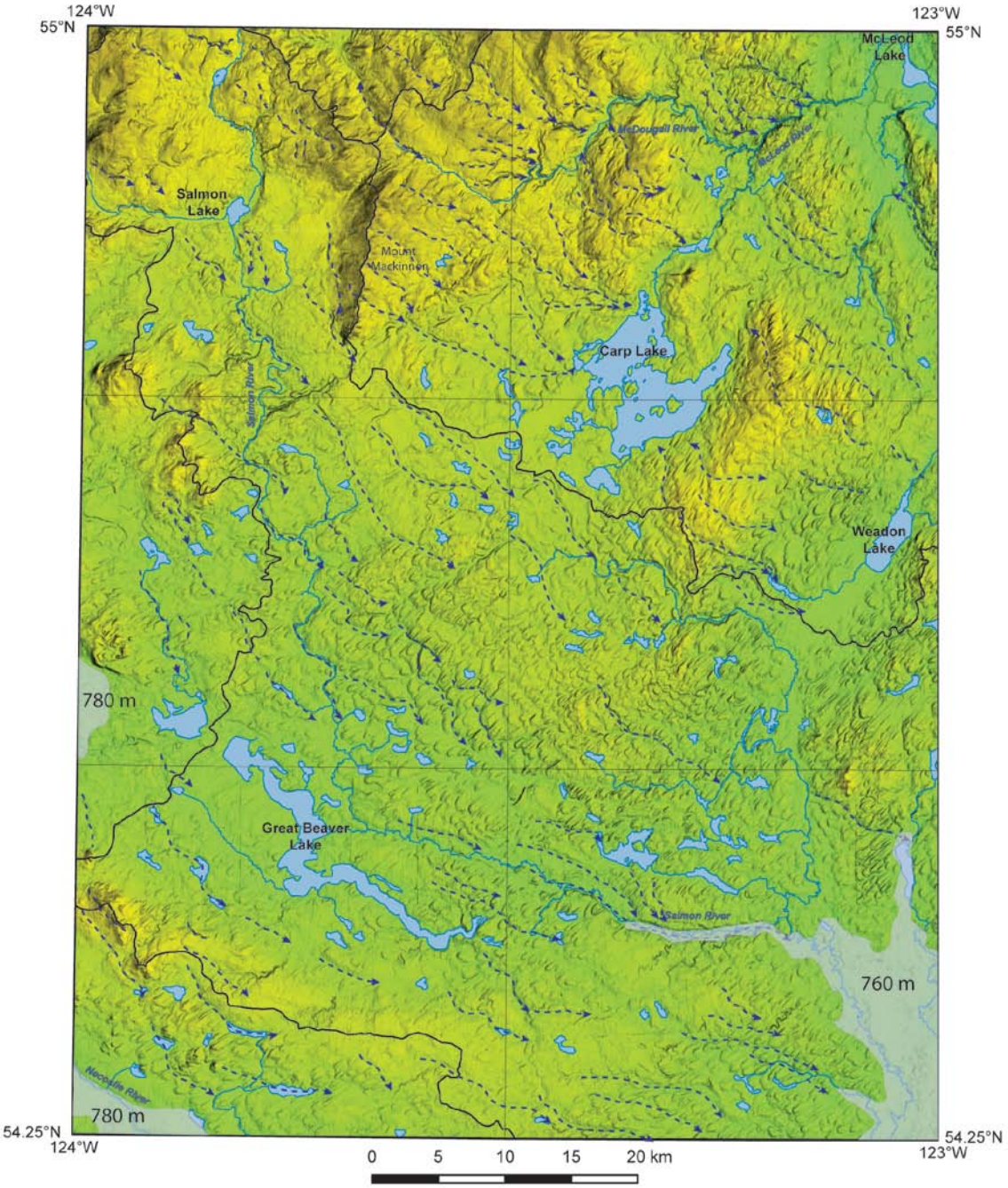
124°W
55°N
123°W
55°N
McLeod Lake
McDougall River
Salmon Lake
Mount Mackinnon
Carp Lake
Salmon River
Weadon Lake
780 m
Great Beaver Lake
Salmon River
760 m
Nechako River
780 m
54.25°N
124°W
0 5 10 15 20 km
54.25°N
123°W

Figure 5.10 F

Figure 5.10: ***Morphology of the glacier and drainage networks during deglaciation. The ice margin is estimated based on the trend of successive lateral meltwater channels and is not necessarily representative of the configuration at a specific time as there is no chronologic control linking the channels. Deglaciated areas are shades of yellow and green. A) Near complete ice cover; subglacial meltwater flowing northeast. B) Linear ice margin retreating into study area; lateral meltwater channels cut into topography; proglacial meltwater flowing northeast into glacial lake. C) Linear ice margin continues to retreat; ice marginal lakes develop against uplands in north and around Weadon Lake in south. D) Linear margin retreats past drainage divede; proglacial meltwater drains southeast along ice margin. E) Ice margin curves, trending more north-south in the north and east-west in the south; proglacial meltwater continues to drain southeast; glacial lake develops around Great Beaver Lake. F) Study area is deglaciated; a lake develops at 780 m around the Necoslie River and west of Great Beaver Lake as drainage is blocked to the south; it is unclear when the lake developed in the southeast corner; it may have been much earlier.***

Glacial Lake McLeod formed in the McLeod Lake and Crooked River valleys (Fig. 5.11a). The ice mass that impeded northerly drainage is delineated by hummocky gravels, a large esker complex and a large kettle lake (Tudyah Lake). The southern limit of the lake was the retreating ice margin and the lake expanded as this margin retreated down the valley. During this retreat, an ice mass stagnated in the McLeod Lake basin, against which outwash from the McLeod River formed a delta. Localized ice-contact deposits indicate that another ice block was left about 10 km south of McLeod Lake in the Crooked River valley. The highest water level was at least 750 m a.s.l. as indicated by deltaic sediments at the mouth of the McLeod River and a spillway draining east into the Parsnip River valley. At the southern end of the lake, an ice-marginal channel dips south that connected glacial lakes McLeod and Fraser. At this water level, the lake occupied about a 100 km length of the valley between the ice mass on the north and the ice margin on the south (Fig. 5.11a).

Continued ice retreat exposed the southern part of the Crooked River valley and connected glacial lakes McLeod and Fraser. The water elevation was likely controlled by the ice mass in the north. When the water level lowered to an elevation of 715 m a.s.l., the connection was limited to a spillway in the south end of the valley that drained

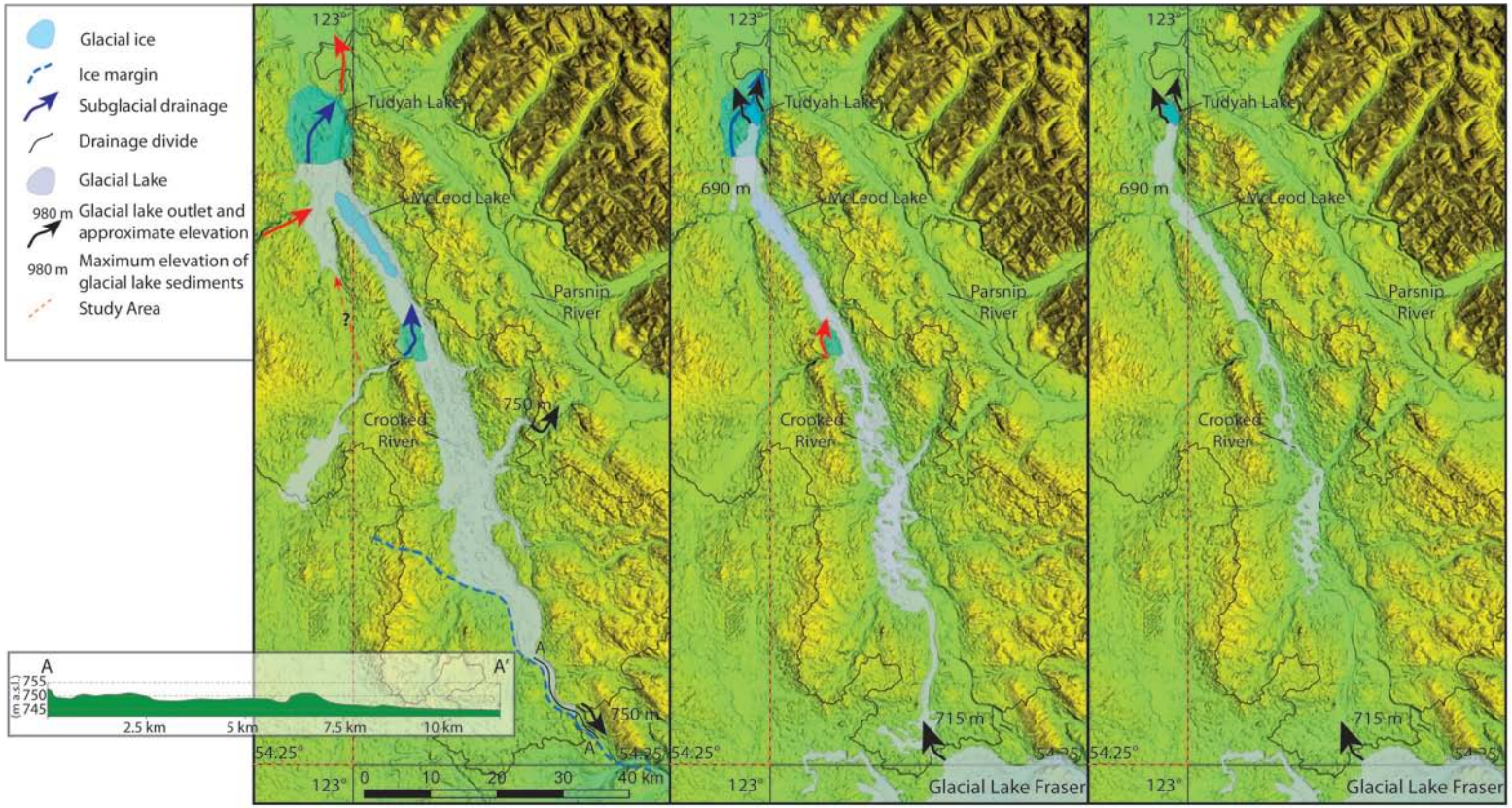

Figure 5.11 ***Configurations of glacial Lake McLeod. Minimum water-level elevation for the maximum extent is determined from ice-marginal spillway in south (A-A') and a spillway on east valley wall at 750 m a.s.l. (A). Second extent at a minimum water-level elevation of 715 m a.s.l. determined from channel on the southern limit (B). Glacial Lake McLeod was connected to glacial Lake Fraser at this stage. Third extent at a water-level elevation of 690 m a.s.l. inferred from elevation of deltaic sediments (C). Glacial Lake Fraser drained into glacial Lake Mcleod at this stage.***

glacial Lake Fraser into glacial Lake McLeod (Fig. 5.11b). A third lake elevation of 690 m a.s.l. is inferred from the surface elevation of a lower delta. At this elevation, the lake could be contained by an ice mass the size of Tudyah Lake (Fig. 5.11c). Many of the topographic highs in the southern part of the valley were exposed, and the water was not much higher than the Crooked River flood plain. Glacial Lake Fraser was likely still draining into glacial Lake McLeod as its water spilled over the drainage divide and through the channel in the south end of the valley. A rapid draining event during the evolution of glacial Lake McLeod may explain the erosion of glaciolacustrine sediments (unit 7b) in section DS-05 and deposition of ~1 m of pebble gravel (unit 8). Further sedimentological information is needed to verify this theory.

As the ice continued to retreat, meltwater no longer flowed into the McDougall River, and the sediment diminished. Multiple terraces were created as the McDougall River incised its valley fill. Meltwater was then diverted southeast along the ice margin to Carp Lake and flowed northeast into the McLeod Lake valley (Fig. 5.10c). A chaotic system of meltwater channels developed west of Carp Lake. Meltwater likely flowed along several paths into Carp Lake, controlled by the amount of water and the position of the ice front. Nye channels carried water northeast towards the ice margin. As the ice margin retreated, new lateral channels formed that cross-cut the Nye channels. Outwash plains that end abruptly at the limits of Carp Lake suggest that they formed against stagnant ice blocks that formed the lake basin. To the southwest, a proglacial lake developed around Weadon Lake to a minimum elevation of 780 m a.s.l. Northern drainage was impeded by the ice mass in the Crooked River valley (Fig. 5.10c, 5.11a). A series of eskers indicates subglacial drainage. A large channel suggests final drainage occurred between this ice and the valley wall.

When the northern ice margin in NTS 093J13 began retreating down the uplands, several ice-marginal lakes were impounded (Fig. 5.10c). Spillways indicate a minimum elevation of about 1020 m a.s.l. for the northern lake and 1100 m a.s.l. for the southern lake. The size of the channels and lack of sediment on the lee side of the northern outlets suggest that a large amount of water drained through these areas (Fig. 5.12). Numerous eskers, kames, and kettles at the base of the channels indicate that stagnant ice was left in the valley. The lakes existed along the retreating ice margin until the water was able to drain southeast below Mount Mackinnon.

When the ice margin was south of the drainage divide, all proglacial meltwater began flowing southeast along the ice margin into the Fraser River drainage basin (Fig. 5.10d). A series of lateral channels indicate that the ice margin was mostly linear and trended

Figure 5.12 Large meltwater channel cut below a glacial lake spillway on the lee side of the northern uplands.

northwest-southeast as it retreated over the next 15 – 20 km. Beyond this, the channels in the southeast part of the study area are oriented in a more southerly direction, and the channels in the south-central and southwest are oriented more easterly (Fig. 5.10e). This change in orientation suggests that the shape of the ice margin changed, possibly due to the different dynamics of the source areas south and west of the study area. Until this time, the northerly influence of ice from the south and the easterly influence of ice from the west caused a northeasterly flow direction and a northwest-southeast-oriented ice front. Afterwards, the influence of southern ice decreased, allowing east flowing ice to dominate and causing a reorientation of the margin. The transition to easterly ice-flow

is illustrated in the southwest by macroforms (Fig 5.7), till fabrics 10-01 and 10-02, till fabric 09-05 (Fig. 5.9) and striations northwest of Great Beaver Lake (Fig. 5.8, black and red symbols). Striations on the west side of NTS 093J12 (Fig. 5.8, red symbols) and till fabric 09-06 (Fig. 5.9) also indicate easterly ice flow.

The changing ice dynamics during the reorientation of the ice margin caused at least one oscillation of the ice front that is recorded at section DS-06 where a till (unit 9) overlies outwash gravel (unit 8). A glacial lake formed around what is now Great Beaver Lake to a minimum elevation of 795 m a.s.l. (Fig. 5.10e). Two possible outlets at 780 m a.s.l. were blocked by sediment or ice. Localized ice-contact glaciofluvial deposits near the southern outlet suggest that it was stagnant ice. The lake drained through the lower Salmon River valley. Ice retreated south across the southern adjacent map area (Clague 1988) and west through the western adjacent map area (Plouffe 2000), implying that the ice margin continued to diverge beyond the study area.

A large lake developed around the southern part of Stuart Lake and the Stuart and Necoslie rivers (Plouffe 1997, 2000), which Plouffe (2000) suggests was inundated during late stages of glacial Lake Fraser. However, equivalent glaciolacustrine units indicate minimum lake elevations of 780 m a.s.l. in the study area (Fig 5.10f) and 760 m a.s.l. to the west (Plouffe 2000). It is unlikely that glacial Lake Fraser reached this elevation in these regions because its outlet to the Peace River basin is significantly lower (~715 m a.s.l.). To deposit higher glaciolacustrine sediments a separate lake is required, here informally referred to as glacial Lake Stuart. I propose a portion of the ice margin south of the study area impounded glacial Lake Stuart, and also formed the large esker complex that terminates just north of Prince George (Fig. 5.13). The ice margin may have been located where gullied glaciolacustrine sediments transition into a more defined meltwater channel in the Stuart River valley. As the ice thinned, hydrostatic pressure from the lake caused the ice margin to decouple, allowing glacial Lake Stuart to drain subglacially. This cut a large channel leading to glacial Lake Fraser. As the hydraulic gradient between the two lakes decreased, flow slowed and the large esker system was deposited that extends east to Prince George.

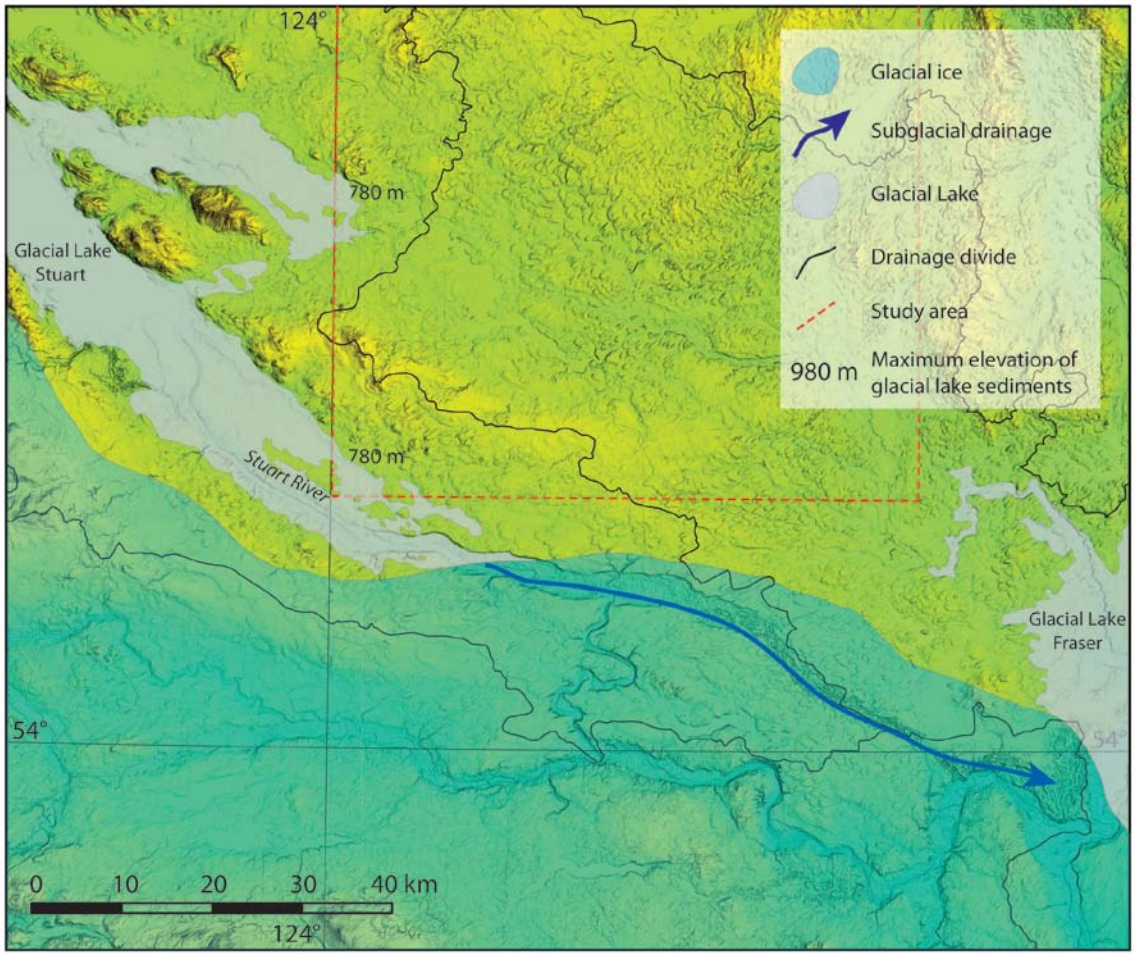

Figure 5.13 Hypothetical ice configuration used to explain glacial Lake Stuart at a water level of 780 m a.s.l., and the formation of the Prince George esker system. Glacial lake Fraser is depicted at a water level of 715 m a.s.l., which was controlled by the outlet draining north in to the Peace River watershed.

The western ice lobe retreated across the Nechako Plateau, eventually breaking up into ice tongues that occupied large valleys such as the Babine, Francois and Ootsa Lake valleys (Levson et al. 1998; Stumpf et al. 2000). Meltwater from these glaciers drained into glacial Lake Fraser, which is thought to have occupied much of the Fraser Basin including the Nechako and Stuart river valleys (Tipper 1971a; Clague 1988,1989; Plouffe 1997, 2000). Glaciolacustrine sediments are mapped to elevations of: 760 m a.s.l. in the Stuart Lake area (Plouffe 2000); 780 m. a.s.l. in the study area; and 800 m a.s.l. south of Prince George (Blais-Stevens and Clague 2007) and in the Nechako River valley (Clague 1998). These data suggest that glacial Lake Fraser reached a minimum

elevation of 800 m a.s.l.; however, the previously discussed channel into the Peace River basin should have limited the elevation of the lake to 715 m a.s.l. (Fig. 5.14). The elevated glaciolacustrine deposits in Stuart Lake area can be explained by the existence of glacial Lake Stuart. The glaciolacustrine sediments to the south, that are ~85 m higher in elevation than that of the outlet, are enigmatic. The occurrence of glacial lake sediment at 760 m a.s.l. in the southeast corner of the study area is also difficult to explain (Fig 5. 10f). It is tentatively suggested here that: 1) rates of isostatic tilting varied due to thicker ice over the Fraser Basin; and 2) glacial Lake Fraser was a complex of interconnected smaller lakes possibly dammed by ice or sediment in valleys.

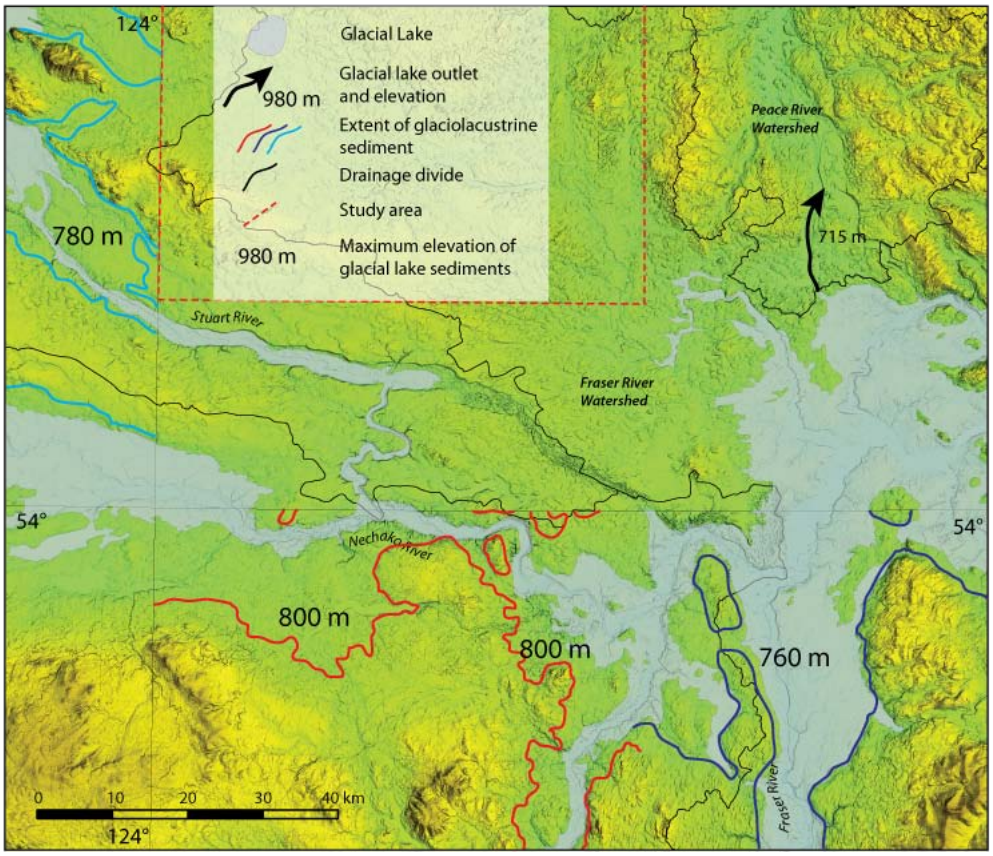

Figure 5.14 ***Glacial Lake Fraser delineated at a water level of 715 m a.s.l. The maximum elevation of the lake was controlled by a spillway into the Peace River watershed. Glaciolacustrine sediments could not have been deposited at the depicted extents (blue lines from Plouffe (2000); red lines from Clague (1998); blue lines from Tipper (1971b)) suggesting that isostasy varied across the region and that glacial Lake Fraser may have been a complex of interconnected smaller lakes.***

A piece of wood was collected from the base of a peat deposit in the esker system. The sample was processed at Paleotec Services and analysed at the W.M. Keck Carbon Cycle AMS Laboratory at the University of California. The wood yielded an age of 8775 ± 30 ^{14}C yr BP (UCAIMS 83989). This age is similar to many radiocarbon ages obtained from basal peat deposits in the area. It provides a minimum age for ice retreat beyond the esker system, but more accurately indicates the timing of initial post-glacial peat development, which significantly post-dates deglaciation.

5.5. Regional ice-flow model

The local glacial history is integrated here with previous work (Tipper 1971; Plouffe 2000; Stumpf et al. 2000; Levson 2001; Plouffe and Levson 2001a) to expand the regional model for ice-flow in central British Columbia during the Fraser Glaciation (Fig. 5.15).

5.5.1. Ice-expansion stage

The ice-expansion phase probably lasted late into the last glaciation (Ryder et al. 1991; Bobrowsky and Rutter 1992; Stumpf et al. 2000). During this time, ice accumulated and then expanded into the Northern Interior of British Columbia from the north, west and southwest (Clague 1988, 1989; Plouffe 1997, 2000; Stumpf et al. 2000; Plouffe and Levson 2001a). The first glaciers that developed in the Omineca and Skeena mountains flowed southeast down the northern Rocky Mountain Trench and the Takla and Babine lake valleys (Ryder and Maynard 1991; Plouffe 1997; Stumpf et al. 2000; Levson 2001; green arrows, Fig. 5.15a). Data from this study suggest that the glaciers also flowed southeast across the east part of the Nechako Plateau and into the northern uplands of the study area. These glaciers were the first to enter the study area and the ice front experienced at least one oscillation.

Ice from the Kitimat Ranges and Hazelton Mountains flowed eastward across the Nechako Plateau (Plouffe 1997, 2000; Stumpf et al. 2000; Plouffe and Levson 2001a). These glaciers interacted with the glaciers sourced in the Skeena and Omineca mountains producing an easterly transition in their ice-flow direction (yellow arrows, Fig.

5.15a). Eventually, ice from the Pacific Ranges reached the northern part of central British Columbia (Clague 1988, 1989; Plouffe 1997, 2000), which caused a deflection in flow to the northeast (blue arrows, Fig. 5.15a). The exact locations of the ice confluences are unknown. Based on the proximity of the Omineca and Skeena mountains to the north and the Kitimat Ranges and Hazelton Mountains to the west, it is likely that ice masses from these source areas coalesced, in or near the study area prior to the arrival of ice from the Pacific Ranges.

5.5.2. Maximum stage

In the Northern Interior of British Columbia the glacial maximum is thought to be marked by an eastward shift of the ice divide from the Coast and Skeena mountains over Babine Lake Valley, extending south to the Francois and Ootsa Lake areas (Levson et al. 1998; Stumpf et al. 2000; Fig. 2.5). The easterly oriented macroforms in the adjacent map-area, NTS 093K (Plouffe 2000) reflect the influence of this ice divide. In the study area, the dominance of northeastern ice-flow indicators suggest that flow was controlled by the interaction between this ice divide and an ice divide in the south through the maximum stage (Fig. 5.15b). In the southwest part of the study area and to the south, some macroforms are more easterly oriented, but these probably were modified during the late-glacial period (see below). Ice flow during the glacial maximum may be better represented in these areas by the northeast-oriented striations (Fig. 5.8).

5.5.3. Late-glacial phase

During the late-glacial phase, the ice sheet thinned and retreated from the Rocky Mountains, and ice flow at the margin became more influenced by the local topography. Initially, northern deviations occurred as the ice surface lowered through the valleys north of the study area (orange arrows, Fig. 5.15c). As the ice retreated past the influence of these valleys, it began to flow more easterly in the northwest part of the study area.

Easterly oriented macroforms, striations and till fabrics occur dominantly in the southwest part of the study area and continue farther south and west. These features record an easterly transition in the ice-flow direction. The distribution of these indicators

suggests that ice retreated through the northeast corner of the study area or was too thin to substantially modify the substrate in that region during the easterly transition. The transition was likely affected by the reduced influence from ice flowing from the south, due to downwasting and stagnation (Fulton, 1967, 1991; Plouffe et al. 2011). This allowed an increased influence from the ice divide to the west, causing the final regional easterly ice-flow (red arrows, Fig. 5.15c).

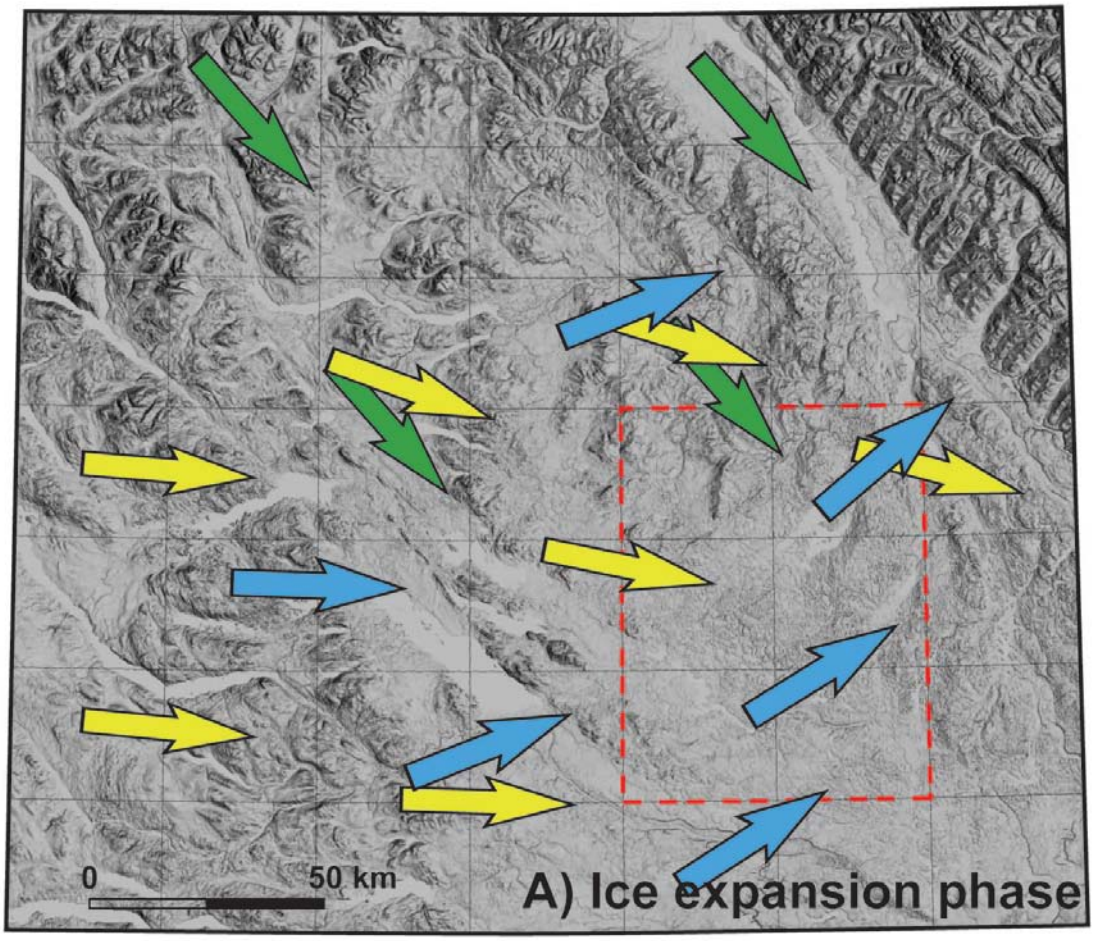

Figure 5.15 A

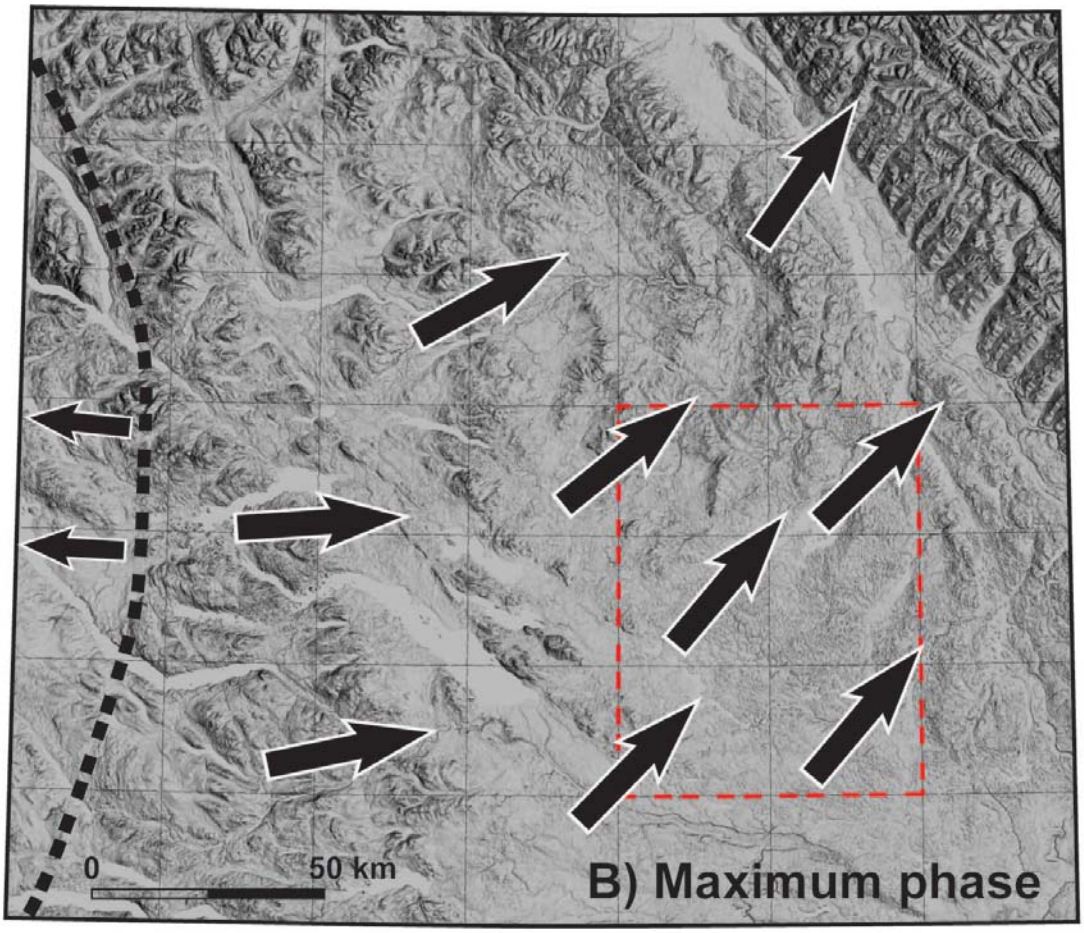

Figure 5.15 ***Regional ice flow model for the northern Interior with data from Tipper (1971); Plouffe (2000); Stumpf et al. (2000); Levson (2001); Plouffe and Levson (2001) and this study. (A) Glaciers first flowed southeast from the Omineca Mountains (green arrows) until more dominant ice from the west and south deflected the flow direction to the northeast (yellow and blue arrow). (B) During the maximum phase, the ice divide shifted east from the Coast Mountains and ice flow maintained a dominantly north eastern flow direction. (C) During the late glacial phase, ice flow was initially modified by topography on the foothills of the Rocky Mountains until it retreated (orange arrows). The influence from the south diminished and the glaciers sourced in the west became dominant causing an easterly shift in ice flow (red arrows).***

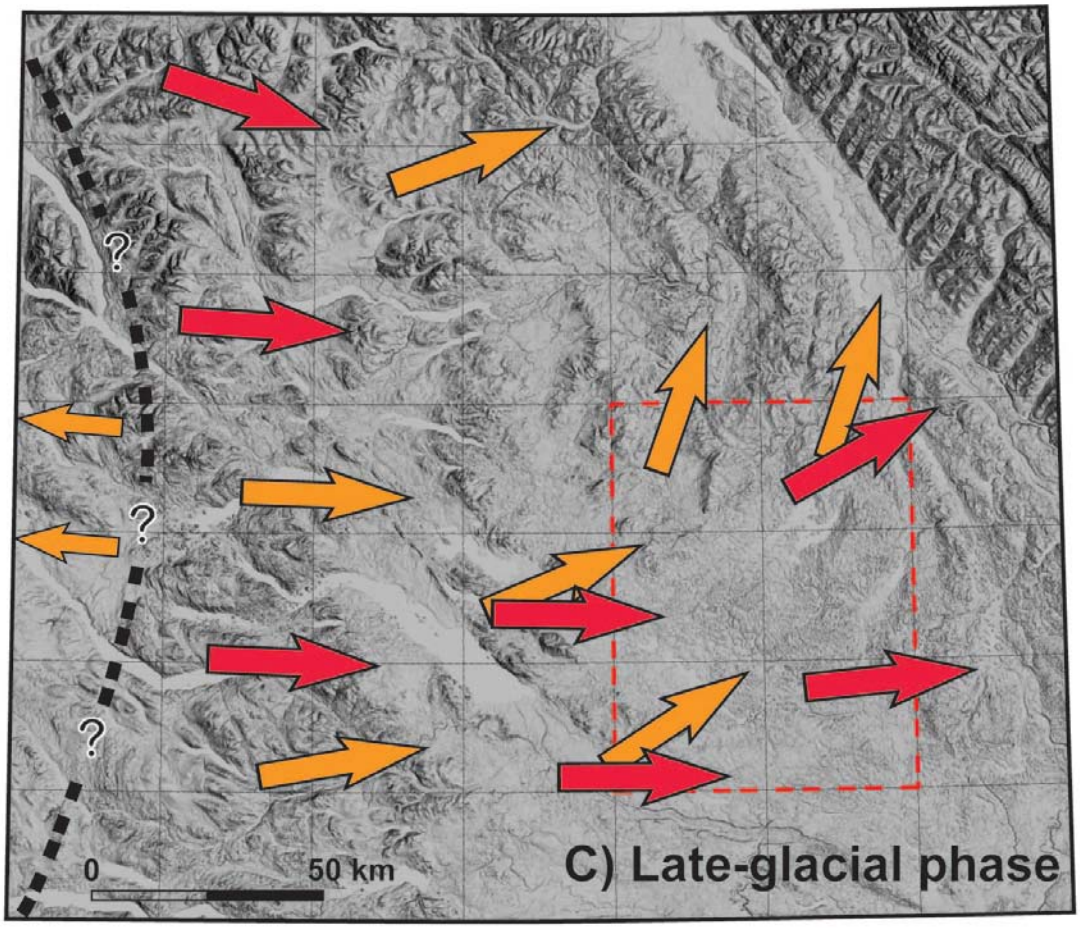

Figure 5.15 C

5.6. Conceptual models for deglaciation

Fulton's (1967, 1991) deglacial model for the Southern Interior describes active ice, transitional upland, stagnant ice and dead ice phases (Chapter 2). Similar patterns of deglaciation were reported for the Bonaparte Lake map-area (NTS 092P) where the thinnest ice in the upland areas melted first and ice remained in the valleys (Plouffe et al. 2011). Alternately, Lesemann and Brennand (2009) propose a reverse theory for the southern Interior Plateau that has thick ice over the uplands and thin ice over subglacial lakes in valleys (e.g. Okanagan Valley). They postulate that erosion during underbursts from subglacial lakes developed drumlin swarms throughout the Thompson Plateau and parts of the Fraser Plateau and Okanagan Valley. The volume and location of the proposed valley lakes are not conducive to the formation of all the drumlins in the region,

thus Lesemann and Brennand (2009) theorize the formation of a large sub- or supraglacial lake over the Fraser Plateau. Mapping of the surficial geology in the area underlying the proposed lake identified no sedimentological evidence for a subglacial lake, and if a supraglacial lake existed, its formation and maintenance on a frozen ice sheet during glaciation requires explainion (Plouffe et al. 2011).

Although there are physiographic similarities between northern and southern parts of the Interior, the absence of landforms associated with large-scale dead and stagnant ice indicate Fulton's model is not entirely applicable in the north (*cf.* Plouffe 2000). This is likely due to the ice divide in the Northern Interior that largely remained east of the Coast Mountains during the early phases of deglaciation and maintained connection with valley glaciers when it shifted back to the mountains (Levson et al. 1998; Stumpf et al. 2000); the proximity to local accumulation centres (Plouffe 2000); and the limited occurrence of deep topographic lows that served as loci for stagnation in the south.

Margold et al. (in press) present a model of the CIS retreat in central British Columbia reconstructed from regional-scale investigations of meltwater landforms. Based on ice surface profiles delineated through inversion modeling, they conclude that the pattern of retreat was similar to that of the Fennoscandian ice sheet (*cf*. Kleman et al. 1997), in which ice retreated back into the source area along an irregular ice front with minimal stagnation. Specifically, the CIS retreated westward and southwestward back into the Coast Mountains. The proposed style of frontal retreat is in general agreement with the findings of this study; however, the suggested ice front locations and morphology of the ice mass are not congruent. Their reported retreat patterns for the northern Interior Plateau are likely oversimplified due to the large scale of their investigation. These discrepancies may be caused by the inability of the profile modeling to accommodate the complex topography of British Columbia and the influence of multiple major ice accumulation zones.

Plouffe (2000) applied Fulton's (1967) model of deglaciation with minor modifications to map-areas NTS 093N/K, west of the study area. He illustrates that ice tongues remained active and connected to their sources throughout deglaciation. Levson et al. (1998) and Stumpf et al. (2000) also conclude ice movement and connectivity late into deglaciation over the Nechako Plateau. Data from this study illustrates localized

stagnation, and large-scale modifications to ice-flow and the shape of the ice margin as local source areas became more influential during deglaciation. Here, Fulton's (1967, 1991) model of deglaciation is refined with these findings to emphasize the reorganization of the ice sheet, continued ice movement, and local rather than regional ice stagnation. The refined model is specific to the northern Interior Plateau of British Columbia and consists of four phases: 1) confluent ice sheet; 2) ice sheet reorganization; 3) valley; and 4) alpine.

The confluent ice sheet phase is analogous with Fulton's (1967, 1991) active ice phase. During this phase the northwest-southeast-oriented ice front retreated southwesterly from the Rocky Mountains into the northern Interior Plateau. The general ice-flow direction was similar to that of the glacial maximum, but large topographic features caused local ice-flow variations at the margin. Locally, ice masses detached from the ice front as it retreated across topographic irregularities. Examples of local ice stagnation are: the ice dam for glacial Lake McLeod and large kettle lakes further north in the Parsnip River valley; ice stagnation topography on the northeast side of the uplands in NTS 093J13; and Carp Lake. During the ice sheet reorganization phase, ice dynamics shifted to reflect major source areas. Specifically, the southern part of the margin began to trend more east-west and northern part more north-south, and ice-flow near the northern margin shifted east. Closer to the major source areas, ice was thinning and ice-flow became increasingly influenced by topography (Stumpf et al. 2000). Ice-flow continued through this phase and the ice front continued to retreat west through the Nechako Plateau (Plouffe 2000) and south through the Fraser Basin (Clague 1988). The valley phase (analogous with Fulton's (1967, 1991) transitional upland phase) occurred when accumulation zones shifted back into the local mountains and ice was limited to large valleys such as the Babine and Ootsa lake valleys. Topographically controlled ice-flow continued in valley glaciers that were still attached to source areas in the northern mountain ranges (Levson et al. 1998; Plouffe 2000; Stumpf et al. 2000). Local ice stagnation presumably occurred during this phase as ice blocks detached from retreating ice margins. During the final alpine phase, active ice was limited to alpine regions. Climate fluctuations such as the Younger Dryas may have caused some readvances in alpine areas (e.g. Lakeman et al. 2008). Ice left in the lower valleys during these readvances likely stagnated.

6. Summary and conclusions

This project was designed to determine the glacial history of part of the Quesnel Terrane to guide mineral exploration and to add to the body of knowledge of glaciation in central British Columbia. The main objectives of the project were to: 1) describe and document the distribution of the surficial materials; 2) develop a stratigraphic framework; 3) determine the local ice-flow history; and 4) determine the local pattern and chronology of deglaciation. Aerial photograph interpretation and field-based investigations were done to produce two 1:50 000-scale terrain maps and an inventory of surficial materials and landforms. Stratigraphic exposures were logged to determine the succession of depositional environments. Large- and small-scale ice-flow indicators and their relative chronologies were used to determine the ice-flow history. The data were used to determine the pattern and events of deglaciation, and minimum ages for deglaciationwere determined through optical and radiocarbon dating.

6.1. Summary of glacial history and surficial geology

The study area is in the northern Interior Plateau where glaciers sourced from the Coast, Skeena and Omineca mountains coalesced. Ice first flowed southeasterly into the region from the Omineca Mountains and covered at least the northwest part of the study area. This advance impeded northern drainage, forming a glacial lake in parts of the Peace River watershed within the study area. Later, ice from the Kitimat and Pacific ranges of the Coast Mountains coalesced with ice from the Skeena and Omineca mountains, causing a northeast shift in ice flow that streamlined the sediment and bedrock at the glacial maximum.

When the northeast part of the study area became deglaciated, ice first flowed to the northeast, with minor northerly deviations near the margin due to topography. The ice margin retreated to the southwest along a northwest-southeast-trending margin.

Northerly drainage was impeded by ice in the northern McLeod Lake valley, causing a large glacial lake to form within it and the Crooked River valley. When the ice margin retreated beyond the Arctic and Pacific drainage divide, meltwater was diverted to the southeast, cutting lateral channels along the ice margin that drained into glacial Lake Fraser. The channels delineate ice margin locations and depict the reorganization of the ice sheet as it began to separate and retreat to major source areas in the south and west. During this reorganization there was an easterly shift in ice flow in the southwest part of the study area and several time-transgressive ice-marginal lakes developed.

After the ice retreated, sand was deflated from unvegetated glaciofluvial and glaciolacustrine units and deposited as localized mantles and dunes throughout the study area. Optical ages on K-feldspar of 9.35 ± 0.64 ka, 9.94 ± 0.77 and 13.3 ± 1.0 ka provide new limiting ages for ice retreat. An organic sample obtained from peat in the hollow of an ice-contact glaciofluvial deposit yielded an age of 9910 - 9642 cal yr BP (8775 ± 30 ^{14}C yr BP; UCAIMS 83989) that is a minimum age for peat development and does not closely delimit deglaciation. The agreement between the radiocarbon age and younger optical ages suggest that those optical ages are too young to tightly constrain the timing of deglaciation.

Fulton's (1969, 1991) conceptual model for deglaciation in the Southern Interior of British Columbia is refined for the northern Interior Plateau. The refined model emphasises the separation of the CIS into lobes that retreated to different source areas, continued ice-flow through the late-glacial phase and local ice-stagnation. It consists of four phases: 1) confluent ice sheet; 2) ice sheet reorganization; 3) valley; and 4) alpine. During the confluent ice sheet phase, ice flowed northeast with minor deviations at the margin due to topographic influence. The ice sheet reorganization phase is marked by modifications to the ice margin and ice flow to reflect different source areas that became dominant during deglaciation. During the valley phase, accumulation zones shifted back to local mountains and active trunk glaciers occupied large valleys. In the final alpine phase, active ice was limited to alpine regions where minor oscillations occurred during climate fluctuations.

The surficial geology is dominantly a result of the Fraser Glaciation, with minor modifications during the Holocene. The study area is characterized by thick drift that

conceals most bedrock except in the northern uplands where rock outcrop and sediment mantles are more numerous. Till is the most aerially extensive material. It occurs as blankets and veneers in the uplands and large fields of drumlins and flutings in the remaining areas. Stratigraphic exposures in the north suggest that till is dominantly underlain by bedrock or glaciolacustrine sediments. Both glaciofluvial and glaciolacustrine deposits occur locally overlying the till. Large, northerly flowing proglacial meltwater systems deposited thick gravel units in the northeast corner of the study area. Throughout the rest of the study area, thin glaciofluvial units were deposited in lateral meltwater channels that flowed southeast. Ice-contact gravels are common in topographic depressions. Glaciolacustrine deposits are limited in the north and mostly occur within valleys. They are typically ice-proximal deposits composed of sand, gravel and diamict. In the southern part of the study area, glaciolacustrine deposits are dominantly silty and form expansive blankets and plains in most depressions.

6.2. Recommendations for research

A main deliverable from this project is information to guide mineral exploration. In conjunction with this study, a regional till geochemical and mineralogical survey was conducted that highlighted several anomalous zones with the potential for economic mineralization (Ward et al. 2009, 2011, 2012; Sacco et al. 2010). Using the terrain maps and ice-flow history, a local-scale till survey should be carried out to better define the indicator trains and locate the source areas of anomalous samples.

There are still many unanswered questions regarding the events of the Fraser Glaciation that can only be answered with chronological data. Radiocarbon dating is relatively inexpensive, precise, and easily accessible. Organics, however, from the immediate deglacial period are rare. Optical dating of post-glacial aeolian sediments is an alternative means of constraining the time of deglaciation. Additional experimentation with the method could increase the accuracy of the ages. Dating the numerous aeolian deposits in and around the study area would provide a large data set from which a detailed chronology for deglaciation could be established.

Stratigraphic exposures are dominantly located in the northern part of the study area, and a comprehensive story of events was established in that area. However, more information on the early ice advance could be attained by measuring clast fabric orientations and lithological composition of the lower till and the lower sections of till units in these exposures. Stratigraphic information is lacking in south. Locating exposures along the Salmon and Necoslie rivers could yield more data and provide more information on local glacial events.

Despite the large amount of work completed on glacial Lake Fraser and its sediments, the dynamics are still poorly understood. This is likely due to the large extent of the lake and the limited knowledge of isostacy in the region. Studies that quantify the extent of isostatic uplift by measuring the elevations of related glaciolacustrine units could provide the means to more accurately model the extent of the lake and identify the outlets that controlled it.

Another research topic that could be addressed is the formation of subglacial bedforms; a topic that has been debated for many years. Numerous drumlins and flutings in the study area are easily accessible through a network of forest service roads. The roads expose sections in hundreds of features and provide an excellent opportunity to investigate their internal structure and composition. A data set of this size could lend evidence to a present theory for the formation of subglacial bedforms, or provide new alternatives.

7. References

Adamiec, G. and Aitken, M. J. 1998. Dose-rate conversion factors: update. Ancient TL, **16**: 37-39.

Aitken, M. J. 1985. Thermoluminescence dating. Academic Press, New York.

Alley, N. and Young, G. 1978. Environmental significance of geomorphic processes in northern British Columbia west of the Rocky Mountains. BC Ministry of the Environment, Resource Analysis Branch, Bulletin 3.

Armstrong, J. E., and Tipper, H. W. 1948. Glaciation in north-central British Columbia. American Journal of Science, **246**: 283-310.

Armstrong, J. E., Crandell, D. R., Easterbrook, D. J., and Noble, J. B. 1965. Late Pleistocene stratigraphy and chronology in southwestern British Columbia and northwestern Washington. Geological Society of America Bulletin, **76**: 321-330.

Ballantyne, C. K. 2002. Paraglacial geomorphology. Quaternary Science Reviews, **21**: 1935-2017.

Bateman, M. and Murton, J. 2006. The chronostratigraphy of late Pleistocene glacial and periglacial aeolian activity in the Tuktoyaktuk coastlands, NWT, Canada. Quaternary Science Reviews, **25**: 2552-2568.

Bednarski, J. M. and Smith, I. R. 2007. Laurentide and Montane glaciation along the Rocky Mountain foothills of northeastern British Columbia. Canadian Journal of Earth Sciences, **44**: 445-457.

Benn, D. I. and Evans, D. J. A. 1998. Glaciers & glaciation. Oxford University Press Inc., New York.

Berger, G. W, Clague, J. J., and Huntley, D. 1987. Thermoluminescence dating applied to glaciolacustrine sediments from central British Columbia. Canadian Journal of Earth Sciences, **24**: 425-434.

Bobrowsky, P. and Rutter, N. W. 1992. The Quaternary geologic history of the Canadian Rocky Mountains. Géographie physique et Quaternaire, **46**: 5-50.

Boulton, G. S. 1987. A theory of drumlin formation by subglacial sediment deformation. *In* Menzies, J. and Rose, J. (eds), Drumlin Synopsium. Balkema, Rotterdam, pp. 25–80.

Brennand, T. A. 1994. Macroforms. large bedforms and rhythmic sedimentary sequences in subglacial eskers, south-central Ontario: implications for esker genesis and meltwater regime. Sedimentary Geology, **91**:9-55.

Burke, M. J., Woodward, J., Russell, A. J., Fleisher, P. J., and Bailey, P. K. 2010. The sedimentary architecture of outburst flood eskers; a comparison of ground-penetrating radar data from Bering glacier, Alaska and Skeidararjokull, Iceland. Geological Society of America Bulletin, **122**: 1637-1645.

Church, M. and Ryder, J. M. 1972. Paraglacial sedimentation; a consideration of fluvial processes conditioned by glaciation. Geological Society of America Bulletin, **83**: 3059-3072.

Clague, J. J. 1987. Quaternary stratigraphy and history, Williams Lake, British Columbia. Canadian Journal of Earth Sciences, **24**: 147-158.

Clague, J. J. 1988. Quaternary stratigraphy and history, Quesnel, British Columbia. Géographie physique et Quaternaire, **42**: 279-288.

Clague, J. J. (Compiler). 1989. Chapter 1. Quaternary geology of the Canadian Cordillera. *In* Quaternary geology of Canada and Greenland *Edited by* R.J. Fulton and J.O. Wheeler. Geological Survey of Canada, Geology of Canada, No. 1: 15-96.

Clague, J. J. 1998. Surficial geology, Cluculz Lake, British Columbia. Geological Survey of Canada, Open File 3638.

Clague, J. J., Armstrong, J. E., and Mathews, W. H. 1980. Advance of the Late Wisconsinan Cordilleran Ice Sheet in southern British Columbia since 22,000 yr B.P. Quaternary Research, **13**: 322-326.

Clague, J. J., Hebda, R. J., and Mathewes, R. W. 1990. Stratigraphy and paleoecology of Pleistocene interstadial sediments, central British Columbia. Quaternary Research, **34**: 208-226.

Clark, P. U. and Hansel, A. K. 1989. Clast ploughing, lodgement and glacier sliding over a soft glacier bed. Boreas, **18**: 201-207.

Davis, N. F. G. and Mathews, W. H. 1944. Four phases of glaciation with illustrations from southwestern British Columbia. Journal of Geology, **52**: 403-413.

Dawson, G. M. 1878. On the superficial geology of British Columbia. Quarterly Journal of the Geological Society of London, **34**: 89-123.

Dawson, G. M. 1881. Report on an exploration from Port Simpson on the Pacific Coast to Edmonton on the Saskatchewan, embracing a portion of the northern part of British Columbia and the Peace River country, 1879. Geological Survey of Canada, Progress Report, **1879-1880**.

Dawson, G. M. 1888. Recent observations on the glaciation of British Columbia and adjacent regions. Geological Magazine, **5**: 347.

Dawson, G. M. 1889. Glaciation of high points in the southern Interior of British Columbia. Geological Magazine, **6**: 350.

Dawson, G. M. 1891. On the later physiographical geology of the Rocky Mountain region in Canada, with special reference to changes in elevation and to the history of the glacial period. Transactions of the Royal Society of Canada, **8**: 3-74.

Demarchi, D. 2011. The British Columbia ecoregion classification. BC Ministry of Environment, Victoria, British Columbia.

Demuro, M., Roberts, R., Froese, D., Arnold, L., Brock, F., and Bronk Ramsey, C. 2008. Optically stimulated luminescence dating of singe and multiple grains of quartz from perennially frozen loess in western Yukon Territory, Canada: Comparison with radiocarbon chronologies for the late Pleistocene Dawson tephra. Quaternary Geochronology, **3**: 346-364.

Dreimanis, A. 1989. Tills: Their genetic terminology and classification. *In* Genetic Classification of Glaciogenic Deposits *Edited by* R. Goldthwait and C. Matsch. A.A. Balkema, Rotterdam: 17-83.

Edwards, B. R, Russell, J.K, and Anderson, R. G. 2002. Subglacial, phonolitic volcanism at hoodoo mountain volcano, northern Canadian Cordillera. Bulletin of Volcanology, **64**: 254-272.

Eyles, N. and Clague, J. J. 1991. Glaciolacustrine sedimentation during advance and retreat of the Cordilleran Ice Sheet in central British Columbia. Géographie physique et Quaternaire, **45**: 317-331.

Flint, R. F. 1971. Glacial and Quaternary geology. Wiley, New York.

Fulton, R. J., Irving, E., and Wheadon, P. M. 1992. Stratigraphy and paleomagnetism of Brunhes and Matuyama (>790 ka) Quaternary deposits at Merritt, British Columbia. Canadian Journal of Earth Sciences, **29**: 76-92.

Fulton, R. J. 1967. Deglaciation studies in Kamloops region, an area of moderate relief, British Columbia. Geological Survey of Canada, Bulletin 165.

Fulton, R. J. 1991. A conceptual model for growth and decay of the Cordilleran Ice Sheet. Géographie physique et Quaternaire, **45**: 281-286.

Galbraith, R. F. and Olley, J. M. 1999. Optical dating of single and multiple grains of quartz from Jinmium rock shelter, northern Australia, part 1, experimental design and statistical models. Archaeometry, **41**: 339-364.

Geike, J. 1984. The great ice age, 3rd ed. Edward Stanford, London.

Hartman, G. M. D., and Clague, J. 2008. Quaternary stratigraphy and glacial history of the Peace River valley, northeast British Columbia. Canadian Journal of Earth Sciences, **45**: 549-564.

Harder, M. and Russell, J. K. 2007. Basanite glaciovolcanism at Llangorse Mountain, northern British Columbia, Canada. Bulletin of Volcanology, **69**: 329-340.

Harington, C. R., Plouffe, A., and Jette, H. 1996. A partial bison (bison *cf*. B. Latifrons) skeleton from Chuchi Lake, and its implications for the Middle Wisconsinan environment of central British Columbia. Géographie physique et Quaternaire, **50**: 73-80.

Harington, C. R., Tipper, H. W., and Mott, R. J. 1974. Mammoth from Babine Lake, British Columbia. Canadian Journal of Earth Sciences, **11**: 285-303.

Hebda, R. J. 1995. British Columbia vegetation and climate history with focus on 6 ka BP. Geographie Physique et Quaternaire, **49**: 55-79.

Hickson, C. J. and Souther, J. G. 1984. Late Cenozoic volcanic rocks of the Clearwater-Wells Gray area, British Columbia. Canadian Journal of Earth Sciences, **21**: 267-277.

Hickson, C. J., Moore, J. G., Calk, L. C., and Metcalfe, P. 1995. Intraglacial volcanism in the Wells Gray-Clearwater volcanic field, east-central British Columbia, Canada. Canadian Journal of Earth Sciences, **32**: 838-851.

Hicock, S. R., Hobson, K., and Armstrong, J. E. 1982. Late Pleistocene proboscideans and early Fraser glacial sedimentation in eastern Fraser lowland, British Columbia. Canadian Journal of Earth Sciences, **19**: 899-906.

Hicock, S. R., Goff, J. R., Lian, O. B., and Little, E. C. 1996. On the interpretation of subglacial till fabric. Journal of Sedimentary Research, **66**: 928-934.

Holland, S. S. 1976. Landforms of British Columbia: A physiographic outline. Department of Mines and Petroleum Resources, Victoria, B.C.

Howes, D. E. and Kenk, E. 1997. Terrain classification system for British Columbia. Version 2. British Columbia Ministry of Environment, Lands and Parks, Victoria, B.C.

Hugenholtz, C.H., Moorman, B.J., and Wolfe, S. A. 2007. Ground-penetrating radar (GPR) imaging of the internal structure of an active parabolic sand dune. Geological Society of America. Baker, G.S., Jol, H. M. (eds), Special Paper, **432**: 35-45.

Hugenholtz, C. H, Wolfe, S. A., and Moorman, B. J. 2008. Effects of sand supply on the morphodynamics and stratigraphy of active parabolic dunes, Bigstick Sand Hills, southwestern Saskatchewan. Canadian Journal of Earth Sciences, **45**: 321-335.

Huntley, D. J. and Lamothe, M. 2001. Ubiquity of anomalous fading in K-feldspars and the measurement and correction for it in optical dating. Canadian Journal of Earth Sciences, **38**: 1093-1106.

Jackson, L. E. Jr. and Clague, J. J. 1991. The Cordilleran Ice Sheet; one hundred and fifty years of exploration and discovery. Geographie physique et Quaternaire, **45**: 269-280.

Jol, H. M, Bristow, C. S., and Havholm, K. G. 2002. GPR stratigraphic investigation of modern and ancient aeolian environments. SEG Annual Meeting Expanded Technical Program Abstracts with Biographies, **72**: 1535.

Jol, H. M., Comas, X., Slater, L., Fisher, T. G., and Reeve, A. 2007. Ground penetrating radar; a noninvasive, high resolution method for the development of facies models in eskers. - Geological Society of America Abstracts with Programs, **39**: 117.

Kelman, M. C., Russell, J. K., and Hickson, C. J. 2002. Glaciovolcanism at Ember Ridge, Mount Cayley Volcanic Field, southwestern British Columbia. Geological Survey of Canada, Current Research, 2002-A15.

Kerr, F. A. 1934. Glaciation in northern British Columbia. Transactions of the Royal Society of Canada, **28**: 17-31.

Kleman, J.K., Hattestrand, C., Borgstrom, I., and Stroeven, A. 1997. Fennoscandian palaeoglaciology reconstructed using a glacial geological inversion model. Journal of Glaciology, **43**: 283-299.

Lakeman, T. R., Clague, J. J., and Menounos, B. 2008a. Advance of alpine glaciers during final retreat of the Cordilleran Ice Sheet in the Finlay River area, northern British Columbia, Canada. Quaternary Research, **69**: 188-200.

Lakeman, T. R., Clague, J. J., Menounos, B., Osborn, G. D., Jensen, B. J. L., and Froese, D. G. 2008b. Holocene tephras in lake cores from northern British Columbia, Canada. Canadian Journal of Earth Sciences, **45**: 935-947.

Lesemann, J. E., and Brennannd, T. A. 2009. Regional reconstruction of subglacial hydrology and glaciodynamic behaviour along the southern margin of the Cordilleran Ice Sheet in British Columbia, Canada and northern Washington State, USA. Quaternary Science Reviews, **28** (23-24): 2420-2444.

Levson, V. M. 2001. Quaternary geology of the Babine porphyry copper district; implications for geochemical exploration. Canadian Journal of Earth Sciences, **38**: 733-749.

Levson, V. M. and Giles, T. R. 1997. Quaternary geology and till geochemistry studies in the Nechako and Fraser plateaus, central British Columbia (NTS 93C/1, 8, 9, 10; F/2, 3, 7; L/16; M/1). British Columbia Geological Survey, Paper 1997-2: 121-145.

Levson, V. M., Giles, T. R., Bobrowsky, P. T., and Matysek, P. F. 1990. Geology of placer deposits in the Cariboo mining district, British Columbia; implications for exploration (93A, B, G, H). Ministry of Energy, Mines and Petroleum Resources, Paper 1990-1: 519-529.

Levson, V. M., Stumpf, A. J., Stuart, A. J., and Smyth, W. R. 1998. Quaternary geology and ice-flow studies in the Smithers and Hazelton map-areas (93 L and M); implications for exploration. Ministry of Energy, Mines and Petroleum Resources Paper 1998-1: 5-16.

Levson, V. M., Stumpf, A. J., Meldrum, D. G., O'Brien, E. K., and Broster, B. E. 1997. Quaternary geology and ice-flow history of the babine copper porphyry belt, british columbia (NTS 93 L/NE, M/SE). British Columbia Geological Survey, Paper 1997-1: 427-438.

Lian, O. B. and Roberts, R. 2006. Dating the Quaternary: Progress in luminescence dating of sediments. Quaternary Science Reviews, **25**: 2449-2468.

Lian, O. B. 2007. Optically-stimulated luminescence. *In* Encyclopedia of Quaternary Geology *Edited by* S. Elias. Elsevier, Oxford, pp. 1491-1505.

Lian, O. B. and Hickin, E. J. 1993. Late Pleistocene stratigraphy and chronology of lower Seymour valley, southwestern British Columbia. Canadian Journal of Earth Sciences, **30**: 841-850.

Lian, O. B., Barendregt, R. W., and Enkin, R. J. 1999. Lithostratigraphy and paleomagnetism of pre-Fraser glacial deposits in south-central British Columbia. Canadian Journal of Earth Sciences, **36**: 1357-1370.

Lian, O. B., Hu, J., Huntley, D. J., and Hicock, S. R. 1995. Optical dating studies of Quaternary organic-rich sediments from southwestern British Columbia and northwestern Washington State. Canadian Journal of Earth Sciences, **32**: 1194-1207.

Logan, J. M., Schiarizza, P., Struik, L. C., Barnett, C., Nelson, J. L., Kowalczyk, P., Ferri, F., Mihalynuk, M. G., Thomas, M. D., Gammon, P., Lett, R., Jackaman, W., and Ferbey, T. 2010. Bedrock geology of the QUEST map-area, central British Columbia. Geological Survey of Canada, Open File 6476.

Lowdon, J. A. and Blake, W. J. 1980. Geological Survey of Canada radiocarbon dates; XX. Geological Survey of Canada, Paper 80-7.

Margold, M., Jansson, K., Kleman, J., Stroeven, A., and Clague, J. J. In press. Late-glacial retreat pattern of the Cordilleran ice sheet in central British Columbia reconstructed from glacial meltwater landforms.

Mate, D. J. and Levson, V. M. 2000. Quaternary geology of the Marilla map area NTS 93F/12. British Columbia Geological Survey, Paper 1999-1: 25-32.

Mate, D. J. and Levson, V. M. 2001. Quaternary stratigraphy and history of the Ootsa Lake-Cheslatta River area, Nechako Plateau, central British Columbia. Canadian Journal of Earth Sciences, **38**: 751-765.

Mathews, W. H. 1980. Retreat of the last ice sheets in northeastern British Columbia and adjacent Alberta. Geological Survey of Canada, Bulletin 331.

Mathews, W. H. and Rouse, G. E. 1986. An early Pleistocene proglacial succession in south-central British Columbia. Canadian Journal of Earth Sciences, **23**: 1796-1803.

Maynard, D., Geertsema, M., Sacco, D. A., and Ward, B. C. 2012a. Terrain inventory map, NTS 093J11, central British Columbia. Geoscience BC.

Maynard, D., Sacco, D. A., and Ward, B. C. 2012b. Terrain inventory map, 093J05, central British Columbia. Geoscience BC.

Maynard, D., Sacco, D. A., and Ward, B. C. 2012c. Terrain inventory map, NTS 093J06, central British Columbia. Geoscience BC.

McConnell, R. G. 1891. Report on an exploration in the Yukon and Mackenzie basins, Northwest Territories. Geologic Survey of Canada, Annual Report.

Murray, A. S., and Wintle, A. G. 2000. Luminescence dating of quartz using an improved single-aliquot regenerative-dose protocol. Radiation Measurements, **32**: 57-73.

Murray, A.S. and Wintle, A.G. 2003. The single aliquot regenerative dose protocol; potential for improvements in reliability. Radiation Measurements, **37**: 377-381.

Neal, A. 2004. Ground-penetrating radar and its use in sedimentology; principles, problems and progress. Earth-Science Reviews, **66**: 261-330.

Nye, J. 1973. Water at the bed of a glacier. *In* Symposium on the Hydrology of Glaciers, IASH Publication, Cambridge, **95**, pp. 189-194.

Parent, M., Paradis, S. J., and Doiron, A. 1996. Palimpsest glacial dispersal trains and their significance for drift prospecting. Journal of Geochemical Exploration, **56**: 123-140.

Paulen, R. and Bobrowsky, P. 2003. Multiphase flow of late Wisconsinan ice in the Quesnel highlands: Piecing together discordant ice-flow indicators. GAC-MAC-SEG, Program with Abstracts, **28**: 132.

Plouffe, A. 1992. Quaternary stratigraphy and history of central British Columbia. *In* Current Research, Part A, Geological Survey of Canada, Paper 92-1A: 189-193.

Plouffe, A. 1997. Ice-flow and late-glacial lakes of the Fraser glaciation, central British Columbia. *In* Current Research, Geological Survey of Canada, Paper 1997-A/B: 133-143.

Plouffe, A. 2000. Quaternary geology of the Fort Fraser and Manson River map-areas, central British Columbia. Geological Survey of Canada, Bulletin 554.

Plouffe, A. and Levson, V. M. 2001a. Late quaternary glacial and interglacial environments of the Nechako River-Cheslatta Lake area, central British Columbia. Canadian Journal of Earth Sciences, **38**: 719-731.

Plouffe, A. and Levson, V. M. 2001b. Surficial geology, Tatelkuz Lake, British Columbia. Geological Survey of Canada, Open-File 4001.

Plouffe, A. and Jette, H. 1997. Middle Wisconsinan sediments and paleoecology of central British Columbia; sites at Necoslie and Nautley rivers. Canadian Journal of Earth Sciences, **34**: 200-208.

Plouffe, A. and Levson, V. M. 2002. Surficial geology, Entiako Lake, British Columbia. Geological Survey of Canada, Open-File 4157.

Plouffe, A., Bednarski, J. M., Huscroft, C. A., Anderson, R. G, and McCuaig, S. J. 2011. Late Wisconsinan glacial history in the Bonaparte lake map-area, south-central British Columbia; implications for glacial transport and mineral exploration. Canadian Journal of Earth Sciences, **48**: 1091-1111.

Prescott, J. and Hutton, J. 1994. Cosmic ray contributions to dose rates for luminescence and ESR dating: Large depths and long term time variations. Radiation Measurements, **23**: 497-500.

Resources Inventory Committee. 1996. Guidelines and standards for terrain mapping in British Columbia. Government of British Columbia, Victoria, B.C.

Röthlisberger, H. 1972. Water pressure in intra- and sub-glacial channels. Journal of Glaciology, **11**: 177-203.

Rutter, N.W. 1977. Multiple glaciations in the area of Williston Lake, British Columbia. Geological Survey of Canada, Bulletin 273.

Ryder, J. and Maynard, D. 1991. The Cordilleran Ice Sheet in northern British Columbia. Geographie physique et Quaternaire, **45**: 355-363.

Sacco, D. A., Ward, B. C., Maynard, D., Geertsema, M., and Reichheld, S. 2010. Terrain mapping, glacial history and drift prospecting in the northwest corner of McLeod lake map-area (part of NTS 093J), central British Columbia. *In* Geoscience BC Summary of Activities 2009. Report 2010-1: 33-42.

Sensors and Software. 1999. Ground penetrating radar survey design.

Shaw, J. 1989. Drumlins, subglacial meltwater floods, and ocean responses. Geology, **17**: 853-856.

Souther, J. G., Armstrong, R. L., and Harakal, J. 1984. Chronology of the peralkaline, late Cenozoic Mount Edziza Volcanic Complex, northern British Columbia, Canada. Geological Society of America Bulletin, **95**: 337-349.

Spooner, I. S., Osborn, G. D., Barendregt, R. W., and Irving, E. 1995. A record of early Pleistocene glaciation on the Mount Edziza Plateau, northwestern British Columbia. Canadian Journal of Earth Sciences, **32**: 2046-2056.

Spooner, I. S., Osborn, G. D., Barendregt, R. W., and Irving, E. 1996. A middle Pleistocene (isotope stage 10) glacial sequence in the Stikine River valley, British Columbia. Canadian Journal of Earth Sciences, **33**: 1428-1438.

Stokes, C. R., Lian, O. B., Tulaczyk, S., Clark, C. D. 2008. Superimposition of ribbed moraines on a paleo-ice-stream bed: implications for ice stream dynamics and shutdown. Earth Surface Processes and Landforms, **33**: 593–609.

Struik, L. C. 1994. Geology of the McLeod Lake map-area (93J), British Columbia. Geological Survey of Canada, Open-File 2439.

Stumpf, A. J., Broster, B. E., and Levson, V. M. 2000. Multiphase flow of the late Wisconsinan Cordilleran Ice Sheet in western Canada. Bulletin of the Geological Society of America, **112**: 1850-1863.

Tipper, H. W. 1971a. Glacial geomorphology and Pleistocene history of central British Columbia. Geological Survey of Canada, Bulletin 196.

Tipper, H. W. 1971b. Multiple glaciations in central British Columbia. Canadian Journal of Earth Sciences, **8**: 743-752.

van der Meer, J. J. M., Kjaer, K. H., Krueger, J., Rabassa, J., and Kilfeather, A. A. 2009. Under pressure; clastic dykes in glacial settings. Quaternary Science Reviews, **28**: 708-720.

Visser, J. N. J. 1989. Stone orientations in basal glaciogenic diamictite; four examples from the Permo-Carboniferous Dwyka ormation, South Africa. Journal of Sedimentary Petrology, **59**: 935-943.

Ward, B. C., Geertsema, M., Telka, A., and Mathewes, R. W. 2008. A paleoecological record of climatic deterioration from middle to late Wisconsinan time on the Interior Plateau of British Columbia, Canada. 33rd International Geological Congress, August 6–14, 2008, Oslo, Norway.

Ward, B. C, Leybourne, M., and Sacco, D. A. 2011. Drift prospecting within the quest project area, central British Columbia (NTS 093J): Potential for porphyry copper-gold, volcanogenic massive sulphide mineralization and gold-copper veins. *In* Geoscience BC Summary of Activities 2010, Report 2011-1: 73-96.

Ward, B. C., Leybourne, M., and Sacco, D. A. 2012. Heavy mineral analysis of till samples within the QUEST project area, central British Columbia. *In* Geoscience BC Summary of Activities 2011, Report 2012-1:59-68.

Ward, B. C., Maynard, D., Geertsema, M., and Rabb, T. 2009. Ice-flow history, drift thickness and drift prospecting for a portion of the QUEST project area, central British Columbia (NTS 093G, H [west half], J). *In* Geoscience BC Summary of Activities, Report 2009-1: 25-32.

Ward, B. C., Sacco, D. A., and Maynard, D. 2012. Terrain inventory map, NTS 093J13, central British Columbia. Geoscience BC.

Wintle, A. G. 2008. Luminescence dating: Where it has been and where it is going. Boreas, **37**: 471-482.

Wintle, A. G. and Murray, A. S. 2006. A review of quartz optically stimulated luminescence characteristics and their relevance in single-aliquot regeneration dating protocols. Radiation Measurements, **41**: 369-391.

Woodcock, N. H. and Naylor, M. A. 1983. Randomness testing in three-dimensional orientation data. Journal of Structural Geology, **5**: 539-548.

Appendices

Appendix A.

Supplementary CD

A1. Digital terrain inventory database

Filename: TerrinInventoryDatabase.gdb.zip

Creator: David Sacco

Description: Digital database of terrain mapping data and shapefiles

A2. GPR profiles

Filename: AppendixA2_GPR_profiles.pdf

Creator: David Sacco

Description: Additional GPR profiles

A3. Striation Data Table

Filename: Appendix_A3_striation_data.pdf

Creator: David Sacco

Description: Description of striations

Appendix B.

Map Pocket

B1. Terrain Map, NTS 093J13

Creator: David Sacco

Description: Terrain map for NTS 093J13

B2. Terrain Map, NTS 093J14

Creator: David Sacco

Description: Terrain map for NTS 093J14